Transport Phenomena in Polymer Electrolyte Membranes

by

Jeffrey Anders Fimrite
B.Eng., University of Victoria, 2002

A Thesis Submitted in Partial Fulfillment of the Requirements for the Degree of

MASTER OF APPLIED SCIENCE

in the Department of Mechanical Engineering

We accept this thesis as conforming
to the required standard

Dr. N. Djilali, Supervisor (Department of Mechanical Engineering)

Dr. H. Struchtrup, Supervisor (Department of Mechanical Engineering)

Dr. D. Harrington, Outside Member (Department of Chemistry)

Dr. B. Wetton, External Examiner (Mathematics Department, UBC)

© Jeffrey Anders Fimrite, 2004
University of Victoria

Abstract

This thesis presents a thorough review of the available literature on issues relevant to transport phenomena in polymer electrolyte membranes. The insight gained in the literature review is used in the development of a transport model based on the Binary Friction Model (BFM). A competing model, the Dusty Fluid Model (DFM), is not used because there are still some unanswered questions regarding the introduction of additional viscous terms. The transport model is then applied to 1100 *EW* Nafion. In order to investigate the unknown parameters in the transport model, a simplified conductivity model, termed the Binary Friction Conductivity Model (BFCM), is developed. Available experimental conductivity data measured using the AC impedance method is translated to give conductivity as a function of the number of water sorbed per sulfonate head using curve fits to sorption isotherm data. The unknown parameters are then fit so that the results of the BFCM lay within the expected range of conductivity values at 30°C. Whenever possible, values obtained in literature are used to corroborate the magnitude of unknown parameters. The diffusion coefficients are then assumed to all have the same temperature dependence and are adjusted to fit to experimental data at 70°C. The diffusion coefficients are assumed to have Arrhenius-type temperature dependence. Activation energy is calculated using the reference diffusion coefficients found at 30°C and 70°C. The temperature dependence is found to be reasonable by comparison of our predicted conductivity to data at 40°C. The conductivity model is compared to two other models and found to provide a more reasonable fit over the entire range of water contents. The BFCM is also implemented with slightly modified parameters to show its ability to predict conductivity of membranes within the family of perfluorosulfonic acid membranes. One advantage of the BFCM model and the associated transport model is that by fitting the BFCM to conductivity data we are able to gain insight into all the transport parameters, which could be used to predict water transport through the membrane.

Examiners:

_____

Dr. N. Djilali, Supervisor (Department of Mechanical Engineering)

_____

Dr. H. Struchtrup, Supervisor (Department of Mechanical Engineering)

_____

Dr. D. Harrington, Outside Member (Department of Chemistry)

_____

Dr. B. Wetton, External Examiner (Mathematics Department, UBC)

Table of Contents

List of Figures

List of Tables

Nomenclature

A	Cross-sectional area	m^2
A_1, A_2	Model fitting parameters	1
a	Activity of species i	1
B_0	Permeability	m^2
B_Φ	Electrokinetic permeability	m^2
B_H	Hydraulic permeability	m^2
c	Molar density	$mol\ m^{-3}$
$\mathcal{D}_i$	Diffusion coefficient (Nernst-Planck equation)	$m^2\ s^{-1}$
$\mathcal{D}_{O2}$	Diffusion coefficient for oxygen	$m^2\ s^{-1}$
D_{ij}^e	Effective concentration diffusion coefficient	$m^2\ s^{-1}$
D_{ij}^{S-M}	Stefan-Maxwell diffusion coefficient	$m^2\ s^{-1}$
D_{iK}^e	Effective Knudsen diffusion coefficient	$m^2\ s^{-1}$
D_{iM}^e	Membrane diffusion coefficient	$m^2\ s^{-1}$
D_σ	Proton mobility	$m^2\ s^{-1}$
D_{H2O}	Water mobility	$m^2\ s^{-1}$
E_a	Activation energy	$J\ mol^{-1}$
E_η	Activation energy for viscosity of water	$J\ mol^{-1}$
EW	Equivalent weight	$g\ mol^{-1}$
$\mathbf{F}$	External body force per mole	$N\ mol^{-1}$
f	Friction coefficient	1
g	Molar specific Gibb's free energy	$J\ mol^{-1}$
ΔH^0	Enthalpy change for proton solvation	$J\ mol^{-1}$
IEC	Ion exchange capacity	$mol\ g^{-1}$
i	Current density	$A\ m^2$
J	Molar flux in GDL	$mol\ m^{-2}\ s^{-1}$
K	Equilibrium Constant	1
$K_{A,C}$	Equilibrium constant for proton solvation in terms of concentration	1
k_ϕ	Electrokinetic permeability (Nernst-Planck equation)	m^2
k_p	Hydraulic permeability (Nernst-Planck equation)	m^2
L	Pore length	m
L_M	Membrane thickness	m
l	Distance between reference electrodes	m
$\mathbf{N}, N$	Molar flux relative to fixed reference frame	$mol\ m^{-2}\ s^{-1}$
M	Molar mass	$kg\ m^{-3}$
N_i^{N-P}	Molar flux (Nernst-Planck equation)	$mol\ m^{-2}\ s^{-1}$
n	Molecular density (DGM equations)	$molecules\ m^{-3}$
or		
n	Number of moles of a species (within our counting section)	1
n_{drag}	Electro-osmotic drag coefficient	1
p	Pressure	Pa
q	Bruggeman exponent	1

R_{mem}	Measured membrane resistance	Ω
R_{ij}	Resistance between species i and j	m^2 s mol^{-1}
r_{iM}	Resistance between species i and the membrane	m^2 s mol^{-1}
r	Pore radius	m
r_p	Average pore radius	m
S	Pore specific surface area	m^{-1}
s	Diffusion coefficient exponent	1
s	Molar specific entropy	J mol^{-1} K^{-1}
SA	Surface area of pore	m^2
SE	Standard error	1
T	Temperature	K
T_{cell}	Cell temperature (Springer's model)	°C
u	Molar specific internal energy	J mol^{-1}
$\mathbf{u}$	Molar average velocity	m s^{-1}
$\overline{V}$	Partial molar volume	m^3 mol^{-1}
V_M	Molar volume	m^3 mol^{-1}
V	Volume	m^3
$\mathbf{v}$	Convective velocity	m s^{-1}
$\mathbf{v}_i$	Average velocity of species i	m s^{-1}
$\hat{v}$	Non-dimensional molar volume	1
v_S	Solvent velocity from Schloegl equation	m s^{-1}
v_{pw}	Pore water velocity	m s^{-1}
X	Mole fraction	1
x	Relative humidity	1
z	Charge number	1

Greek

α	Degree of dissociation of acidic heads	1
β	Dimensionless parameter	1
γ	Number of waters fixed to sulfonate head (not participating in transport)	1
γ_i	Activity coefficient for species i	1
$\overline{\gamma}$	Water transfer coefficient	1
δ	Ratio of mutual to membrane effective diffusion coefficients	1
ε	Porosity	1
ε_0	Threshold porosity	1
η	Viscosity	kg m^{-1} s^{-1}
Θ	Dimensionless parameter	1
θ	Contact angle	1
κ	Membrane spring constant	1
λ	Number of waters sorbed per acid head	1
λ_i^C	Number of fixed species i molecules per sulfonate head	1
$\lambda_{i,M}$	Empirical solvation parameter for species i	1
λ_i^0	Equivalent conductance for species i at infinite dilution	S m^2 mol^{-1}
μ	Chemical potential	J mol^{-1}

μ^e	Electrochemical potential	J mol^{-1}
$\mu_{i,\alpha}$	Chemical potential of species i in phase α	J mol^{-1}
ν	Number of chemical equilibrium steps for a reaction	1
$\nu_{\rho i}$	Stoichiometric coefficient of component i in reaction ρ	1
Π_σ	Capillary pressure difference	Pa
Π_M	Pressure difference due to elasticity of membrane	Pa
ρ	Mass concentration	kg m^{-3}
ρ_{dry}	Dry membrane density	kg m^{-3}
σ	Conductivity	S m^{-1}
σ_w	Surface tension of water	N m^{-1}
τ	Tortuosity factor	1
Φ	Potential	V
ϕ	Volume fraction	1
ω_{pw}	Number of waters within hydrated proton complex	1

Constants

R	Universal gas constant	8.314 J mol^{-1} K^{-1}
F	Faraday's constant	96485 C mol^{-1}
ξ	Fixed charge density	1200 mol m^{-3}
k_B	Boltzmann's constant	1.3807×10^{-23} J K^{-1}

Subscripts

A	Reaction A
a	Anode
c	Cathode
$diff$	Diffusive
F	Phase external to the membrane
f	Fixed species in membrane
fw	Fixed waters
i	Species I
K	Knudsen
L	liquid
M	Membrane or a phase within the membrane
min	Minimum
p	Pore
pw	Waters in protonated complex
ref	Reference quantity
sat	Corresponding to saturated vapor conditions
sh	Sulfonate heads
t	Total
V	Vapor
$visc$	Viscous
W	Total sorbed waters
w	Water
α	Phase α

xiv

ρ	Reaction number ρ
1	Protonated complex (typically hydronium ion)
2	Waters participating in transport

Superscripts

a	anode
C	Fixed waters
c	cathode
diff	Diffusive
e	effective
m	Per unit mass
o	Standard state
visc	Viscous
*	Equilibrium value
'	Pore averaged flux per unit pore area

Abbreviations

BPS	Berg, P., K. Promislow, J. St-Pierre, J. Stumper and B. Wetton. [40]
BV	Verbrugge, M., and D. Bernardi. [47][48]
CD	Choi, P. and R. Datta. [30]
GH	Gierke, T. D. and W. Y. Hsu. [24][25]
SES	Sone, Y., P. Ekdunge and D. Simonsson. [29]
SZG	Springer, T. E., T. A. Zawodzinski and S. Gottesfeld. [39]
TMT	Thampan, T., Malhotra, S., Tang, H. and R. Datta. [41]
WN	Weber, A. Z. and J. Newman. [3][66]
YS	Yeager, H. L. and A. Steck [27]
ZDV	Zawodzinski, T. A., Davey, J., Valerio, J. and S. Gottesfeld. [38]
ZSD	Zawodzinski, T. A, Springer, T. E., Davey, J., Jestel, R., Lopez, C., Valerio, J. and S. Gottesfeld [14]

Acknowledgements

I would like to thank my supervisors; Dr. Henning Struchtrup and Dr. Ned Djilali. This dynamic duo provided me with a broad base of experience to draw on when investigating a topic that covers so many disciplines. I would like to thank them both for maiking themselves available for lengthy discussions, despite their busy schedules. I would also like to thank them for all the excellent advice throughout the entire process, which has made my experience as a graduate student significantly more relaxed than I anticipated.

I would like to thank my fiancée, Jen Zacharias, for being supportive and understanding, helping me to keep things in perspective, and always being there for me, no matter what. I would also like and my family (Doris, Elroy and my sister Jenn) and friends for being such a strong support group and also helping to keep things in perspective - apparently there is a world outside of school, who knew?

I would also like to thank everyone from IESVic, including Ms. Susan Walton, for their advice, insight and support.

1 Introduction

Polymer electrolyte membrane fuel cells (PEMFCs) are a power source that can be used to supply energy in a wide range of power applications, from the sub-Watt to Megawatt scale. PEMFCs use a solid polymer electrolyte, typically a perfluorosulfonic acid (PFSA) membrane as opposed to a liquid electrolyte or solid electrolyte, to electrically and mechanically isolate the anode and cathode while allowing for ion migration [1][2]. Nafion, manufactured by DuPont, is one of the most thoroughly used and studied membranes [1][3]. Another family of membranes that holds some promise for use in PEMFCs are sulfonated polyaromatic membranes, typically sulfonated polyetherketones. There is also research being performed into other types of membranes and hybrid membranes that might have even better suited properties, unfortunately information on these membranes is scarce [4][5][6][7][8][9][10].

There is a strong desire to develop transport models for the membrane that can be included in computational models of fuel cells. It is the hope of many that such computational models will be able to provide valuable insight into the phenomena occurring within a fuel cell and save valuable time in the design and optimization of existing and new fuel cell architectures. Obviously, better models for transport in the membrane will provide better insight, and prove to be more useful.

It is the need to better understand the phenomena that are occurring within the membrane and the desire to improve the way in which transport in membranes is modeled that is the impetus for the work contained herein. Part 1 (Chapters 2 – 8) of this work contains a thorough literature review, performed with an eye to unifying the works of many authors into a comprehensive understanding of the microstructure [1], and in fact nanostructure, of the membrane, and its effect on the transport phenomena. Part 2 (Chapters 9-17) of this work uses the insight gleaned through the literature review to guide in the development of an improved transport model for the membrane that addresses several limitations in previous models:

- Use of equations based on physics rather than purely empirical curve fits, thus allowing one model to be used to describe behaviour in numerous membranes, using physically significant parameters determined for each membrane.

- The binary friction model can be used instead of the dusty fluid model, thus eliminating the additional viscous terms.

- The restriction to equimolar counter diffusion can be removed.

- The effect of temperature on the sorption isotherm can be accounted for.

The objective of Part 1 is to present a comprehensive overview of the microstructural aspects of PEMs and highlight the various approaches taken in attempting to model the observed behavior. We shall look at all phenomena that occur in the membrane, including Schroeder's Paradox and the mechanisms of proton transport, and attempt to provide a unified view of the transport phenomena in PEMs. In addition we will discuss some of the classical and recently proposed models and identify their novel contributions.

Part 1: Literature Review

2 Membrane Families

Proton conductivity across PEMs is possible due to the presence of carboxylic or sulfonated acid groups with a cation exchange counterion. The counterion dissociates and eventually becomes mobile as the membrane swells [11]. Membranes for use in fuel cells should exhibit three key properties:

1. high conductivity; conductance can be increased by decreasing the membrane thickness, increasing the water content, and/or increasing the ion exchange capacity;

2. good stability, both mechanical and chemical, within the operating environment of the fuel cell;

3. high permselectivity for non-ionised molecules to limit crossover of reactants; permselectivity is decreased as swelling increases [11].

We note that the ion exchange capacity (*IEC*) is the inverse of the equivalent weight (*EW*), defined as

$$(2.1) \quad EW = \frac{\text{weight of dry polymer sample in grams}}{\text{number of moles of acid groups}}.$$

Sulfonated fluoropolymers exhibit these desired properties and are thus widely used in fuel cells. Investigation into the use of sulfonated polyetherketone membranes, as well as other membranes such as Flemion and Aciplex, is being driven by the demand for membranes that exhibit better characteristics than those currently used:

1. It is desirable to increase the operation temperature above 100°C to reduce catalyst poisoning that occurs if CO is present [11]. Perfluorinated membranes cannot be used in this regime due to degradation of their mechanical properties, and due to the fact that almost all the water present in the membrane will have evaporated resulting in poor conductivity [12].

2. In attempts to reduce the cost of fuel cell stacks, it is highly desirable to mitigate the cost of the membrane - perfluorinated membrane costs can approach 600 \$ m^{-2} [1][11].

3. It is also desirable to switch to membranes that are not fluorinated due to environmental considerations [11].

2.1 Sulfonated Fluoropolymers

Sulfonated fluoropolymers (also referred to as perfluorinated ion exchange membranes or perfluorosulfonic acid membranes (PFSAs)) are commonly used in fuel cells, the best known membrane of this type being the Nafion family of membranes produced by DuPont [2]. Because of its commercial availability, stability in the environment of the fuel cell, and mechanical strength, Nafion has become the most widely used and studied PEM [1]. The sulfonated fluoropolymer membranes (including the Nafion family of membranes) start with a polytetrafluoroethylene (PTFE) backbone that is sulfonated. In the sulfonation process, a side chain ending in a sulfonic acid group ($-SO_3H$) is added to the PTFE backbone. The resulting macromolecule of Nafion, shown in Figure 1 below, is both hydrophobic and hydrophilic.

$$-(CF_2\text{-}CF_2)_X\text{-}(CF\text{-}CF_2)_Y\text{-}$$

$$(X=6\text{-}10)$$
$$(Y,Z=1)$$
$$O(CF_2\text{-}CF)_Z\text{-}O\text{-}(CF_2)_2SO_3H$$

$$CF_3$$
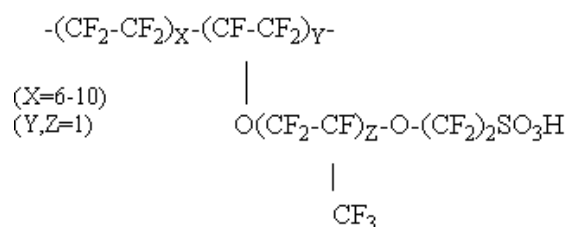
Figure 1: Chemical Structure of Nafion Perfluorosulfonic Acid Ionomer Membrane, after [11].

The polytetrafluoroethylene backbone, which is essentially Teflon, is hydrophobic and thus tends to minimize its interaction with water. The sulfonate head, however, is hydrophilic and thus has a strong affinity for water [13]. It is generally agreed that a hydrated fluoropolymer membrane forms a bi-phasic system, one phase containing water and the dissociated ions, the other made up of the polymer matrix [3][12][11]. Since all sulfonated fluoropolymers have a hydrophobic backbone and hydrophilic sulfonate head groups on a side chain, they all form two-phase systems when hydrated.

Altering the length of the chains, and location of the side chain on the backbone, makes the different variants comprising the family of membranes.

The family of sulfonated fluoropolymers includes Dow chemical membranes (Figure 2) and Membrane C (Chlorine Engineers, Japan). Membrane C is an ionomer with an equivalent weight (*EW*) of 900, with the same side chain as Nafion [14]. The Dow family of membranes has shorter side chains than the Nafion family [15].

$$(CF_2\text{-}CF_2)_X\text{-}(CF\text{-}CF_2)_Y\text{-}$$

(X=3-10)
(Y=1) $O(CF_2)_2SO_3H$
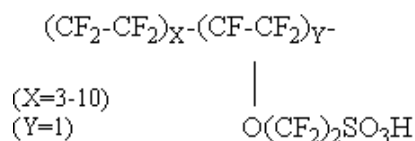
Figure 2: Chemical Structure of Dow Ionomer Membrane, after [11].

Within the family of Nafion, a number - such as 117 - differentiates the various types of Nafion. The first two digits refer to the equivalent weight of the membrane, e.g. Nafion 117 has an equivalent weight of 1100 g/mol. The last digit refers to the thickness of the membrane in mil (1 mil = 0.001 inch = 2.54×10^{-3} cm), e.g. Nafion 117 has a thickness of 7 mil. The equivalent weight of the membrane is varied by changing the length of the backbone, i.e. the value of x, as depicted in Fig. 1.

The Flemion (Asahi Glass) and Aciplex (Asahi Chemical) membranes, also members of the perfluorinated membrane family, have also been investigated for use in PEMFCs [16][17]. Both the Aciplex and the Flemion membranes have a bi-layer structure that is comprised of sulfonic acid functional groups on the anode side and carboxylic acid functional groups on the cathode side [16][3]. Flemion and Aciplex membranes can be made thinner, while still providing the same acid activity and thus have a higher cation exchange capacity, and therefore a better conductivity [3]. Information on Flemion and Aciplex membranes can be found in the papers of Yoshida et al. [16] and Du et al. [17].

2.2 Sulfonated Polyetherketone Membranes

Sulfonated polyetherketones (also referred to as sulfonated polyaromatic) membranes are being investigated for use in PEMFCs [13][1]. Sulfonated polyetherketone membranes consist of a polyetherketone (i.e. PEK, PEEKK and PEEK) backbone that has a sulfonic acid functional group attached to it (see Figure 3 below). Once again, the backbone is hydrophobic and the sulfonate head is hydrophilic, however, the backbone is less

hydrophobic than the PTFE backbone and the sulfonic acid group is less acidic and therefore less hydrophilic [13]. The polyetherketone backbone is less flexible than the PTFE backbone of the sulfonated fluoropolymer family of membranes [13]. As a result of the differences between the two membranes, the sulfonated polyetherketone membranes are not separated into a two-phase system as well as the sulfonated fluoropolymer family of membranes [13]. The advantage of the polyaromatic membranes is that they are easier to manufacture than the sulfonated fluoropolymer membranes, and as a result are significantly cheaper [18].
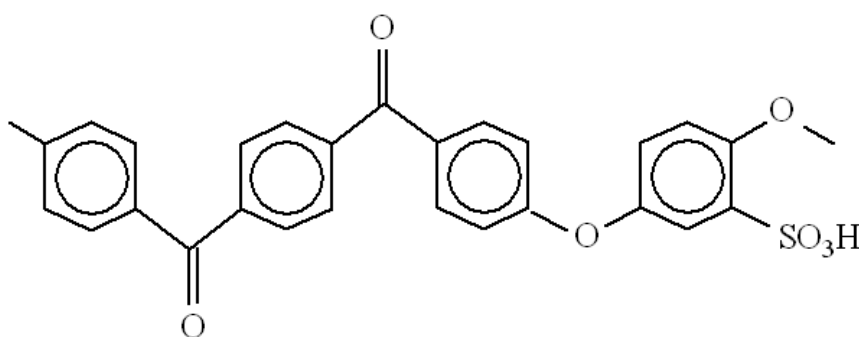
Figure 3: Chemical Structure of Sulfonated Polyetherketone, after [13].

2.3 Other Membranes

In addition to the sulfonated polyetherketone and sulfonated fluoropolymer membranes there are several other types of membranes being investigated for use in fuel cells. This includes the DAIS membranes based on sulfonated styrene-(ethylene-butylene)-styrene triblock copolymers [1][19], Ballard Advanced Materials (BAM) membranes based on α,α,β-trifluorostyrene [1][19][20], perfluorinated sulfonamides [1][21], radiation-grafted membranes [1][20], polybenzimidazole membranes [20][22] and sulfonated polyimides [20]. Unlike Nafion and sulfonated polyetherketone membranes, information on the use of these membranes in fuel cells, as well as their properties, is scarce and these membranes will not be considered further.

3 Hydrated Membrane Morphology

3.1 Sulfonated Fluoropolymer Membrane Morphology

3.1.1 Nafion

There is a general consensus that the hydrated membrane forms a two-phase system consisting of a water-ion phase distributed throughout a partially crystallized perfluorinated matrix phase [11][3][12]. The crystallized portion of the membrane cross-links the polymer chains, preventing complete dissolution of the polymer at temperatures below which the crystalline portion of the polymer network is affected [11]. The glass transition temperature of Nafion is reported to be approximately 405K [12].

There are two widely cited models to explain the resulting morphology of the hydrated Nafion membrane, the cluster network model by Gierke, Hsu et al. (hereafter referred to as GH) [23][24][25][26], and the model of Yeager and Steck (hereafter referred to as YS) [27].

GH developed the cluster network model of the Nafion membrane morphology according to which the ion exchange sites form clusters within the membrane. This model is supported by evidence developed from numerous experimental techniques, including small angle X-ray experiments, X-ray experiments, electron microscopy, NMR, and IR [24]. Using transmission electron micrographs of ultra-microtomed Nafion sections, GH were able to show that the clusters are approximately spherical [24].

As the membrane is hydrated, the sorbed water molecules are attracted to the hydrophilic sulfonate heads, which aggregate into clusters. As more water is sorbed, the clusters grow, and eventually short narrow channels form and connect the clusters [24][25]. The polymeric charges are located close to the cluster surface, at the phase interface between the liquid and polymer phases [24].

Figure 4 shows the proposed morphology of the membrane. The spherical clusters are determined to be approximately 4 nm in diameter [3], or 3-5 nm according to Ref. [24],

when the membrane is fully hydrated. The channels, which connect the clusters, are determined to have a maximum diameter of approximately 1 nm [3].
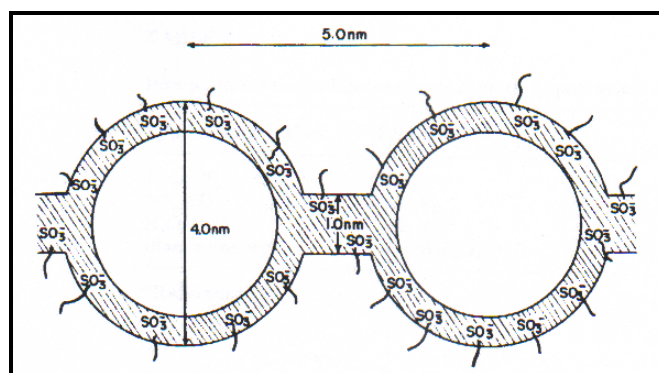
Figure 4: Cluster-network model for Nafion Membranes. The polymeric ions and absorbed electrolyte phase separate from the fluorocarbon backbone into approximately spherical clusters connected by short narrow channels [24].

The second model to explain the morphology of hydrated Nafion is that proposed by YS [27] who claim that the ionic clusters are not spherical. YS identify three regions that comprise the membrane morphology. Region A is the fluorocarbon phase, made up of the hydrophobic backbone where it is energetically unfavorable for water to be. Region C is comprised of the ionic clusters; it also incorporates the sulfonate heads. Region B is an interfacial region between region A and C and contains fewer sorbed waters, sulfonate heads that have not been incorporated into the clusters, and a portion of the counterions [27].

Figure 5A is a schematic of the morphology described by YS. Figure 5B is a schematic of the morphology of Nafion discussed by Kreuer et al. in several of their papers [13][28]. They do not specifically state whether their morphology is consistent with YS's or GH's models; however, their schematic model is more in line with YS's, since it is not as simplified as the model of GH. Essentially regions B and C combined form the water-ion phase. The interfacial region, region B, comes about because there are certain areas where the density of sulfonate heads is lower. In this region, the sulfonate heads cannot cluster together, while the hydrophilic sulfonate heads will still attract waters and dissociate.
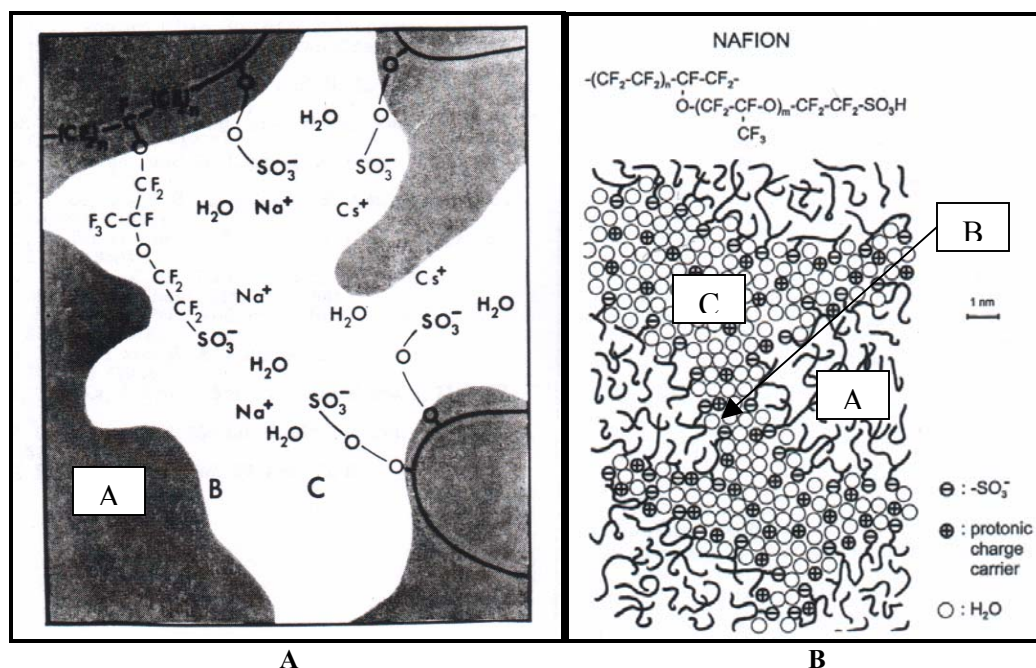
Figure 5: A) Three region structural model for Nafion [27], B) Schematic representation of microstructure of Nafion [13].

Weber and Newman in Ref. [3] (hereafter referred to as WN) consider the model of GH to be an idealization of the model of YS. The ideas of WN provide the best insight into the structure of the membrane, allowing us to unify our view of the morphology of the membrane. Within the membrane, ionic clusters form where there is a high density of sulfonate heads. These clusters are approximately spherical in shape. The interfacial regions introduced by YS are what GH consider to be the channels that connect the ionic clusters [3].

We can consider the interfacial region as collapsed channels that can fill with water to form a liquid channel, but note that even in their collapsed form they allow for conductivity, since sorbed waters can dissociate from the sulfonate heads located in the collapsed channels - however, not enough water is sorbed to form a continuous liquid pathway [3]. The collapsed channels form in membrane regions with lower sulfonate head concentrations. Figure 6 and 7 below show how the morphology can be described in terms of collapsed channels with ionic clusters.
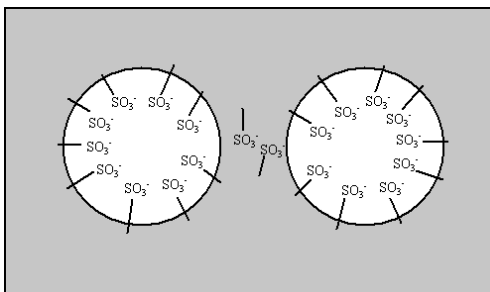
Figure 6: Schematic of membrane showing the collapsed interconnecting channel, after [3].
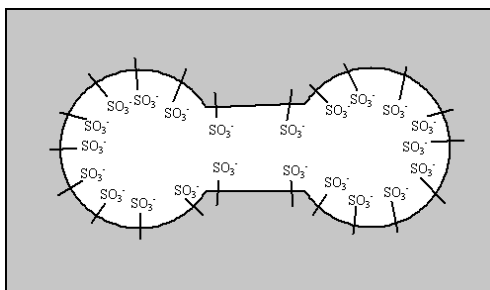
Figure 7: Schematic of a membrane showing the interconnecting channel swollen, after [3].

3.1.2 Other Membranes

Compared to Nafion, relatively little is known about the morphology of the other membranes; however, we still do have some insight into their microstructure.

The Dow family of membranes has a structure similar to Nafion except with a shorter side chain. As a result of the shorter side chain WN predict that the clusters formed within the Dow membranes will be smaller due to the higher elastic deformation energy [3].

The formation of smaller clusters will mean that there will be a higher volume of interconnecting channels than for Nafion, and thus higher water content for a liquid-equilibrated membrane [3]. This would occur because the interconnecting channels are what are assumed to swell to allow for the additional uptake from liquid water than from water vapor. In addition, for membranes with the same type of sulfonic acid sites, and the same number of sites, the uptake from vapor should be less for Dow's membranes than for Nafion due to the smaller clusters formed [3].

WN also considered Flemion and Aciplex. They predict a microstructure with clusters that are closer together and also predict that the network is more hydrophilic and also better interlinked [3]. WN verify these results by evaluating trends in experimental data.

3.2 Sulfonated Polyetherketone Membranes

It has already been established that the backbone of the sulfonated polyetherketone membranes is stiffer than that of Nafion, and that the sulfonate heads are less hydrophilic and the backbone less hydrophobic than Nafion. Because the hydrophobic/hydrophilic difference is smaller than for Nafion and the backbone is stiffer, the separation into two domains, one hydrophobic and one hydrophilic, is not as well defined as in Nafion [13]. The structure of the sulfonated polyetherketone membranes is, as a result, one with narrower channels and the clusters are not as well connected as in Nafion [13][3]. Figure 8 below is a schematic of the microstructure of Nafion and a sulfonated polyetherketone membrane illustrating the less pronounced phase separation.
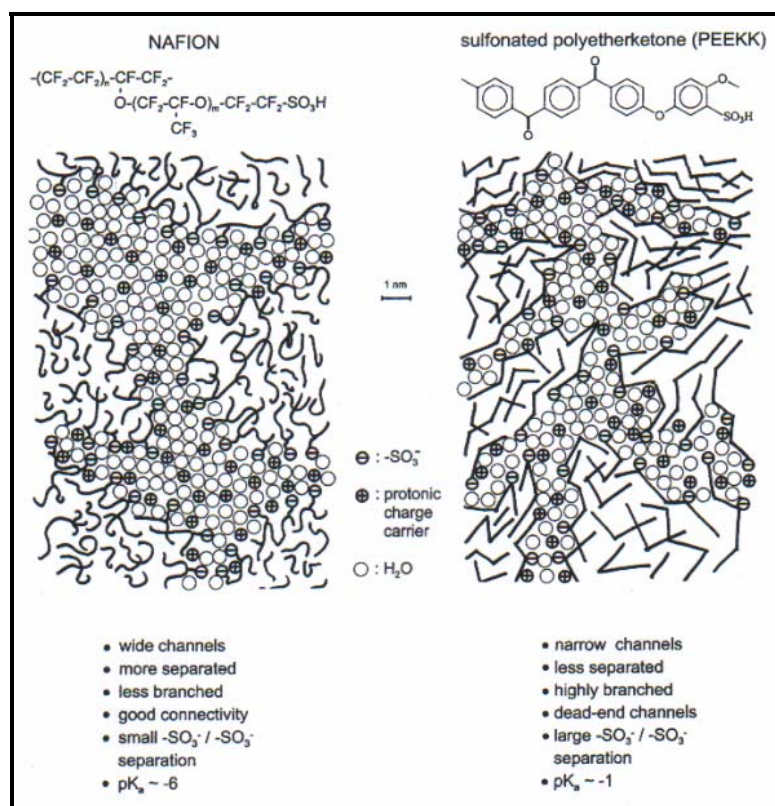
Figure 8: Schematic representation of the microstructure of Nafion and a sulfonated polyetherketone membrane illustrating the less pronounced hydrophilic/hydrophobic separation of the latter compared to the former [13].

4 Overview of Transport Parameters

When considering transport within the membrane, we are interested in determining the conductivity of the membrane, which tells us how easily protons travel through the membrane, and in finding how much water is transported through the membrane. Since we would like to produce as much power from our fuel cell as possible we would like to operate our fuel cell in regimes where the conductivity is high (resistance is low). Therefore, the conductivity is a key parameter, since it tells us how much resistance is provided to the flow of protons through the membrane.

Modeling of water transport through the membrane is important, because the conductivity of the membrane depends highly on the water content within the membrane: if part of the membrane dries out, the conductivity will drop significantly. Also, the accumulation of too much water in certain areas of the fuel cell can lead to flooding of the fuel cell. When this occurs, the performance of the fuel cell is extremely degraded as liquid blocks the passage of gases in the gas diffusion layers and flow channels. The water content in the membrane is not only dictated by the water transport within the membrane but also by the amount of water sorbed by the membrane from the surrounding solvent.

The discussion in the following chapters will focus first on the membrane hydration and the sorption mechanisms within the membrane. We then introduce the concept of sorption isotherms, which relate the amount of water sorbed by a membrane equilibrated with an external solvent (vapor or liquid) to the activity of that solvent. Once we have developed the picture of how the solvent interacts with the polymer membranes, we look at the transport mechanisms occurring within "bulk" solvent, in particular we study how these are coupled, and how they change for transport within a membrane. Finally, we discuss the various models that have been introduced to describe the physical phenomena occurring.

5 Membrane Hydration

In order to understand the transport and swelling behavior of a PFSA membrane, we must first look at what happens as the membrane sorbs water molecules. The sorption of water

by Nafion membranes has been studied extensively, while, unfortunately, other membranes have not been studied in such great detail. Thus results presented in this section are for the Nafion family of membranes only. However, it is anticipated that due to similarities between all the membranes, similar trends to those found for Nafion can be found in other membranes.

When considering the water sorption behavior of PEMs it is common to consider the number of sorbed waters per sulfonate head (λ = # sorbed waters/# sulfonate heads), see Eqn. (2.1). We first consider the behavior of Nafion for λ in the range from one to two. Note that the anhydrous form ($\lambda = 0$) of the membrane is not common, since removing all the water requires raising the temperature of the membrane to a point where decomposition of the membrane begins to occur. As a result, approximately one and a half waters per sulfonate head remain in a membrane that is not in contact with any water vapor or liquid water [12]. The first waters sorbed by the membrane cause the sulfonate heads to dissociate, resulting in the formation of hydronium ions as indicated by Fourier transform-infrared spectroscopy (FT-IR) data [12]. The water that hydrates the membrane forms counter-ion clusters localized on sulfonate sites with the sulfonate heads acting as nucleation sites [12].

Due to the hydrophobic nature of the backbone, and the hydrophilic nature of the sulfonate heads, it is very reasonable to consider all water molecules sorbed by the membrane at this low water content as being associated with the sulfonate heads. Moreover, the hydronium ions will be localized on the sulfonate heads, and since not enough water has been sorbed for the formation of a continuous water phase, the conductivity will be extremely low. Figure 9, below, is a schematic of what occurs within a membrane for λ in the range between one and two. The separation of sulfonate groups and size of molecules is taken from rough approximations of sizes presented by Laporta, Pegoraro and Zanderighi [12] in order to have approximately the right proportions for the description. Note also that the distance between sulfonate heads will be somewhat less in an actual membrane as sulfonate heads cluster together, thus some transport is possible at lower water contents ($\lambda \sim 2$).
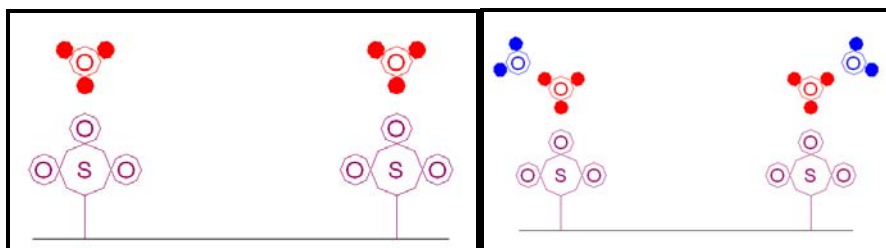
Figure 9: Schematic hydration diagram for Nafion for λ=1 and λ=2. Hydronium ions are shown in red, molecules forming the primary hydration shell are shown in blue and sulfonate heads in purple.
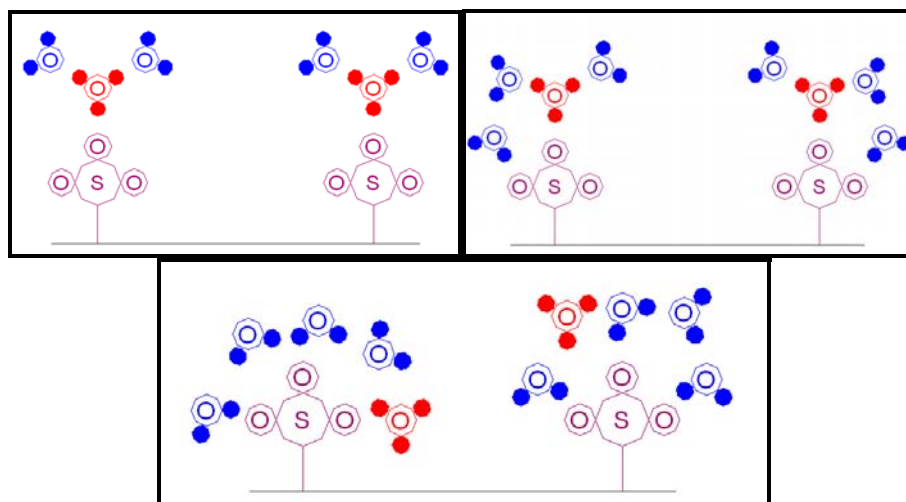
Figure 10: Schematic hydration diagram for Nafion for water contents of λ = 3 – 5. Hydronium ions are shown in red, molecules forming the primary hydration shell are shown in blue and sulfonate heads in purple.
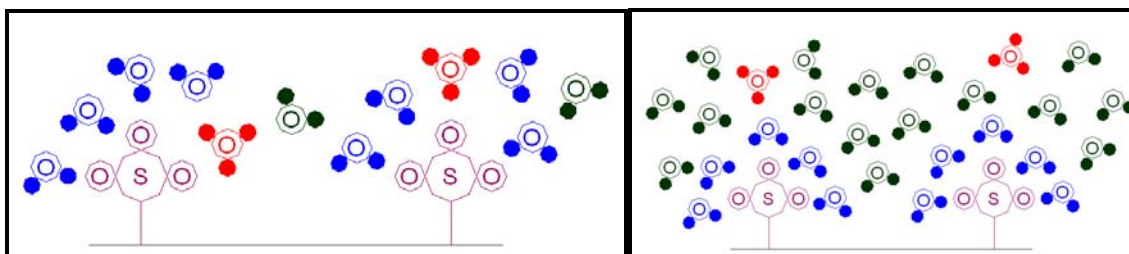
Figure 11: Hydration schematic for Nafion for λ = 6 and λ = 14. Hydronium ions are shown in red, molecules forming the primary hydration shell are shown in blue, "free" waters are shown in green and sulfonate heads in purple.

We next consider what happens as the relative humidity of the external solvent is increased, and λ lies in the range of three to five. When λ is in the range of one to two, the hydrogen bonds are approximately 80% the strength of those in pure water, but as more water is added to counter-ion clusters, the hydrogen bonds are weaker since the

cluster shape does not allow for the formation of stronger bonds [12]. In this range, the counter-ion clusters continue to grow while the excess charge (proton) becomes mobile over the entire cluster, as indicated by the disappearance of the bending band of hydronium and the appearance of the water bending band in FT-IR data [12].

Infrared spectra data has shown that for water contents in this range the proton is highly mobile within the counter-ion clusters [12]. For λ of approximately or greater than two, the membrane will conduct some charge as the excess protons are delocalized on the counter-ion clusters and some pathways may be formed through the membrane to allow for conductivity. Figure 12 shows conductivity measurements for Nafion as function of λ; note that the membrane exhibits low conductivity below a λ value of five. As λ approaches five the membrane becomes slightly conductive as some counter-ion clusters may be connected while there is still not enough water present for all clusters to coalesce [12]. It should also be noted that λ of five is considered a threshold value below which the conductivity begins to drops significantly [12][14].
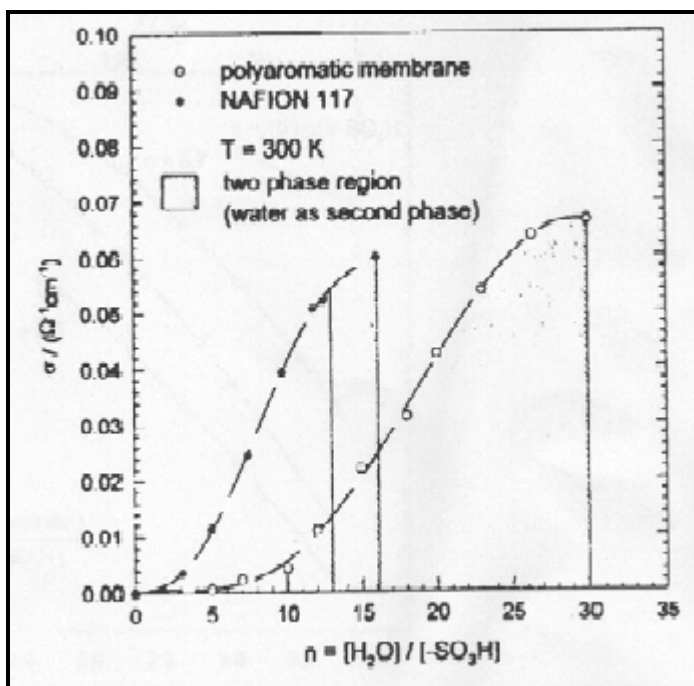
Figure 12: Room temperature proton conductivity of Nafion and a sulfonated polyaromatic membrane as a function of water content [18].

Figure 13 shows the conductivity data of Sone, Ekdunge and Simonsson (hereafter referred to as SES) for Nafion in the expanded form[1]. Note that when the relative humidity drops from approximately 60% (corresponding to circa five water per sulfonate head) to approximately 13% (corresponding to circa two waters per sulfonate head) the conductivity drops approximately two orders of magnitude. So in the range of two to five waters per sulfonate head there is a two order of magnitude conductivity change, while in the range of water contents between five and fourteen waters per sulfonate head (corresponding to relative humidity in the range of 60% to 100%) there is only a one order of magnitude variation. The extreme variation in conductivity in the range of λ from two to five indicates how significant an effect the formation of a continuous phase has on the conductivity of the membrane.
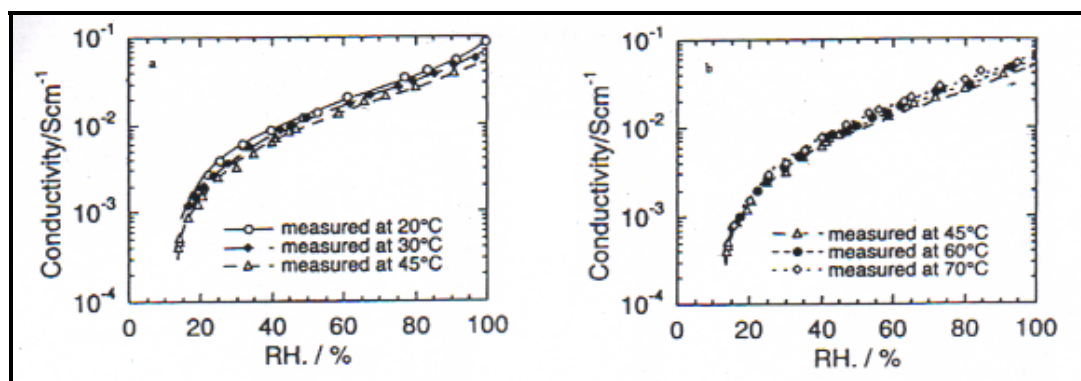
Figure 13: Conductivity dependence on temperature and relative humidity for the E-form of Nafion [29].

Figure 10 shows schematics for the water content in the range of three to five waters per sulfonate head. The number of water molecules forming the primary hydration shell for Nafion is expected to lie in the range of four to six [30]. Molecular dynamics simulations of Nafion indicated that five waters form the primary hydration shell for the sulfonate head, and any additional waters are not as strongly bound and thus form a free phase [31][32]. Choi and Datta (hereafter referred to as CD) have assumed that five waters form the primary hydration shell [30].

---

[1] The E (expanded) form of Nafion has not been subjected to any heat treatment. The N (normal) form and the S (shrunken) form are heat treated at 80˚C and 105˚C respectively. The N form has some of the micropores joined and some closed compared to the E form and the S form has even more pores closed compared to the E form [29]

We next consider λ values greater than or equal to six. In this range, counter-ion clusters coalesce to form larger clusters, and eventually a continuous phase is formed with properties that approach those of bulk water [12]. This is supported by measurements, which show that water mobility, and water self-diffusion values approach the bulk water values [33]; the mobility of protonic charge carriers approaches the value in bulk water as well [13]. The free water phase is screened (or shielded) from the sulfonate heads by the strongly bound water molecules of the primary hydration shell [13][30].

Figure 11 gives a schematic representation of the hydration state for λ equal to six (near the conductivity threshold) and fourteen (saturated vapor equilibrated).

Although this hydration scheme is developed specifically for Nafion, we can see that it can describe conduction in other membranes. However, the number of waters in the primary hydration shell will vary according to the charge on the head group, and the distance between sulfonate heads will affect the conductivity threshold, which will vary with the amount of water needed to connect the clusters. These are just a few of the ways in which the description may vary for different membranes, however, it is assumed that similar phenomena will occur in all PFSAs as they are hydrated, due to similarities in the morphology of the membranes.

6 Sorption Isotherms

6.1 Schroeder's Paradox

The so-called Schroeder's Paradox refers to an observed difference in the amount of water sorbed by a liquid-equilibrated membrane and a saturated vapor-equilibrated membrane, with both reservoirs at the same temperature and pressure [3][14][34]. Figure 14 shows sorption isotherms for Nafion and a sulfonated polyaromatic membrane. Note that both of these membranes exhibit the difference in water uptake characteristics of Schroeder's Paradox.

Several explanations for the observed difference in water uptake have been proposed. Some of these suggest experimental error such as difficulty in attaining truly unit vapor phase activity, temperature fluctuations or not allowing enough time for equilibration [34]. These possibilities have, however, been ruled out [34]. When a water-equilibrated membrane was placed in a situation where it was allowed to equilibrate with saturated vapor at the same conditions (*T* and *p*) the water content of the membrane dropped, thus there is no support for the argument of insufficient equilibration time [34]. Experimental error explanations have also been ruled out since the membranes do not exhibit Schroeder's paradox for all polymer/solvent combinations [34].
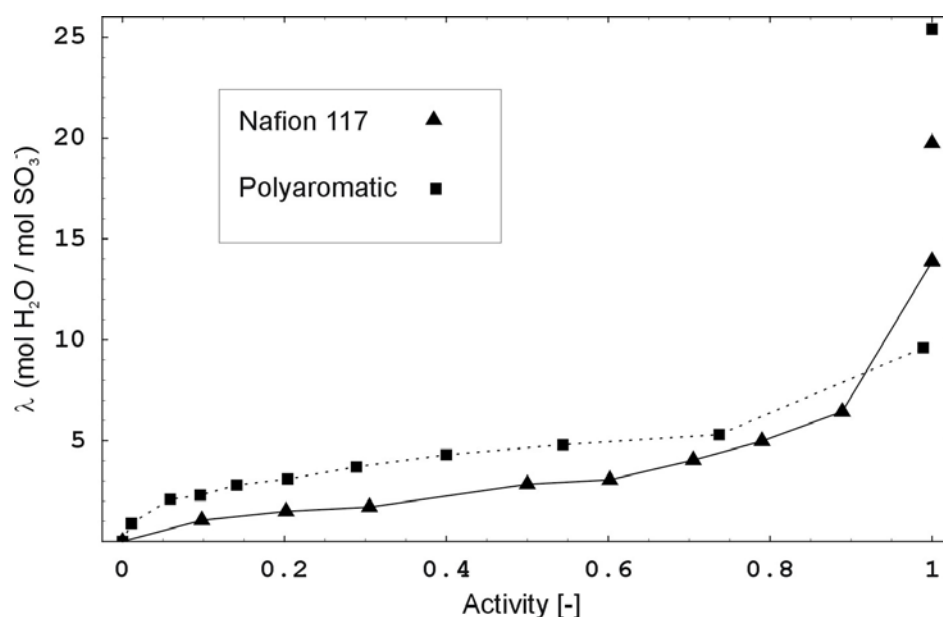
Figure 14: Water sorption isotherm for Nafion 117 and a sulfonated polyaromatic membrane at 300K, after [18].

Possibly the best explanation of Schroeder's paradox is that proposed by CD [30], who present a physicochemical model for water sorption which stands in accordance with the hydration scheme presented in the previous section. CD assume that water molecules sorbed by the membrane are either strongly (chemically) bound to the sulfonate heads or are 'free' waters, which are free to physically equilibrate with the external solvent [30]. The number of chemically bound waters is determined by chemical equilibrium [30]

(6.1) $\sum_{i=1}^{n} v_{\rho i}\mu_i = 0 \ \left(\rho = 1,2,\ldots,q\right),$

where $v_{\rho i}$ is the stoichiometric coefficient of component i in reaction[2] ρ and μ_i is the chemical potential of species i in the external solvent phase. In the case of sorption with water as the only solvent then species i is water, however, if other solvents were present then species i could represent any solvent sorbed by the membrane.

CD recognize that the first chemically sorbed molecules will sorb strongly, while the second and subsequent chemically sorbed water molecules will sorb with decreasing strength. However, as an idealization they assume that the first water molecule sorbs strongly and the rest sorb with equal strength, described by the equilibrium constant $K_\rho = 1$.

To correct for this simplification, they include an empirical solvation parameter to better represent the sorption behavior, and arrive at an expression for the number of chemically bound solvent molecules [30]

(6.2) $\lambda_i^C = \lambda_{i,M} \dfrac{K_1 a_i}{1-a_i}\left(\dfrac{1-(v+1)(a_i)^v + v(a_i)^{v+1}}{1+(K_1-1)a_i - K_1(a_i)^{v+1}}\right);$

in the above expression λ_i^C is the number of species i molecules fixed (i.e. water molecules, but, the model is left with the subscript i by the authors so as not to sacrifice generality) fixed per sulfonate head, $\lambda_{i,M}$ is an empirical solvation parameter for species i, v is the number of chemical equilibrium steps for the reaction (also the number of water molecules forming the primary hydration shell), K_1 is the equilibrium constant for the first reaction step and a_i is the activity of species i in the external solvent. Although this expression is a simplification, it still leaves room to change the model for different

---

[2] The formation of the hydration shell is described by sequential reactions between the polymer acid groups (A⁻H⁺), and the solvent (BOH), the reactions are of the form $A^-H^+ + BOH \leftrightarrow A^-BOH_2$, $A^-BOH_2 + BOH \leftrightarrow A^-BOH_2(BOH)$, $A^-BOH_2(BOH), + BOH \leftrightarrow A^-BOH_2(BOH)_2$, etc. [30].

membranes. For example, the number of water molecules forming the primary hydration shell (ν) can be modified. Also the introduction of the empirical solvation parameter $\lambda_{i,M}$ allows to "fit" the model to the data to better account for the chemical sorption behavior that actually occurs.

The number of free waters is determined by phase equilibrium [30]

$$(6.3) \quad \mu_{i,M} = \mu_{i,F},$$

where the subscripts i, *M, and F* refer to the species, to the free membrane phase, and the external phase, respectively. The chemical potential of species i in phase α is given by [30]

$$(6.4) \quad \mu_{i,\alpha} = \mu_i^o(T,p^o) + \int_{p^o}^{P} \left(\overline{V}_{i,\alpha}\right)dp + RT \ln a_{i,\alpha},$$

where $\mu_i^o\left(T,p^o\right)$ is the chemical potential of species i at standard pressure, $\overline{V}_{i,\alpha}$ is the partial molar volume of i in phase α, and $a_{i,\alpha}$ is the activity of i in phase α.

Evaluating Eqn. (6.3) for the two phases, i.e. free waters inside the membrane and external solvent, CD arrive at [30]

$$(6.5) \quad \ln \frac{a_{i,M}^F}{a_{i,\alpha}} = -\left(\frac{\overline{V}_i}{RT}\right)(p_M - p_\alpha),$$

where $\alpha = L$ if the external solvent is a liquid and $\alpha = V$ if the external solvent is a vapor. p_M is the pressure of the constituents of the membrane liquid phase, p_α is the pressure of the constituents of the membrane in phase α, and $\overline{V}_i$ is the partial molar volume of species i in the liquid form.

CD assume that the pressure difference between the membrane and external solvent arises due to two effects. The first contribution to the pressure difference is caused by the

elastic force of the membrane: as the membrane swells, the elasticity of the membrane causes the pressure of the free solvent to increase. In addition it is assumed that the interaction between the free waters and the hydrophobic backbone can be included in this pressure [30]. The second contribution to the pressure difference occurs only for a vapor-equilibrated membrane. The interface between the liquid within the membrane and the external vapor causes a pressure increase in the membrane due to capillary forces [30]. As a result, for the vapor-equilibrated membrane we have [30]

$$(6.6) \quad \Pi_M + \Pi_\sigma = p_M - p_V$$

and for the liquid-equilibrated membrane we have [30]

$$(6.7) \quad \Pi_M = p_M - p_L$$

where p_M, Π_M, and Π_σ, are the pressure of the constituents in the membrane liquid phase, pressure increase due to membrane elasticity ($\Pi_M = \kappa\varepsilon$) and capillary pressure respectively. κ is the effective spring constant for the membrane and ε is the pore volume fraction occupied by the liquid,

$$(6.8) \quad \varepsilon = \frac{\lambda_i}{\dfrac{\overline{V}_M}{\overline{V}_i} + \lambda_i}.$$

CD combine the models for the chemical equilibrium and phase equilibrium to arrive at an expression for the number of sorbed water molecules per sulfonate head (λ) in a vapor-equilibrated membrane [30]

$$(6.9) \quad \left\{ \lambda_i - \lambda_{i,M} \frac{K_1 a_{i,V}}{1 - a_{i,V}} \left(\frac{1 - (v+1)(a_{i,V})^v + v(a_{i,V})^{v+1}}{1 + (K_1 - 1)a_{i,V} - K_1(a_{i,V})^{v+1}} \right) \right\}^{-1} = \frac{1}{a_{i,V}} \exp \left\{ \left(\frac{\overline{V}_i}{RT} \right) \left[\kappa \frac{\lambda_i}{\lambda_i + \dfrac{\overline{V}_M}{\overline{V}_i}} - (S\sigma_w \cos\theta) \left(1 + \frac{\overline{V}_M}{\overline{V}_i} \frac{1}{\lambda_i} \right) \right] \right\} - 1,$$

and a liquid-equilibrated membrane [30]

$$(6.10) \quad \left\{ \lambda_i - \lambda_{i,M} \frac{K_1 a_{i,L}}{1 - a_{i,L}} \left(\frac{1 - (\nu+1)(a_{i,L})^{\nu} + \nu(a_{i,L})^{\nu+1}}{1 + (K_1 - 1)a_{i,L} - K_1(a_{i,L})^{\nu+1}} \right) \right\}^{-1} = \frac{1}{a_{i,L}} \exp\left\{ \left(\frac{\overline{V}_i}{RT} \right) \kappa \frac{\lambda_i}{\lambda_i + \frac{\overline{V}_M}{\overline{V}_i}} \right\} - 1,$$

where λ_i is the total number of sorbed waters per sulfonate head, R is the universal gas constant, T is the temperature, σ_w is the surface tension of water, S is the pore specific surface area, κ is the membrane spring constant and θ is the contact angle of saturated water vapor in Nafion.

The explanation of Schroeder's Paradox lies in the additional capillary pressure Π_σ of the sorbed free water phase in vapor-equilibrated membranes. Eqns. (6.9) and (6.10) are solved to find λ, due to the additional capillary pressure term in Eqn. (6.9), less water is sorbed by the vapor equilibrated membrane for external solvent with the same activity.

6.2 Sorption Isotherms

The sorption isotherms are important as they tell us the equilibrium water content of the membrane for given external solvent activity and given temperature of the system. CD's model of the membrane, considered in some detail above, was developed to determine sorption isotherms for the Nafion membranes. Moreover, CD consider the chemical equilibrium for the strongly bound solvent molecules. They assume that ν water molecules are chemically sorbed by a sulfonate head to form the primary solvation shell [30]. Any subsequently sorbed waters are considered free to equilibrate with the surroundings [30]. As considered in the previous section on hydration, for Nafion there are five strongly bound waters in the hydration shell of a sulfonate head.

CD use Eqn. (6.9) to plot the sorption isotherm for vapor-equilibrated Nafion and this is compared to experimental data, see Figure 15. Note that the model of CD provides for a

good visual fit to the experimental data at 30°C and at all times falls within the range of experimentally determined values.
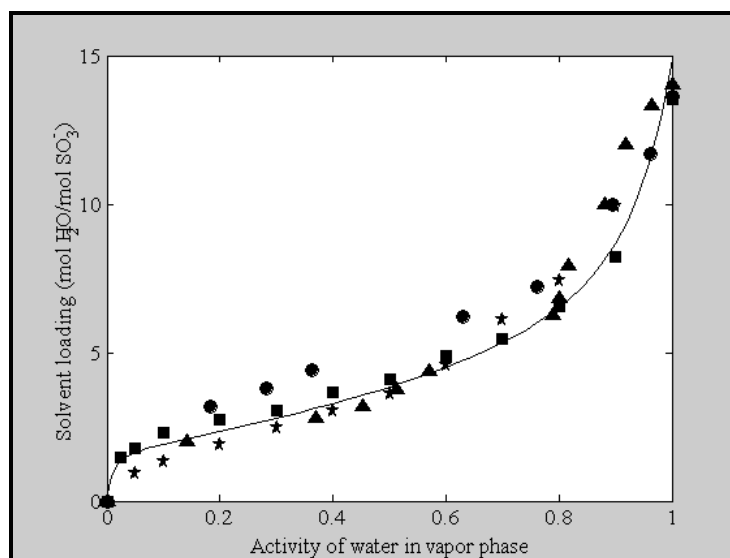
Figure 15: Water sorption isotherm for water vapor-equilibrated Nafion Membrane at 30°C (solid line is model prediction) [30].

It has been shown that the water content of Nafion does not drop below approximately 1.5 water molecules per sulfonate head even when vacuum dried [12]. It is also acknowledged that it is not possible to remove all the waters from the membrane without raising the temperature of the membrane above a point where decomposition of the polymer begins to occur [12]. Looking at the measured data in the above sorption isotherm, no water contents lower than ~1-2 waters per sulfonate head are found, besides the trivial data point of no waters per sulfonate head at zero activity. Although the model predicts behavior for water contents less than approximately 1.5 water molecules per sulfonate head, the membranes do not exhibit the predicted behavior.

However, this low water content behavior would not impact a model of a fuel cell. In typical operation, the water content of the membrane would not be allowed to drop anywhere near the one to two water per sulfonate head region, some corrective control action would be taken to ensure the membrane did not dehydrate to this point, since performance of the membrane (i.e. conductivity) is extremely poor in this region.

6.3 Predicting Trends in Membrane Behavior

By means of the model of CD, we can also explain the behavior of other membranes. The expression for capillary pressure [30]

$$(6.11) \quad \Pi_\sigma = -\frac{2\sigma_w \cos\theta}{r_p}$$

indicates that the capillary pressure is proportional to the inverse of the average pore radius

$$(6.12) \quad \Pi_\sigma \propto \frac{1}{r_p}.$$

Comparing Nafion and the sulfonated polyetherketone membrane sorption isotherms in Fig. 14, we note the larger difference between the vapor-equilibrated and liquid-equilibrated uptake for the sulfonated polyetherketone membrane compared to Nafion. The contact angle θ will depend on the material, however, we assume that the contact angle will be similar for Nafion and the sulfonated polyetherketone membrane. As discussed previously, the sulfonated polyetherketone membrane has narrower channels than Nafion, which implies that the average pore radius will be smaller for the sulfonated polyetherketone membrane, resulting in a higher capillary pressure and consequently the observed larger difference in water uptake for the former compared to the latter.

The model of CD includes the interactions between the free water molecules and the hydrophobic portion of the membrane in the elastic force of the membrane, which affects the activity of the free waters sorbed by the membrane. Since the sulfonated polyaromatic backbone is less hydrophobic, the activity of the free waters is smaller, thus more water must be sorbed to reach phase equilibrium with the surroundings. The sorption isotherms in Fig.14 show that for the water-equilibrated membrane more water is sorbed by the sulfonated polyaromatic membrane than by the Nafion membrane; this stands in accordance with the above discussion.

7 Transport Mechanisms

7.1 Aqueous Solutions (Bulk Water)

Having considered the sorption behavior of membranes, we now switch our focus to conductivity. Within pure water, the formation of protonic defects is suppressed by both, the stability of the sp^3 hybrid (favoring ordered distribution of protons in space), and strong solvent effects [35]. However, the mobility of protonic defects in aqueous solutions is significantly higher than that observed for other ions [35][36]. The high mobility of protons is due to the ease of proton transport afforded by the fact that the excess protons within the hydrogen bonded water network become indistinguishable from the "sea" of protons already present [37].

An excess proton in bulk water is typically found as a member of one of two structures, the first being a hydronium (H_3O^+) that is a proton donor to three other strongly bound waters [35]. The three strongly bound waters form the primary hydration shell of the hydronium and the result is an "Eigen" ion $(H_9O_4)^+$ [35][33][37]. The excess proton may also reside between two water molecules forming a "Zundel" ion $(H_5O_2)^+$ [35][33][37].

The Zundel and Eigen ions are part of a fluctuating complex [35], with the structure fluctuating between the Zundel and Eigen ions on a time scale of the order of approximately 10^{-13} seconds [33]. Figure 16 shows the structure of a Zundel and Eigen ion as well as the fluctuation between the two structures.

The transformation from an Eigen ion to a Zundel ion is triggered by relaxation of two of the three bonds in the primary hydration shell, accompanied by tightening of the third - this results in a shift of the structure to that of a Zundel ion [35]. The contraction of one of the three bonds is induced by changes in the second hydration sphere, more specifically the breaking of a hydrogen bond in the second hydration sphere [35][33]. The reverse process occurs for the transition from Zundel ion to Eigen ion. The shift from a Zundel to Eigen ion is triggered by the formation of a hydrogen bond.
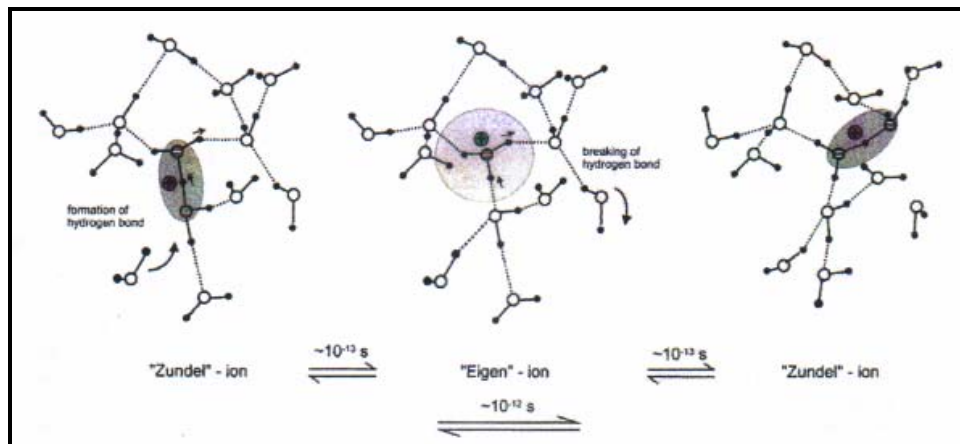
Figure 16:Transport mechanism of a protonic defect in water as obtained from an ab-initio MD simulation. The contracted hydrogen bonded structures are shaded [33].

Proton diffusion can occur via two mechanisms, structural diffusion (also referred to as the Grotthuss mechanism) or vehicle diffusion [35]. Structural diffusion occurs during the transition of the fluctuating complex formed by an excess proton in water from Zundel to Eigen, back to Zundel ions. Note in the above figure how the structure of a Zundel ion has "diffused" through the medium because of the fluctuation between structures. This "hopping" mechanism often referred to as the Grotthuss mechanism, and also referred to as the "Moses" mechanism [36], can be thought of as a process where the breaking of hydrogen bonds propels a moving proton in the direction of the broken bond with new hydrogen bonds forming behind the moving defect [36]. Essentially it is "structural diffusion triggered by molecular diffusion" [35].

The second diffusion mechanism is simply molecular diffusion (also referred to as vehicle diffusion) of a charged Zundel or Eigen ion as a whole [35]. It is the combination of these two diffusion mechanisms that gives protonic defects prodigious conductivity in liquid water.

7.2 Acidic Membranes

The conductivity of protons in aqueous systems of "bulk" water can be seen as the limiting case in conductivity. When aqueous systems interact with the environment, such as occurs in an acidic polymer membrane, the interaction reduces the conductivity of protons compared to that in "bulk" water [35]. The transport properties of the aqueous

phase of the acidic polymer membrane can be understood in the context of the mechanisms described above, with additional effects on conductivity arising due to interactions with the sulfonate heads and the restriction of the size of the aqueous phase that forms within acidic polymer membranes [33].

When considering the effects of the introduction of the membrane, we can consider effects occurring on the molecular scale and on a longer-range scale. First we consider what occurs on a molecular scale. Two main effects can be considered, the first is due to the confinement of water within the hydrophilic phase, and the second is due to the polarization of the hydrogen towards the anion.

When the water content is low, the hydrophilic phase is small, and the number of water/water interactions is reduced, as a result hydrogen bonds are tightened and thus the rate of hydrogen bond cleavage and formation is reduced [33]. We expect the conductivity to be lower, since the rate of bond formation and cleavage is key in determining how effective the Grotthuss structural diffusion mechanism is.

The presence of the dissociated acidic heads causes a polarization of the hydrogen bonds towards the anion, which in turn raises the energy of the Eigen ion (which is symmetrical) and thus reduces the rate of proton mobility [33]. As the amount of water sorbed by the membrane increases and the molecular scale effects are reduced, the properties approach those of bulk water on the molecular scale [33]. Figure 17 shows the trend in proton mobility and water self-diffusion for Nafion and a sulfonated polyetherketone membrane.
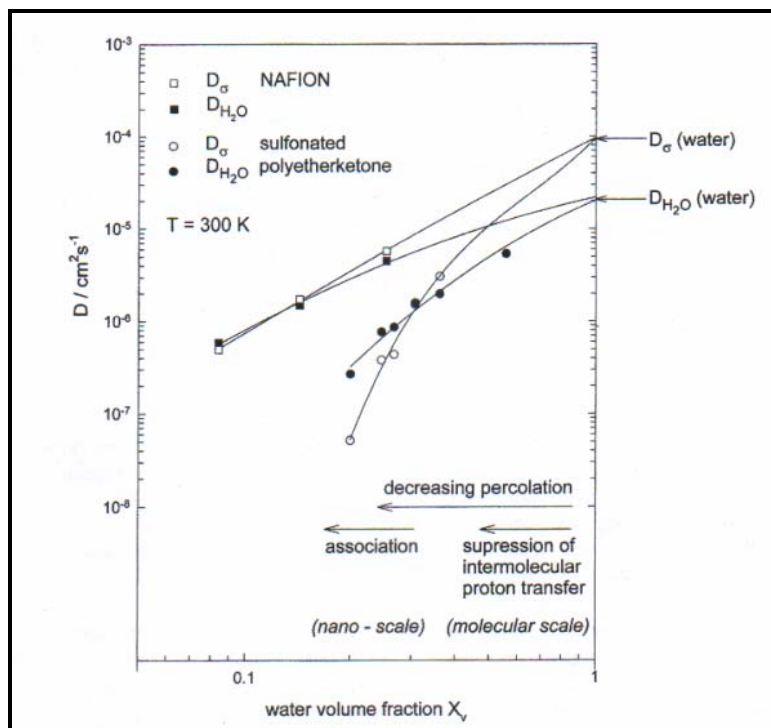
Figure 17: Proton conductivity diffusion coefficient D_σ and the molecular diffusion coefficient D_{H2O} for two different polymers as a function of the water volume fraction. The values for pure water are given for comparison [13].

In addition to the effects observed on the molecular scale, there are effects that occur on longer ranges. Two key effects, which tend to reduce proton conductivity, are the association of the protons with the acidic heads, and the geometrical restrictions provided by the membrane [33]. Within the membrane the dissociated protons remain localized near the acidic functional groups. The energy with which the protons associate with the acidic groups increases as the separation between sulfonate heads increases and as acidity decreases [33].

The sulfonate heads are less acidic in a sulfonated polyetherketone membrane than in Nafion, and the channels are not as well connected, and this leads to the reduced mobility of protons and water in sulfonated polyetherketone membranes compared to Nafion observed in Figure 17.

7.2.1 Electro-osmotic Drag in Nafion
Another phenomenon linked to the conductivity within membranes is electro-osmotic drag, which refers to the fact that as a proton travels through the liquid phase within the

membrane a certain number of water molecules associated with the proton are dragged through. A paper by Zawodzinski, Davey, Valerio et al. [38] (hereafter referred to as ZDV) investigated the dependence of electro-osmotic drag on water content and found that for a membrane equilibrated with water vapor the electro-osmotic drag has a value of approximately one water molecule dragged per proton over a wide range of water vapor activities. Considering Figure 6, for a vapor-equilibrated membrane, within the collapsed channels there are only those waters present which strongly bind to the sulfonate heads while the lower concentration of sulfonate heads means that this portion of the membrane is more hydrophobic than areas where clusters form, thus there is no free water phase present in the collapsed channels.

Because there is no free water phase present, we cannot expect large hydrated structures to diffuse through the membrane as we see in bulk water, instead we expect the delocalized hydronium ions, which are delocalized on the water molecules hydrating the sulfonate heads within the collapsed channels, to allow for conduction within the collapsed channels. Therefore, we have hydronium diffusing through the membrane liquid phase and we have an electro-osmotic drag coefficient of one, as is expected for a vapor equilibrated membrane.

When the membrane is equilibrated with liquid water, the collapsed channels swell, see Fig. 7. Within the collapsed channels there is now free waters and the membrane liquid phase is more bulk-like, as discussed above. Since the membrane liquid phase is now well interconnected, and the effect of the sulfonate heads on the free water is reduced due to shielding, larger structures such as Eigen and Zundel ions can diffuse through the membrane liquid phase and thus we have more waters dragged through the membrane per proton. Approximately 2.5 water molecules accompany each proton through the membrane for a liquid-equilibrated membrane [39][3].

In the model of Springer, Zawodzinski and Gottesfeld [39] (hereafter referred to as SZG), the authors assume that the number of water molecules dragged through a Nafion

membrane by a proton (the electro-osmotic drag) varies linearly with the water content, i.e.

$$(7.1) \quad n_{drag} = \frac{2.5\lambda}{22} \; .$$

This result is based on the assumption that the electro-osmotic drag varies linearly with water content (λ = # waters sorbed by the membrane per sulfonate head) and a water drag of 2.5 is measured in a fully hydrated membrane (membrane equilibrated with liquid water at 100°C [39]). They corroborated this assumption by comparing the value calculated using the linear approximation to a value of approximately 0.9 water molecules per proton at water content of 11 (vapor-equilibrated membrane). This commonly used linear dependence was later shown to be incorrect by experimental investigation in ZDV [38].

As discussed previously, approximately one water is carried through the membrane per proton over a wide range of water vapor activities and approximately 2.5 water are carried through per proton when liquid-equilibrated. This has led to the common assumption that within the liquid phase of a vapor-equilibrated membrane, we need only to be concerned with the transport of hydronium and water [40][41]. That said, WN have proposed a novel model, where as the membrane transitions from vapor-equilibrated to liquid-equilibrated, the number of waters transported through the liquid-equilibrated portion of the membrane per proton is 2.5, while 1 water molecule accompanies a proton for the vapor-equilibrated portion.

8 Membrane Transport Models

8.1 Microscopic Models
"In terms of both quantitative and qualitative modeling, PEMs have been modeled within two extremes, the macroscopic and the microscopic" [3]. The microscopic modeling work for PEMs focuses primarily on Nafion membranes. The breadth of the work performed in microscopic modeling includes molecular dynamics simulations [17] and

statistical mechanics modeling [42][43][44][45]. Some models even apply macroscopic transport relations to the microscopic transport within a pore of a Nafion membrane [46]. The merit of exploring such models is that they provide insight into what occurs within the membrane. The drawback of microscopic models is that, generally, such models are restricted to solution domains including only a portion of the membrane, and are far too complex to be integrated into a macroscopic model of a complete fuel cell. Macroscopic models deal with the problem of transport within PFSA membranes on a scale that can be integrated into a fuel cell model far easier.

8.2 Macroscopic Models

8.2.1 Fuel Cell Models

Macroscopic models can be classified into two broad categories: (i) models that attempt to model the conductivity of the membrane, and (ii) models attempting to represent fuel cell processes, typically for water management purposes. We will consider first the fuel cell models.

These models typically are further classified into hydraulic models, where a pressure gradient drives the water flow through the membrane, and diffusion models, where a concentration gradient drives the water.

8.2.1.1 Hydraulic Models

One of the earliest models is that of Bernardi and Verbrugge [47][48] (hereafter referred to as BV), whose work is closely coupled to the work of Verbrugge and Hill [49][50]. BV's model is a hydraulic model that uses the Nernst-Planck equation, including convection, for the transport of ionic species within the fluid phase [47]

$$(8.1) \quad N_i^{N-P} = -z_i \frac{F}{RT} \mathcal{D}_i c_i \nabla \Phi - \mathcal{D}_i \nabla c_i + c_i v_s,$$

and the Schloegl equation [47]

$$(8.2) \quad v_s = \frac{k_\phi}{\eta} z_f c_f F \nabla \Phi - \frac{k_p}{\eta} \nabla p$$

to describe the fluid transport. In the above expression $\mathcal{D}_i$ is the diffusion coefficient of species i in the membrane pore fluid, z_f is the charge number of the fixed species, c_i is the concentration of species i, F is Faraday's constant, N_i^{N-P} is the molar flux of species i, k_ϕ and k_p are the electrokinetic and hydraulic permeability, p is the pressure, η is the pore fluid viscosity and Φ is the potential. BV do not consider variations in conductivity with water content, rather they assume the membrane is fully hydrated at all times.

The model of BV also considers transport of gases through the membrane, considering the gases to be dissolved in the pore fluid. Since BV only consider the cathode side of the fuel cell system, they only account for transport of oxygen through the membrane, [47]

$$(8.3) \quad \mathcal{D}_{O_2} \frac{d^2 c_{O_2}}{dz^2} = v \frac{dc_{O_2}}{dz}.$$

A more sophisticated hydraulic model is that of Eikerling, Kharkats, Kornyshev et al. [51]. Their model differs slightly from BV's, in that it considers the existence of separate gas, and liquid channels within the membrane. Their model is also significantly more advanced in that water content is allowed to vary throughout the membrane, and conductivity, permeability, and electro-osmotic drag coefficient, are dependent on the local water content.

The problem that arises when using hydraulic models is that in membranes with lower water contents, interactions between the sulfonate heads and the backbone are significant, the water is less "bulk" like and the clusters are no longer well connected. Conceptually, the concentration gradient seems to be a more appropriate driving force than the pressure gradient [3].

8.2.1.2 Diffusion Models

One of the classical diffusion models is that of SZG [39]. The distinguishing feature of this paper, compared to prior studies, is the consideration of variable conductivity of the membrane electrolyte. In the development of this model, the authors performed their own experimental investigations to determine the model parameters, such as variation of the water sorption isotherms and membrane conductivity as a function of the water content.

In contrast with SZG's treatment, the membrane model is simplified in other studies using a variety of assumptions. This includes the assumption of fully hydrated operation at all times—and thus constant conductivity [48]; the use of concentrated solution theory to describe transport in the membrane [52] (Stefan-Maxwell equations for three species: membrane, water and protons); or the assumption of a thin membrane with uniform hydration [53]. The advantage of considering the dependence of the conductivity of the membrane on water content is that it allows for modeling of the increase in resistance of the membrane at lower water contents, which can not be replicated by the other models.

There are, however, several shortcomings in SZG's conductivity model. The conductivity is related to membrane water content and temperature by an empirical relationship. This is significant for two reasons. First, the equations used are not based on the physics of conductivity, they are empirical and the equations are essentially a curve fit. Secondly, the constants in the equations have no physical significance. This means that the model has very limited predictive capabilities and is restricted to Nafion 117. Even with parameter adjustments, SZG's model is not expected to be useful in predicting or correlating the behaviour of other types of membranes.

Since no physically-based model is presented for Nafion 117, it would be necessary to investigate the conduction mechanism in Nafion and other membranes to determine if similar conduction expressions could be applied to different membranes. Ultimately, the conductivity expression should be derived based on physical considerations, and the resulting theoretical model could then possibly be applied to membranes exhibiting similar physical behavior.

Berg, Promislow, St-Pierre et al. [40] (BPS) use the Nernst-Planck equation in their model, however, they consider a concentration gradient as a driving force for the water flux, and thus the model can be classified as a diffusion model. This is in contrast to BV who use the so called Schloegl equation, making their model a hydraulic model.

The model of BPS only considers the flux of water and protons within the membrane. The novel idea in this work is the introduction of a water transfer coefficient ($\bar{\gamma}$) and a water transfer mechanism to the membrane of the form

$$(8.4) \quad J_w^a / \xi = -\bar{\gamma} \left[c_w^a - c_{w,a}^* \right]$$

for the anode side and

$$(8.5) \quad J_w^c / \xi = \bar{\gamma} \left[c_w^c - c_{w,c}^* \right]$$

for the cathode side. In these expressions, the starred quantity is the equilibrium water content per sulfonate head within the membrane, calculated from the water activity in the corresponding channel, c_w^a and c_w^c are the membrane water contents on the anode and cathode side respectively, J_w is a flux of water on either the anode or cathode side and ξ is the fixed charge density. The transfer mechanism is introduced to model some of the effect of the time required for a membrane to reach its equilibrium state as well as transport limitations introduced by the gas diffusion layer.

The problem with diffusion models is that when the water content of the membrane is high (near fully hydrated), there is essentially no water concentration gradient and diffusion models are unable to produce a water concentration profile in the membrane. In this situation, a hydraulic model is more appropriate.

Altogether, we can conclude that diffusion models correctly predict the behavior at low water contents, while hydraulic models correctly predict the behavior in saturated membranes [3].

Janssen [54], and Thampan, Malhotra, Tang et al. [41] (TMT) use chemical potential gradients in their membrane transport models. Conceptually, this simplifies the models since use of the chemical potential eliminates the need to ascribe transport to hydraulic or diffusion mechanisms.

WN [3] developed a novel model where chemical potential gradients are considered as the driving force for vapor-equilibrated membranes, while hydraulic pressure gradients are considered as the driving force for liquid-equilibrated membranes. A continuous transition is assumed between vapor-equilibrated and liquid-equilibrated operation, where the transport mechanism is assumed to be a superposition of the two.

8.2.2 Membrane Conductivity Models.

The model of TMT [41] is one of the few models that is solely targeted at predicting conductivity behavior of a membrane, and which is based on physical rather than purely empirical considerations. It is in this vein they use a combination of the dusty fluid model (DFM) to model transport in the membrane, percolation theory to account for the structural aspects of the membrane, and a finite Brunauer-Emmett-Teller (BET) model to account for the membranes sorption of solvent from vapor. Before considering the model of TMT we examine the background of the DFM, and of the binary friction model (BFM) and we examine relevant aspects of the Stefan-Maxwell Equations on which these two models are based.

8.2.2.1 The Stefan-Maxwell Equations

The Stefan-Maxwell equation for transport in a multicomponent system is [55]

$$(8.6) \quad d_i = -\sum_{j=1}^{n} \frac{X_i X_j \left(\mathbf{v}_i - \mathbf{v}_j \right)}{D_{ij}^{S-M}},$$

where d_i are the forces driving molecular diffusion (e.g. molar density gradients or pressure gradients), X is the mole fraction and $\mathbf{v}$ is the average velocity of a species (note that the velocity can be converted into a molar flux by multiplying by the molar density, e.g. $\mathbf{N}_i = c_i \mathbf{v}_i$). D_{ij}^{S-M} is the Stefan-Maxwell diffusion coefficient, and has the significance of an inverse friction coefficient between species i and j. Note also that these diffusion coefficients are independent of concentration [55]. The essence of the Stefan-Maxwell equations is that the driving forces cause the molecules of a given species to move, while interactions with the molecules of the other species present in the mixture provide a resistance to this movement.

8.2.2.2 The Binary Friction Model

The BFM is developed by considering the free solution within the membrane and applying the Stefan-Maxwell equations to the pore fluid mixture to arrive at [56]

$$(8.7) \quad \frac{X_i}{RT} \widetilde{\nabla}_{T,p} \mu_i + \frac{\phi_i}{c_t RT} \widetilde{\nabla} p - \frac{\rho_i}{c_t RT} \widetilde{\mathbf{F}}_i^m = \sum_{j=1}^{n} \frac{\left(X_i \widetilde{\mathbf{N}}_j' - X_j \widetilde{\mathbf{N}}_i' \right)}{c_t D_{ij}^{S-M}}.$$

In the above expression, X_i is the mole fraction of species i, c_t is the total mole density, ρ_i is the mass concentration, $\widetilde{\mathbf{F}}_i^m$ is the external body force per unit mass (indicated by the superscript m), ϕ_i is the volume fraction of species i and D_{ij}^{S-M} are the Stefan-Maxwell diffusion coefficients.

The next steps in the derivation of the BFM are to assume that local equations (written with a ~ above them) also apply to pore-averaged values (written with arrows above them) and to introduce the friction with the membrane (which is fixed and thus has zero velocity), thus we have [56]

$$(8.8) \quad \frac{1}{c_t RT} \left(c_i \vec{\nabla}_{T,p} \mu_i + \phi_i \vec{\nabla} p - \rho_i \vec{\mathbf{F}}_i^m \right) = \sum_{j=1}^{n} R_{ij} \left(X_i \vec{\mathbf{N}}_j - X_j \vec{\mathbf{N}}_i \right) - r_{iM} \vec{\mathbf{N}}_i.$$

The resistance between species i and the other species is [56]

$$(8.9) \quad R_{ij} = \frac{1}{c_t D_{ij}^{S-M}}$$

while the resistance between species i and the membrane has been added in Eqn. (8.8), and is defined as [56]

$$(8.10) \quad r_{iM} = \frac{X_M}{c_t D_{iM}} = \frac{1}{c_t D_{iM}^e},$$

where D_{iM}^e is the inverse friction coefficient between species i and the membrane.

Inserting Eqns. (8.9) and (8.10) into Eqn. (8.8) yields, after dropping the arrows, to simplify notation,

$$(8.11) \quad \frac{-1}{c_i RT}\left(c_i \nabla_{T,p}\mu_i + \phi_i \nabla p - \rho_i \mathbf{F}_i^m\right) = \sum_{j=1}^{n} \frac{X_j}{D_{ij}^{S-M}}\left(\frac{\mathbf{N}_i'}{c_i} - \frac{\mathbf{N}_j'}{c_j}\right) + \frac{1}{c_i D_{iM}^e}\mathbf{N}_i'.$$

Using the relation to convert an external force per unit mass of species i to an external force per mole of species i

$$(8.12) \quad \frac{\rho_i}{c_i}\mathbf{F}_i^m = \mathbf{F}_i.$$

Considering the driving force we know that [56]

$$(8.13) \quad \nabla_{T,p}\mu_i + \frac{\phi_i}{c_i}\nabla p - \mathbf{F}_i = \nabla_{T,p}\mu_i + \overline{V}_i \nabla p - \mathbf{F}_i = \nabla_T \mu_i - \mathbf{F}_i.$$

Also if the only forces acting on the charged ions are due to the gradient in potential, then

(8.14) $\mathbf{F}_i = -z_i F \nabla \Phi$.

We can combine (8.13) and (8.14) to obtain the electrochemical potential gradient

(8.15) $\nabla_{T,p} \mu_i + \dfrac{\phi_i}{c_i} \nabla p - \mathbf{F}_i = \nabla_T \mu_i^e = \nabla_T \mu_i + z_i F \nabla \Phi$.

Substituting (8.15) back into (8.11), yields

$$(8.16)\quad \boxed{\dfrac{-1}{RT} \nabla_T \mu_i^e = \sum_{j=1}^{n} \dfrac{X_j}{D_{ij}^{S-M}} \left(\dfrac{\mathbf{N}_i'}{c_i} - \dfrac{\mathbf{N}_j'}{c_j} \right) + \dfrac{1}{D_{iM}^e} \left(\dfrac{\mathbf{N}_i'}{c_i} \right)}$$

There is yet another model referred to in the literature as the diffusion model [57]. This model is similar in nature to the BFM, however it is derived by assuming that the membrane can be modeled as a dust component (at rest) present in the fluid mixture. The equations governing species transport are developed from the Stefan-Maxwell equations with the membrane as one of the mixture species. The resulting equation for species i is the same as Eqn. 8.16 above [57], thus the BFM and diffusion models are equivalent.

In the BFM, as well as in the DFM and dusty gas model (DGM) described in detail in the next section, the structure of the porous media is considered independent of the transport equations. In the transport equations, the prime on the fluxes indicates that in fact these fluxes are the pore-averaged fluxes, and are taken per unit of *pore* surface area. We must correct these fluxes for the fact that diffusion is occurring in a porous media with a given porosity ε and tortuosity τ [57]. The flux is corrected to a flux per unit of cross sectional area of *membrane* non-primed quantity by multiplying the primed flux by a correction factor that includes the porosity ε and tortuosity factor τ [56]

(8.17) $\quad N_i = \dfrac{\varepsilon}{\tau} N_i'$.

The porosity and tortuosity factor can be pulled into the diffusion coefficients [58]

(8.18) $\quad D_{ij}^{\text{mod}\,ified} = \dfrac{\varepsilon}{\tau} D_{ij}^{S-M}$.

Thus, if we use the modified diffusion coefficients (8.18) then the fluxes are considered to be defined on a *membrane* area basis and include porosity and tortuosity effects. One should note that it is not always desirable to pull the porosity and tortuosity correction into the diffusion coefficient terms, since this only complicates their dependence on water content further.

An alternative to the correction is the Bruggeman correction [41]

(8.19) $\quad D_{ij}^{\text{mod}\,ified} = (\varepsilon - \varepsilon_0)^q D_{ij}^{S-M}$,

where ε_0 is the threshold volume fraction, the minimum fraction of the volume that must be occupied by water before the water phase is well enough connected to allow for transport.

This alternative correction is used because it is often difficult to determine the tortuosity, but relatively easier to determine the porosity as a function of the amount of fluid in the membrane. Thus, the Bruggeman correction simplifies the problem by eliminating the need to determine the tortuosity; rather, the Bruggeman exponent q is either used as a fitted parameter or is given the value of 1.5 [41]. Note that for the appropriate q value the Bruggeman correction is equivalent to ε/τ. For clarity the Bruggeman correction will always be shown explicitly, so that it is clear when we are considering flux per unit of cross sectional area of *membrane*.

8.2.2.3 The Dusty Fluid Model

In order to understand the DFM and the controversy that surrounds it we must first examine the dusty gas model (DGM). The DGM was developed in order to model gas flow through porous media. It is based on the idea that there are four independent mechanisms that drive gas transport through porous media. The first is Knudsen flow, where the gas pressure is low and collisions between the walls of the porous media and the molecules dominate; the second mechanism is viscous flow in which molecule-molecule interactions dominate; the third is continuum diffusion, where molecule-molecule interactions dominate; and the fourth is surface diffusion which, however, is neglected in the development of the model [57].

The DGM equations for the total flux of a species can be derived from a Chapman-Enskog kinetic theory treatment, and, considering an isothermal system, this yields[3] [57]

$$(8.20) \quad \sum_{j=1}^{v} \frac{n_j}{n_t D_{ij}^e} \left(\frac{\mathbf{N}_i'}{n_i} - \frac{\mathbf{N}_j'}{n_j} \right) + \frac{1}{D_{iK}^e} \left(\frac{\mathbf{N}_i'}{n_i} \right) + \frac{B_0}{D_{iK}^e \eta} \left(\nabla p - \sum_i n_i \mathbf{F}_i \right) = -\nabla \ln \left(\frac{n_i}{n_t} \right) - \nabla \ln p + \frac{\mathbf{F}_i}{k_B T} \, .$$

where n_t is the total molecular density of all the gases in the mixture, n_i is the molecular density of species i, D_{iK}^e is the Knudsen diffusion coefficient and D_{ij}^e is the effective mutual diffusion coefficient between species i and j, $\mathbf{F}_i$ is the external body force on species i per mole, B_0 is the viscous flow parameter, p is the pressure, η is the viscosity coefficient of the gas mixture and k_B is the Boltzmann constant. The effective diffusion coefficients (superscript e) are introduced, as the diffusion coefficients are not strictly Stefan-Maxwell diffusion coefficients, but rather they have absorbed constants introduced by changing from considering the porous medium as part of the mixture to only considering the gas when calculating mole fractions [58]. The first term on the left of Eqn. (8.20) accounts for continuum diffusion, the second term accounts for Knudsen diffusion, and the third term accounts for viscous flow. $\mathbf{N}_i'$ is a pore averaged flux

---

[3] Note that we have elected to change the variables used by the original author from **J** to **N**, in light of the fact that these fluxes are molar fluxes relative to the rest frame of the porous medium, and to avoid confusion when comparing to other equations.

relative to the rest frame of the porous medium, indicated by the prime on the flux variable.

In the dusty gas model, the total flux relative to the fixed reference frame is considered as being made up of contributions from diffusion, and convection, i.e. the total velocity of a species is made up of a diffusive contribution and a viscous flow (convective) contribution,

$$(8.21) \quad \mathbf{N}'_i = n_i \left(\mathbf{v}_i^{diff} + \mathbf{v} \right),$$

with

$$(8.22) \quad \mathbf{v} = -\frac{B_o}{\eta} \left(\nabla p - \sum_{i=1}^{v} n_i F_i \right).$$

The DGM was developed to model gas flow through porous media with high, or low, gas density and the transition regime in between the two ranges [57]. As a result of the different pressure dependences of the various terms, certain terms dominate in different regimes, thus allowing the model to predict behavior over a range of pressures.

The simplest derivation of the DFM involves arguments on the DGM. First, the driving forces (right hand side of Eqn. (8.20)) are converted to the chemical potential of the species within the pore liquid plus external body forces acting on that species. Second, molecular units are replaced with molar units, and the Knudsen diffusion term is now referred to as a membrane diffusion coefficient [57]. In the case of an isothermal system this results in [57]

$$(8.23) \quad \sum_{j=1}^{v} \frac{c_j}{c_t D_{ij}^e} \left(\frac{\mathbf{N}'_i}{c_i} - \frac{\mathbf{N}'_j}{c_j} \right) + \frac{1}{D_{iM}^e} \left(\frac{\mathbf{N}'_i}{c_i} \right) + \frac{B_0}{D_{iM}^e \eta} \left(\nabla p - \sum_{j=1}^{v} c_j \mathbf{F}_j \right) = -\frac{1}{RT} \left(\nabla_T \mu_i - \mathbf{F}_i \right),$$

where c_i is the mole density of species i, c_t is the total mole density and μ_i is the chemical potential of species i. If the only external body force is the force acting on the charged ions due to the gradient in potential, then [55]

$$(8.24) \quad \mathbf{F}_i = -z_i F \nabla \Phi \ ,$$

and we have the electrochemical potential gradient defined as

$$(8.25) \quad \nabla_T \mu_i^e = \nabla_T \mu_i + z_i F \nabla \Phi \ ,$$

where z_i is the charge number of species i, F is Faraday's constant and Φ is the electric potential in volts.

Substituting for the electrochemical potential, (8.23) becomes

$$(8.26) \quad \boxed{\frac{-1}{RT} \nabla_T \mu_i^e = \sum_{\substack{j=1 \\ j \neq i}}^{n} \frac{X_j}{D_{ij}^e} \left(\frac{\mathbf{N}_i'}{c_i} - \frac{\mathbf{N}_j'}{c_j} \right) + \frac{1}{D_{iM}^e} \left(\frac{\mathbf{N}_i'}{c_i} \right) + \frac{B_0}{\eta D_{iM}^e} \left[\nabla p + \left(\sum_{j=1}^{n} c_j z_j \right) F \nabla \Phi \right]}$$

where μ_i^e is the electrochemical potential of species i, $\mathbf{N}_i'$ is the pore averaged molar flux of species i, z_i is the charge number of species i, F is Faraday's constant and Φ is the electric potential in volts.

A second way to arrive at the above expressions was developed by Mason and Viehland who started with the statistical mechanical work of Bearman and Kirkwood to derive the above Eqns. (8.26) [56].

A third way to arrive at the DFM is due to TMT, who introduced the membrane as a dust species in the mixture of diffusing species (Figure 18). The membrane has zero velocity since it is mechanically restrained. The new mixture is modeled using the Stefan-Maxwell equations. The resulting equations are assumed to account for the diffusive

velocity for a given species in the mixture that contains the membrane as a dust species (at rest) [41],

$$(8.27) \quad \frac{-c_i}{RT} \nabla_T \mu_i^e = \sum_{\substack{j=1 \\ j \neq i}}^{n} \frac{c_i c_j}{c_t D_{ij}^e} \left(\mathbf{v}_i^D - \mathbf{v}_j^D \right) + \frac{c_i}{D_{iM}^e} \mathbf{v}_i^D \qquad (i = 1, 2, \ldots, n),$$

where $\mathbf{v}_i^D$ is the diffusive velocity of species i.

It is then stated that the total species velocity is the sum of the diffusive and convective velocities, as Eqn. (8.27) does not account for viscous flow $\left\{ \mathbf{N}_i' = c_i \mathbf{v}_i = c_i \left(\mathbf{v}_i^{Diffusive} + \mathbf{v} \right) \right\}$ [41]. The convective velocity, determined by the Schloegl equation [41]

$$(8.28) \quad \mathbf{v} = -\frac{B_0}{\eta} \left[\nabla p + \left(\sum_{j=1}^{n} c_j z_j \right) F \nabla \Phi \right],$$

is then introduced into Eqn. (8.27) [41]

$$(8.29) \quad \frac{-c_i}{RT} \nabla_T \mu_i^e = \sum_{\substack{j=1 \\ j \neq i}}^{n} \frac{1}{c_t D_{ij}^e} \left(c_i \mathbf{N}_i' - c_i \mathbf{N}_j' \right) + \frac{\mathbf{N}_i'}{D_{iM}^e} + \frac{c_i B_0}{\eta D_{iM}^e} \left[\nabla p + \left(\sum_{j=1}^{n} c_j z_j \right) F \nabla \Phi \right].$$

Dividing Eqn. (8.29) by c_i we obtain Eqn. (8.26).
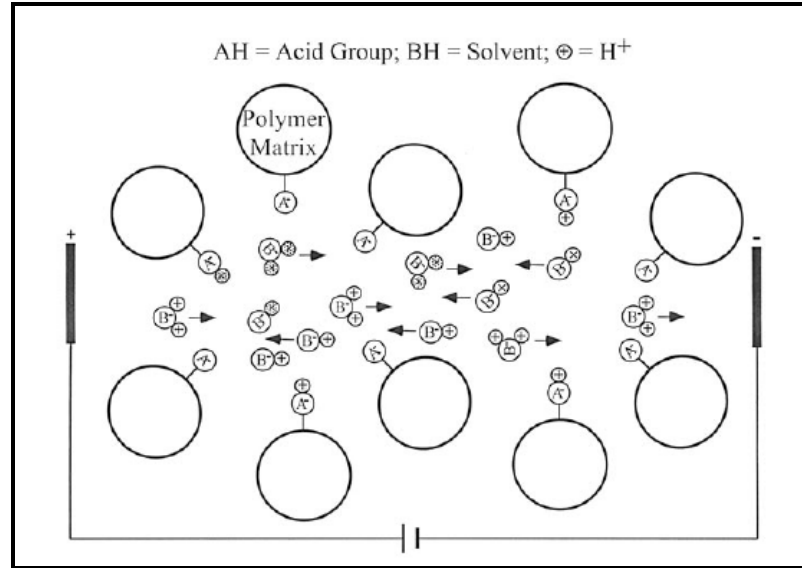
Figure 18: A "dusty-fluid model" depiction of a PEM. The polymer along with an acid group is viewed as "dust" particles, which comprise the PEM [41].

Comparing the DFM and the BFM side by side we have,

Dusty Fluid Model

$$\frac{-1}{RT}\nabla_T\mu_i^e = \sum_{\substack{j=1 \\ j\neq i}}^{n}\frac{X_j}{D_{ij}^e}\left(\frac{\mathbf{N}_i'}{c_i}-\frac{\mathbf{N}_j'}{c_j}\right)+\frac{1}{D_{iM}^e}\left(\frac{\mathbf{N}_i'}{c_i}\right)+\frac{B_0}{\eta D_{iM}^e}\left[\nabla p+\left(\sum_{j=1}^{n}c_j z_j\right)F\nabla\Phi\right],$$

Binary Friction Model

$$\frac{-1}{RT}\nabla_T\mu_i^e = \sum_{\substack{j=1 \\ j\neq i}}^{n}\frac{X_j}{D_{ij}^{S-M}}\left(\frac{\mathbf{N}_i'}{c_i}-\frac{\mathbf{N}_j'}{c_j}\right)+\frac{1}{D_{iM}^e}\left(\frac{\mathbf{N}_i'}{c_i}\right)$$

In this way we can clearly see the extra terms present in the Dusty Fluid Model, and how the addition of the viscous terms distinguishes the DFM from the BFM. There are two schools of thought on the presence of the viscous term in the DFM. There are those who argue that the BFM (which is also referred to as the Lightfoot model [56]) is correct and accounts for all interactions occurring between the membrane, and the species traveling through [56][59], while there are those who argue that the DFM is correct due to the additional viscous terms [41][57][58].

Due to the ad hoc way in which the additional viscous terms are added into the fluid transport equations, and the lack of rigorous justification for the addition of these terms, we have chosen to neglect the additional viscous terms, avoiding unnecessary complication of our model with no evident benefit. Should more rigorous justification for the additional terms be provided, they could then be incorporated into our model, as the additional complexity would be warranted.

8.2.2.4 Transport Model

Having considered the equations used to model transport in the membrane, we can now turn our focus on the conductivity model of TMT [41]. We start by considering what species are present in the pore fluid. In the membrane pore fluid, it is the protons that have dissociated from the sulfonate heads that are the charge carriers. TMT assume that the number of protons that have dissociated will dictate how many free charge carriers there are in the membrane. In order to determine the number of free protons, it is necessary to model the dissociation of the protons from the sulfonate heads. The process of dissociation is coupled with the process of hydration of the sulfonate heads. TMT only consider the first step in the dissociation process, which is responsible for forming the hydronium ions. In this reaction *HA*, where *A* stands for the sulfonate heads, dissociates in the presence of a proton accepting solvent *BH* [41]

$$(8.30) \quad HA + BH \leftrightarrow BH_2^+ + A^- \text{ and } K_A = \frac{a_{BH_2^+} a_{A^-}}{a_{HA} a_{BH}}.$$
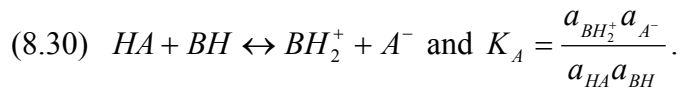
K_A is the equilibrium constant for the reaction. The concentration of charge carriers $c_{BH_2^+}$ can be related to the acid site concentration per unit volume of solution in the pore fluid $c_{HA,0}$ via the degree of dissociation α [41],

$$(8.31) \quad c_{BH_2^+} = c_{HA,0} \alpha.$$

Under the assumption that activity coefficients are unity (typically done in membrane papers to simplify the analysis), the equilibrium constant expression (law of mass action) becomes [41]

$$(8.32) \quad K_{A,C} = \frac{c_{BH_2^+} c_{A^-}}{c_{HA} c_{BH}} = \frac{\alpha^2}{(1-\alpha)(\lambda-\alpha)},$$

which can be solved for α,

$$(8.33) \quad \alpha = \frac{(\lambda+1) - \sqrt{(\lambda+1)^2 - 4\lambda\left(1 - \frac{1}{K_{A,C}}\right)}}{2\left(1 - \frac{1}{K_{A,C}}\right)}.$$

It is reasonable, as discussed previously, to assume that hydronium ions are the charge carriers for vapor-equilibrated membranes. However, this assumption is not valid for liquid-equilibrated membranes, where the transport number is found to be around 2.5 [38]. It is important to note this, as TMT do use this model to predict behavior for liquid-equilibrated membranes, thus the assumption of a hydronium ion being the charge carrier needs to be modified if the membrane is liquid-equilibrated.

It should also be noted that, although hydronium ion formation is the first step in the reaction of water molecules with a sulfonate head [12], the hydronium is not necessarily free to move. Instead, the hydronium will be localized on the sulfonate head for small water contents. Therefore, the number of hydronium ions that are free to conduct is not simply the number that have been dissociated from the sulfonate heads, but rather the number that are sufficiently hydrated so that they can move within the membranes liquid phase.

TMT use the DFM equations in the development of his conductivity model. Recalling the previous discussion on the Bruggeman correction, Eqn. (8.19), TMT use this

correction, with a percolation threshold below which conductivity is zero, in order to convert his fluxes to a per unit cross sectional area of *membrane* basis from a *pore* cross sectional area basis. In this way, TMT have accounted for the requirement of having a minimum amount of water sorbed by the membrane so that the water phase is sufficiently connected to allow charge conduction through the membrane (hydronium ions may be transported).

Membrane water uptake as a function of external solvent activity must be calculated for use in the membrane model, as TMT's conductivity model gives conductivity as a function of water content, and they choose to compare to data that gives conductivity as a function of water vapor activity that the membrane is equilibrated with. When this model was developed, the available options for equations to model the sorption isotherms were polynomial fits, the Flory-Huggins model and the BET model [41]. The BET model was selected because it is based on parameters that have physical significance and it provides a good fit to the experimental data [41]. One way this model could be improved, would be to use the recent model of CD [30] to model the sorption isotherm.

The model of CD could also be used to reduce the number of curve fit parameters as the BET relies on 2 curve fit parameters [41]. Since the BET model provides a good visual fit to the data, it will not induce significant error to use it. One problem with the BET model used is that it is fitted to data at 30°C and does not include temperature dependence; this should be corrected to provide better results.

In the development of the transport equations, several assumptions are made that must be discussed. The model developed by TMT is designed for a closed conductivity cell, where the fluxes of water and hydronium are equal and opposite (equimolar counterdiffusion) [41]. It is acknowledged by TMT that this is not what really occurs in a fuel cell, and that the ratio of water and hydronium flux could be dictated by stoichiometry, or alternatively, a flux equation could also be written for water [41].

There are advantages to either of these two options. If it we wish to simplify the water transport in the membrane, then fixing the ratio of water and hydronium flux is desirable. However, for a more complete transport model, it is desirable to develop a second flux expression for water, which considers the influence of forces (i.e. gradient in water mole density) that drive water flow through the membrane. TMT assume that $D_{1M}^e \approx D_{2M}^e$ due to similarities in water (species 2) and hydronium (species 1) [41]. This assumption is somewhat questionable since, due to the differences in the hydronium ions and water, the interaction forces differ and D_{iM}^e should be different.

The assumption that $D_{1M}^e \approx D_{2M}^e$ coupled with the assumption of a closed conductivity cell forces convection to be zero, [41]

$$(8.34) \quad \nabla p + \left(\sum_{j=1}^{n} c_j z_j \right) F \nabla \Phi = 0 .$$

This implies that any gradient in pressure will cause a gradient in potential, and vice versa.

TMT's expression for conductivity in a closed conductivity cell is [41]

$$(8.35) \quad \sigma = (\varepsilon - \varepsilon_0)^q \left(\frac{\lambda_1^0}{1 + \delta} \right) c_{HA,0} \alpha ,$$

where λ_1^0 is the conductance of hydronium ions in water, ε is the volume fraction of water in the membrane and ε_0 is the percolation threshold volume fraction below which the membrane water clusters are not well enough connected to allow conductivity.

In this model four empirically determined parameters are required. The BET model is fitted to sorption isotherms (Figure 19), which yields C, the BET constant, and n_2, the total number of water layers sorbed on the pore surface. Two more parameters are

required to fit the conductivity expression to conductivity data (Figure 20), the percolation threshold volume fraction ε_0 and the ratio ${D_{12}^e}/{D_{1M}^e} = \delta$.
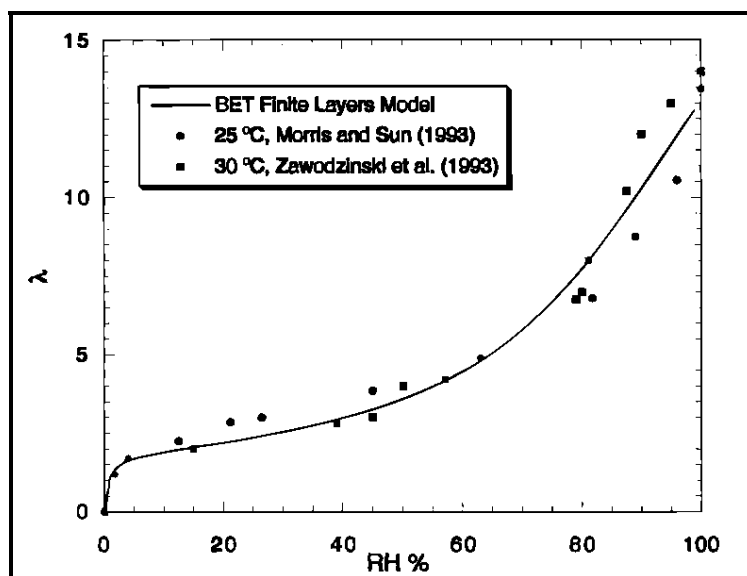
Figure 19: Adsorption isotherm for water uptake by Nafion 117 from water vapor. The finite-layer BET isotherm is compared with the data of Zawodzinski et al. at 30˚C and that of Morris and Sun at 25˚C [41].
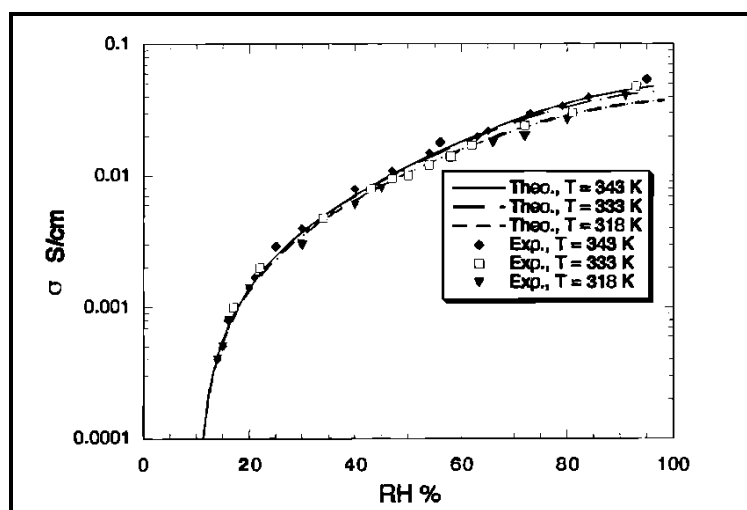
Figure 20: The experimental results of SES for σ of Nafion 117 equilibrated in water vapor vs. RH or water vapor activity at different temperatures along with theoretical predictions of TMT [41].

Expression 8.35 above seems reasonable; when the membrane is well-hydrated there will be a well-connected water phase within the membrane, in which hydronium can diffuse much like a free water phase. Thus, it makes sense to have the maximum conductivity

approach that of hydronium in free water. As the water content drops, the volume fraction of water decreases and thus the conductivity falls. Once the water volume fraction of water drops below the percolation threshold volume fraction, the conductivity vanishes, as the remaining liquid water in the membrane is insufficient to allow proton transport.

As discussed in the prior section on membrane hydration, the membrane will exhibit low conductivity for water contents greater than approximately two waters per sulfonate head, and will be significantly conductive for water contents greater than five. TMT treat the threshold volume fraction as a curve fit parameter and in their model they take a threshold volume fraction corresponding to approximately two waters per sulfonate head. This is done in order to match the data of Sone et al. (Figure 20), which shows that below a relative humidity of approximately 10-15%, the conductivity drops off steeply (almost an order of magnitude). Using the sorption isotherm (Figure 19) we can see that this relative humidity corresponds to approximately two to two and a half waters per sulfonate head.

The above conductivity expression, Eqn. (8.35), provides a good overall fit to the experimental data of SES for vapor-equilibrated membranes (Figure 20). However, the data collected by SES were not obtained from a closed conductivity cell, but from using the four-electrode AC Impedance method on a membrane equilibrated with water vapor; conductivity is determined by measuring the membrane resistance at known water contents. In the AC Impedance method alternating current is passed through the membrane and the resistance is measured. Since alternating current is used, water transport is in fact considered negligible, and no gradients in water molar density are developed during the experiment.

The model of conductive transport in proton exchange membranes presented by TMT in Ref. [41] is significant in that it provides a theoretical framework based on the structure of the membrane and the physics of the transport. This modelling framework is not limited to Nafion, and is applicable to other membranes with similar structures.

However, there is room for improvement:

- The BFM can be used instead of the DFM, thus eliminating the additional viscous terms. An interesting point to note is that Thampan's assumption that $D_{1M}^e \approx D_{2M}^e$ actually causes the additional viscous terms to drop out anyway.

- The restriction to equimolar counter diffusion could be removed.

- The effect of temperature on the sorption isotherm could be accounted for.

As a final note, TMT choose to compare their results to the experimental data in a log-plot format. This can mask discrepancies between model results and experimental data. Comparison should be done in a format where the error in the model can be more readily identified and estimated.

PART II – The Binary Friction Conductivity Model

9 Counting Species for Transport Model

Having investigated the various models used in representing the behavior of membranes and having developed a solid platform of understanding, we can begin to build a transport model for PEMs using the insight we have gained in the previous chapters. In the second part of the work, we focus our attention on the development of a transport model to describe the behavior of the PEMs. We have focused on the Nafion 1100 *EW* family of membranes since they have been studied the most, and thus more information is available on their properties and behavior. We have tried to not sacrifice generality in the development of this model, in the hope that further research into other membranes provides the necessary information to apply this model.

We recall that for the series of 1100 *EW* Nafion membranes, the only difference between the various members of the series is the thickness, e.g. Nafion 117 and Nafion 115 are 7 mil and 5 mil thick respectively, however, they are made up of the same macromolecules, and in fact have the same nanostructure, since the *EW* is the same. The only differences in conductivity that may arise are due to possible surface effects. Surface effects would be expected to have a significant impact, if any, in thinner membranes only. Investigation of such effects is beyond the scope of this work, and no information on these possible effects was noted in the literature survey.

We will start with an exercise in counting of the species involved in transport within the membrane, giving us a fundamental definition of quantities such as mole fractions and porosity. In order to determine the mole densities and mole fractions of the various species within the membrane, we first determine which species are present, and then count how much of a species is present. Using molar volumes, we can determine what volume is occupied by each species and thus determine molar densities.

9.1 Counting

We start by assuming that we have a proton forming a complex with a number of waters residing within the water sorbed by a membrane. A protonated water complex consists of ω_{pw} waters and one extra proton. In order to simplify our analysis, we assume that at all

times the protons are accompanied by the same water molecule(s) in the protonated complex [41][40]. In effect, we are neglecting any contribution of the so-called Grotthuss hopping mechanism to transport. However, the inclusion of such a mechanism is beyond the scope of this work and would significantly complicate the model. Furthermore, we recall that the presence of the membrane reduces the effectiveness of the Grotthuss mechanism [35].

In addition to the protonated complexes we have water and membrane backbone. The water and protonated complexes form one phase, the membrane backbone another. We recall that λ is defined as the number of water molecules sorbed by the membrane per sulfonate head, while α represents the fraction of the sulfonate heads which have dissociated, allowing their protons to combine with waters sorbed by the membrane to form protonated complexes ($0 \leq \alpha \leq 1$). It follows that $\omega_{pw}\alpha$ water molecules per sulfonate head have been converted into protonated complexes. We also introduce γ as the number of fixed waters per sulfonate head, that is waters that are so strongly bound to the sulfonate heads that they effectively become part of the membrane phase, and do not contribute to transport.

In order to perform the counting of species we define the following subscripts:

Table 1: Species Present Within the Membrane

Subscript	Species
1	Protonated complex
2	Free waters
W	Total sorbed waters
fw	Fixed waters
pw	Waters in protonated complex
sh	Sulfonate heads
M	Membrane

The total number of sorbed waters is, due to the definition of λ,

$$(9.1) \quad n_w = \lambda n_{sh}.$$

i.e. the number of sulfonate heads is

$$(9.2) \quad n_{sh} = \frac{n_w}{\lambda}.$$

Due to electroneutrality, the number of protons available to dissociate into the membrane pore fluid must be equal to the number of sulfonate heads,

$$(9.3) \quad n_1 = \alpha n_{sh} = \frac{\alpha}{\lambda} n_w.$$

The number of fixed waters is given as

$$(9.4) \quad n_{fw} = \gamma m_{sh} = \frac{\gamma}{\lambda} n_w.$$

The total number of waters sorbed by the membrane is the sum of the free waters, fixed waters, and waters associated with protonated complexes

$$(9.5) \quad n_w = n_2 + n_{fw} + \omega_{pw} n_1,$$

therefore,

$$(9.6) \quad n_2 = n_w \left(\frac{\lambda - \gamma - \omega_{pw}\alpha}{\lambda} \right).$$

Having counted the numbers of all the species present, we will now determine the molar densities, which involve partial molar volumes. We could not find data on the exact partial molar volume of hydronium or other protonated complexes under the given conditions, i.e. within a hydrated membrane. In order to be able to progress, we make the

reasonable assumption that the partial molar volume of water and hydronium is approximately the same.

Indeed, the addition of an extra proton to bulk water causes the hydrogen bonds to be contracted, and although a proton is added, a volume contraction is measured. In fact the partial molar volume for an individual H^+ ion is -5.4 $cm^3 mol^{-1}$, indicative of this volume contraction [60]. Based on this observation, we shall assume that even though the hydronium ion has an additional hydrogen atom, it has the same partial molar volume as water. We also assume that the partial molar volume of a protonated complex is approximately equal to the number of waters in the complex times the partial molar volume of water,

$$(9.7) \quad \overline{V}_1 \cong \omega_{pw} \overline{V}_2,$$

which implicitly involves assuming that the molar volumes add to give the molar volume of the complex.

Ideally we should use partial molar volumes in this counting exercise, since we are dealing with a solution (water and hydronium ions), and the volumes of the species involved (membrane, water and protons) will not necessarily add as the membrane sorbs water. However, since the water and membranes form a 2 phase system (thus we would expect the volume of membrane and water after sorption to be reasonably close to the sum of the volumes of water and membrane before sorption), and we were unable to find information on the partial molar volumes for a such a system, we assume that the molar volumes of the species are equal to the partial molar volumes. From here on in our analysis we replace partial molar volumes $\overline{V}$ with molar volumes V_M.

The volume occupied by the free waters is

$$(9.8) \quad V_2 = V_{M,2} n_2 = V_{M,2} n_w \left(\frac{\lambda - \gamma - \omega_{pw} \alpha}{\lambda} \right),$$

and the volume occupied by the protonated complex is

$$(9.9) \quad V_1 = \omega_{pw} \mathrm{V}_{M,2} n_1 = \mathrm{V}_{M,2} n_w \omega_{pw} \frac{\alpha}{\lambda}.$$

The volume occupied by the fixed waters is

$$(9.10) \quad V_{fw} = \mathrm{V}_{M,2} n_{fw} = \mathrm{V}_{M,2} n_w \frac{\gamma}{\lambda}.$$

and finally the volume occupied by the membrane is

$$(9.11) \quad V_M = V_{M,M} n_{sh} = \mathrm{V}_{M,M} n_w \frac{1}{\lambda},$$

where $\mathrm{V}_{M,M}$ is the volume of membrane per mole of acid heads ($\mathrm{V}_{M,M} = EW/\rho_{dry}$, where ρ_{dry} is the dry density of the polymer membrane).

We recall that the membrane forms a two-phase system with the sulfonate heads at the interface between the liquid and membrane phases. We assume that the pore fluid consists of only the free waters and the protonated complexes. The fixed waters and the membrane are assumed to be separate from the pore fluid phase, and are thus excluded from the total pore fluid volume.

The total volume of pore fluid is, from Eqns. (9.8 and 9.9),

$$(9.12) \quad V_p = V_1 + V_2 = \mathrm{V}_{M,2} n_w \frac{\lambda - \gamma}{\lambda}.$$

The mole density of protonated complexes within the pore fluid is

$$(9.13) \quad c_1 = \frac{n_1}{V_p} = \frac{1}{V_{M,2}} \frac{\alpha}{\lambda - \gamma},$$

and the mole density of free waters within the membrane is

$$(9.14) \quad c_2 = \frac{n_2}{V_p} = \frac{1}{V_{M,2}} \left(\frac{\lambda - \gamma - \omega_{pw}\alpha}{\lambda - \gamma} \right).$$

The total mole density of the pore fluid is

$$(9.15) \quad c_t = c_1 + c_2 = \left(1 + \frac{(1 - \omega_{pw})\alpha}{\lambda - \gamma} \right) \frac{1}{V_{M,2}}.$$

We can now calculate the mole fraction for the protonated complexes,

$$(9.16) \quad X_1 = \frac{c_1}{c_t} = \frac{\alpha}{\lambda - \gamma + (1 - \omega_{pw})\alpha},$$

and the mole fraction of free waters

$$(9.17) \quad X_2 = \frac{c_2}{c_t} = \frac{\lambda - \gamma - \omega_{pw}\alpha}{\lambda - \gamma + (1 - \omega_{pw})\alpha}.$$

The porosity is defined as the volume of the pore fluid divided by the total volume,

$$(9.18) \quad \varepsilon = \frac{V_p}{V_t},$$

and, since the total volume is the sum of all the volumes that make up the system,

$$(9.19) \quad V_t = V_1 + V_2 + V_{fw} + V_m = n_w \left(V_{M,2} + \frac{V_{M,M}}{\lambda} \right),$$

the porosity can be written as [4]

$$(9.20) \quad \varepsilon = \frac{\lambda - \gamma}{\lambda + \dfrac{V_{M,M}}{V_{M,2}}}.$$

9.2 Simplifying for Transport in Nafion

When considering transport within vapor-equilibrated Nafion, it is reasonable to assume that hydronium is the protonated complex that is formed. We recall that larger hydrated structures (Zundel/Eigen ions) diffuse through the membrane when liquid-equilibrated, thus for liquid-equilibrated membranes we can not assume a hydronium ion is the protonated complex, but rather a larger complex consisting of 1 proton, and approximately 2.5 water molecules should be considered under these conditions. The accounting for species can be simplified, as $\omega_{pw} = 1$ in the case of a vapor-equilibrated membrane, and therefore, we have

$$(9.21) \quad c_1 = \frac{1}{V_{M,2}} \frac{\alpha}{\lambda - \gamma},$$

$$(9.22) \quad c_2 = \frac{1}{V_{M,2}} \frac{\lambda - \gamma - \alpha}{\lambda - \gamma},$$

---

[4] Note that though this expression is different from that of CD and TMT in that we use molar volumes when writing out our expressions, their expressions our the same as ours. We have just explicitly stated our assumption that the molar volumes are equal to the partial molar volumes.

$$(9.23) \quad c_t = \frac{1}{V_{M,2}},$$

$$(9.24) \quad X_1 = \frac{\alpha}{\lambda - \gamma},$$

and finally

$$(9.25) \quad X_2 = \frac{\lambda - \gamma - \alpha}{\lambda - \gamma}.$$

Having considered the accounting of the species within the membrane, we now have the necessary mole fractions, mole densities and porosity expression for the transport model. In the following section we consider the non-dimensionalization of the transport equations.

10 Transport Model

10.1 Non-Dimensionalized Transport Equations

We start our development of the transport model by introducing the chemical potential [61]

$$(10.1) \quad \mu_i = g_i(T, p) + RT(\ln X_i + \ln \gamma_i).$$

Taking the gradient in potential (at constant T) we have,

$$(10.2) \quad (\nabla \mu_i)_T = \frac{dg_i}{dp} \nabla p + RT(\nabla \ln X_i + \nabla \ln \gamma_i),$$

where g is the molar specific Gibb's free energy.

We have that [61]

(10.3) $\quad Tds = du + pdV_M$,

where u is the molar specific internal energy and s is the molar specific entropy, and [61]

(10.4) $\quad dg = d(u + pV_M\text{-}Ts) = du + pdV_M + V_M dp - Tds - sdT$.

Substituting (10.3) into (10.4) and simplifying we get

(10.5) $\quad dg = V_M dp - sdT$.

Taking dg/dp we have

(10.6) $\quad \dfrac{dg}{dp} = V_M$.

Therefore, substituting Eqn. (10.6) into Eqn. (10.2), and recalling the gradient in electrochemical potential (Eqn. (8.15)) we have[5]

(10.7) $\quad \nabla_T \mu_i^e = RT(\nabla \ln X_i + \nabla \ln \gamma_i) + V_{M,i}\nabla p + z_i F \nabla \Phi$.

Recalling the BFM equations, Eqn. (8.16), and introducing the above definition of the electrochemical potential yields, after multiplication by X_i,

(10.8) $-\left(\nabla X_i + X_i \nabla \ln \gamma_i + X_i \dfrac{V_{M,i}}{RT} \nabla p + X_i z_i \dfrac{F}{RT} \nabla \Phi \right) = \displaystyle\sum_{j=1}^{n} \left\{ \dfrac{X_j \mathbf{N}_i'}{c_t D_{ij}^{S-M}} - \dfrac{X_i \mathbf{N}_j'}{c_t D_{ij}^{S-M}} \right\} + \dfrac{\mathbf{N}_i'}{c_t D_{iM}^e}$.

---

[5] Note that this expression for electrochemical potential is different from that in other papers, such as TMT, in that our expression has mole fractions instead of molar densities and molar volumes instead of partial molar volumes. This difference arises because we have chosen to use a different reference state in the development of our chemical potential terms.

Recall that the primed fluxes are pore-averaged values.

We introduce the non-dimensional quantities of length

$$(10.9) \quad \hat{x} = \frac{x}{L_M},$$

where L_M is the membrane thickness, total mole density

$$(10.10) \quad \hat{c}_t = \frac{c_t}{c_{ref}},$$

and mole density of species i

$$(10.11) \quad \hat{c}_i = \frac{c_i}{c_{ref}}.$$

We have chosen the reference molar densities to be the inverse of the partial molar volume of water ($c_{ref} = \frac{1}{V_{M,2}}$), since this will not vary significantly with temperature or pressure ($V_{M,2} = V/\rho_2$, where M_2 is the molar mass of water, which is constant, and ρ_2 is the density of water, which does not vary significantly with temperature, and if we assume incompressible fluids, does not vary with pressure either). The molar volume of water is approximately 18×10^{-6} m^3 mol^{-1} [41], thus the reference mole density is

$$(10.12) \quad c_{ref} = 55.6 \times 10^3 \, \text{mol m}^{-3}.$$

We define the dimensionless mole flux of species i

$$(10.13) \quad \hat{\mathbf{N}}_i' = \frac{\mathbf{N}_i'}{N_{ref}},$$

molar volume for water and hydronium

$$(10.14) \quad \hat{v}_1 = \hat{v}_2 = V_{M,2} c_{ref}$$

and diffusion coefficients

$$(10.15) \quad \hat{D}_{ij} = \frac{D_{ij}^{S-M}}{D_{ref}}.$$

Possible reference diffusion coefficients are D_{ij}^{S-M}, and D_{iM}^{e}. Our analysis of the magnitude of the driving forces – which is the main motivation for deriving non-dimensional equations – focuses only on the magnitude of the driving force terms, thus we need not trouble with finding reference values for the diffusion coefficients.

We now define a reference flux

$$(10.16) \quad N_{ref} = c_{ref} v_{ref}$$

with reference velocity

$$(10.17) \quad v_{ref} = \frac{D_{ref}}{L_M}.$$

We also define reference gradients in pressure and potential to obtain non-dimensional pressure gradients

$$(10.18) \quad \hat{\nabla}\hat{p} = \frac{\nabla p}{\left(\frac{\Delta p_{ref}}{L_M}\right)}$$

and potential gradients

$$(10.19) \quad \hat{\nabla}\hat{\Phi} = \frac{\nabla\Phi}{\left(\dfrac{\Delta\Phi_{ref}}{L_M}\right)},$$

noting that the non-dimensionalized gradient operator can be defined as

$$(10.20) \quad \hat{\nabla} = L_m\nabla .$$

We assume that, as an extreme-case scenario, the pressure drop across the membrane is 5 bar, thus the reference pressure drop is

$$(10.21) \quad \Delta p_{ref} = 5\times10^5 \text{ N m}^{-2},$$

while the maximum potential drop across the membrane is approximately 0.3 V, thus the reference voltage drop is

$$(10.22) \quad \Delta\Phi_{ref} = 0.3 \text{ V} .$$

Substituting the above non-dimensional parameters into the transport equations yields the non-dimensionalized BFM

$$(10.23) \quad -\left(\hat{\nabla}X_i + X_i\hat{\nabla}\ln\gamma_i + \beta X_i\hat{v}_i\hat{\nabla}\hat{p} + \Theta X_i z_i\hat{\nabla}\hat{\Phi}\right) = \sum_{j=1}^{n}\left\{\frac{X_j\hat{\mathbf{N}}_i'}{\hat{c}_t\hat{D}_{ij}} - \frac{X_i\hat{\mathbf{N}}_j'}{\hat{c}_t\hat{D}_{ij}}\right\} + \frac{\hat{\mathbf{N}}_i'}{\hat{c}_t\hat{D}_{iM}^e},$$

where we have introduced the following non-dimensional parameters

$$(10.24) \quad \beta = \frac{\Delta p_{ref}}{RTc_{ref}},$$

and

$$(10.25) \quad \Theta = \frac{F\Delta\Phi_{ref}}{RT}.$$

10.2 Driving Forces

From both physical insight and solution method, we are interested in simplifying the model as much as possible by retaining only important terms. We now consider the magnitudes of the driving forces to assess whether there are any driving forces that can be neglected. For the BFM, the driving forces are on the left hand side of Eqn (10.23).

10.2.1 Gradients in Activity Coefficients

The first simplifying assumption we make is that the gradients in activity coefficients are negligible $\left(X_i\hat{\nabla}\ln\gamma_i = 0\right)$. The activity coefficients for each species depend on the properties of the surrounding solution (i.e. mole fractions, species present, etc.). Throughout the membrane the type of species present will be similar although the mole fractions may vary. In order to simplify the model, and since no information is available on these coefficients for the pore fluid species, we assume the gradients in activity coefficient are negligible. This seems a reasonable approximation, which is commonly invoked in the literature [41]. The driving forces in Eqn. (10.23) become

$$(10.26) \quad \left(\hat{\nabla}X_i + \{X_i\hat{v}_i\beta\}\hat{\nabla}\hat{p} + \{X_iz_i\Theta\}\hat{\nabla}\hat{\Phi}\right).$$

10.2.2 Magnitude of The Driving Forces

We know that F is Faradays constant, R is the universal gas constant, T is the temperature of interest in Kelvin $(T \approx 348\,\text{K})$, η is the pore fluid mixture viscosity $\left(\eta = 3.565\times10^{-4}\ \text{kg}\cdot\text{m}^{-1}\cdot\text{s}^{-1}\right)$ [47], z_i is the charge number of species i $(z_1 = +1, z_2 = 0)$ and the non-dimensionalized mole density of hydronium (species 1) is

$$(10.27) \quad \hat{c}_1 = \frac{c_1}{c_{ref}} = \left(\frac{\alpha}{\lambda - \gamma}\right) = X_1.$$

Recall that we also assumed that the molar volume of hydronium is approximately the same as that for water

$$(10.28) \ \hat{v}_1 \approx \hat{v}_2 \approx V_{M,2} c_{ref} = 1$$

In Appendix A we calculate the coefficients for the driving force terms and they are summarized in Table 2.

Table 2: Comparing the relative magnitude of the driving forces in the transport equations

Gradient of Interest	Coefficient for Gradient Term	Coefficient Value	Approximate Order of Magnitude
$\hat{\nabla} X_1, \hat{\nabla} X_2$	1	1	~1
$\hat{\nabla}\hat{p}$	$X_1 \hat{v}_1 \beta$	$X_1(3.15 \times 10^{-3})$	~10^{-3}
	$X_2 \hat{v}_2 \beta$	$X_2(3.15 \times 10^{-3})$	~10^{-3}
$\hat{\nabla}\hat{\Phi}$	$X_1 \Theta$	$X_1(10.1)$	1-10

The above table helps to identify some of the dominant terms and elucidates several points. The first point is that compared to the potential and mole fraction gradient terms, we can neglect the pressure terms since they are of a significantly lower order than the other potential gradient term and the mole fraction gradient terms. The second observation is that the potential term Θ is the dominant term of the known coefficients.

11 Simplified Binary Friction Model

The objective of this work is to develop a transport model for the membrane that allows prediction of the conductivity of the membrane (transport of ionic species through the membrane) and, eventually, the transport of water through the membrane. Due to the geometry of the membrane and the nature of fuel cell operation we can consider transport through the membrane as being one-dimensional, occurring normal to the plane of the membrane $\left(\hat{\mathbf{N}}_i' = \hat{N}_i' \right)$. Thus we develop a simple 1-D model for transport within the membrane.

We start with the BFM equations for transport within the membrane. We simplify them according to the assumptions made in the previous section arriving at

$$(11.1) \quad -\left(\hat{\nabla}X_i + \Theta X_i z_i \hat{\nabla}\hat{\Phi}\right) = \sum_{j=1}^{n}\left\{\frac{X_j \hat{N}_i'}{\hat{c}\hat{D}_{ij}} - \frac{X_i \hat{N}_j'}{\hat{c}\hat{D}_{ij}}\right\} + \frac{\hat{N}_i'}{\hat{c}\hat{D}_{iM}^e} ,$$

recalling that primed molar fluxes are pore averaged-fluxes per unit *pore* surface area. We consider transport within an 1100 *EW* Nafion membrane assuming that we have only 2 species present in the pore fluid, hydronium ions (species i = 1) and water (species i = 2).

We can now write out the transport equations for both species starting with species 1 ($z_1 = 1$)

$$(11.2) \quad -\left(\hat{\nabla}X_1 + \Theta X_1 \hat{\nabla}\hat{\Phi}\right) = \left\{\frac{X_2 \hat{N}_1'}{\hat{c}\hat{D}_{12}} - \frac{X_1 \hat{N}_2'}{\hat{c}\hat{D}_{12}}\right\} + \frac{\hat{N}_1'}{\hat{c}\hat{D}_{1M}^e}$$

and for species 2, using that $\hat{D}_{ij} = \hat{D}_{ji}$ [56], we have ($z_2 = 0$)

$$(11.3) \quad -\left(\hat{\nabla}X_2\right) = \left\{\frac{X_1 \hat{N}_2'}{\hat{c}\hat{D}_{12}} - \frac{X_2 \hat{N}_1'}{\hat{c}\hat{D}_{12}}\right\} + \frac{\hat{N}_2'}{\hat{c}\hat{D}_{2M}^e} .$$

We can put the above into matrix form

$$(11.4) \quad -\left\{\begin{array}{c}\hat{\nabla}X_1 + \Theta X_1 \hat{\nabla}\hat{\Phi} \\ \hat{\nabla}X_2\end{array}\right\} = \frac{1}{\hat{c}}\left[\begin{array}{cc}\left(\dfrac{X_2}{\hat{D}_{12}} + \dfrac{1}{\hat{D}_{1M}^e}\right) & \dfrac{-X_1}{\hat{D}_{12}} \\ \dfrac{-X_2}{\hat{D}_{12}} & \left(\dfrac{X_1}{\hat{D}_{12}} + \dfrac{1}{\hat{D}_{2M}^e}\right)\end{array}\right]\left\{\begin{array}{c}\hat{N}_1' \\ \hat{N}_2'\end{array}\right\} .$$

We invert the matrix to get an expression for the fluxes in terms of the driving forces

$$(11.5) \quad \begin{Bmatrix} \hat{N}_1' \\ \hat{N}_2' \end{Bmatrix} = -\frac{\hat{c}}{\chi} \begin{bmatrix} \left(\dfrac{X_1}{\hat{D}_{12}} + \dfrac{1}{\hat{D}_{2M}^e} \right) & \dfrac{X_1}{\hat{D}_{12}} \\ \dfrac{X_2}{\hat{D}_{12}} & \left(\dfrac{X_2}{\hat{D}_{12}} + \dfrac{1}{\hat{D}_{1M}^e} \right) \end{bmatrix} \begin{Bmatrix} \hat{\nabla} X_1 + \Theta X_1 \hat{\nabla} \hat{\Phi} \\ \hat{\nabla} X_2 \end{Bmatrix},$$

where χ is the determinant of the matrix of diffusion coefficients in Eqn. (11.4),

$$(11.6) \quad \chi = \frac{X_1}{\hat{D}_{12} \hat{D}_{1M}^e} + \frac{X_2}{\hat{D}_{12} \hat{D}_{2M}^e} + \frac{1}{\hat{D}_{1M}^e \hat{D}_{2M}^e}.$$

We are now able to introduce our definitions of X_1 and X_2 into the above matrix, but first we consider the gradients in mole fraction. We know that both, X_1 and X_2 (Eqns. (9.24) and (9.25)), are functions of λ so that

$$(11.7) \quad \hat{\nabla} X_1 = \frac{\partial X_1}{\partial \lambda} \hat{\nabla} \lambda = \left\{ \frac{-\alpha \left(1 - \dfrac{\partial \gamma}{\partial \lambda} \right) + (\lambda - \gamma) \dfrac{\partial \alpha}{\partial \lambda}}{(\lambda - \gamma)^2} \right\} \hat{\nabla} \lambda$$

and

$$(11.8) \quad \hat{\nabla} X_2 = \frac{\partial X_2}{\partial \lambda} \hat{\nabla} \lambda = \left\{ \frac{\alpha \left(1 - \dfrac{\partial \gamma}{\partial \lambda} \right) - (\lambda - \gamma) \dfrac{\partial \alpha}{\partial \lambda}}{(\lambda - \gamma)^2} \right\} \hat{\nabla} \lambda.$$

Introducing the above expressions for mole fraction gradients and the mole fractions, as previously defined in Eqns. (9.24) and (9.25), into the transport equations we get

$$(11.9) \quad \begin{Bmatrix} \hat{N}_1' \\ \hat{N}_2' \end{Bmatrix} = \frac{-\hat{c}}{(\lambda-\gamma)\chi} \begin{bmatrix} \left(\dfrac{\alpha}{\hat{D}_{12}} + \dfrac{(\lambda-\gamma)}{\hat{D}_{2M}^e} \right) & \dfrac{\alpha}{\hat{D}_{12}} \\ \dfrac{(\lambda-\gamma-\alpha)}{\hat{D}_{12}} & \left(\dfrac{(\lambda-\gamma-\alpha)}{\hat{D}_{12}} + \dfrac{(\lambda-\gamma)}{\hat{D}_{1M}^e} \right) \end{bmatrix} \begin{Bmatrix} \left\{ \dfrac{-\alpha\left(1-\frac{\partial\gamma}{\partial\lambda}\right)+(\lambda-\gamma)\frac{\partial\alpha}{\partial\lambda}}{(\lambda-\gamma)^2} \right\} \hat{\nabla}\lambda + \Theta\left(\dfrac{\alpha}{\lambda-\gamma}\right)\hat{\nabla}\hat{\Phi} \\ \left\{ \dfrac{\alpha\left(1-\frac{\partial\gamma}{\partial\lambda}\right)-(\lambda-\gamma)\frac{\partial\alpha}{\partial\lambda}}{(\lambda-\gamma)^2} \right\} \hat{\nabla}\lambda \end{Bmatrix}$$

with

$$(11.10) \quad \chi = \frac{1}{\lambda-\gamma} \left(\frac{\alpha}{\hat{D}_{12}\hat{D}_{1M}^e} + \frac{(\lambda-\gamma-\alpha)}{\hat{D}_{12}\hat{D}_{2M}^e} + \frac{(\lambda-\gamma)}{\hat{D}_{1M}^e \hat{D}_{2M}^e} \right).$$

The transport equations can be simplified further to yield

$$(11.11) \quad \begin{Bmatrix} \hat{N}_1' \\ \hat{N}_2' \end{Bmatrix} = \frac{-\hat{c}}{(\lambda-\gamma)^2 \chi} \begin{bmatrix} \left(\dfrac{\alpha^2}{\hat{D}_{12}} + \dfrac{\alpha(\lambda-\gamma)}{\hat{D}_{2M}^e} \right)\Theta & \dfrac{\left\{ -\alpha\left(1-\frac{\partial\gamma}{\partial\lambda}\right)+(\lambda-\gamma)\frac{\partial\alpha}{\partial\lambda} \right\}}{(\lambda-\gamma)^2} \\ & \dfrac{\hat{D}_{2M}^e}{} \\ \dfrac{\alpha(\lambda-\gamma-\alpha)}{\hat{D}_{12}}\Theta & \dfrac{\left\{ \alpha\left(1-\frac{\partial\gamma}{\partial\lambda}\right)-(\lambda-\gamma)\frac{\partial\alpha}{\partial\lambda} \right\}}{(\lambda-\gamma)^2} \\ & \dfrac{\hat{D}_{1M}^e}{} \end{bmatrix} \begin{Bmatrix} \hat{\nabla}\hat{\Phi} \\ \hat{\nabla}\lambda \end{Bmatrix}.$$

We now have a set of equations describing transport within the membrane; however, we cannot solve this system because there is no information presently available in membrane literature on the transport coefficients (D_{12}, D_{1M}^e and D_{2M}^e), the number of fixed waters not participating in transport γ and the minimum water content λ_{min}. Therefore, in order to determine the transport coefficients we need to have data on the transport of species within the membrane under known conditions; this will then allow extraction of the transport coefficients.

Conductivity in PEMs is directly related to the transport of hydronium ions through the membrane. Conductivity happens to be currently the best-documented transport phenomenon that we can use to fit the parameters. Using the above transport model (Eqn. (11.11)) we will now explicate the development of what has been termed the Binary Friction Conductivity Model (BFCM), owing to its basis on the BFM.

We then use the BFCM model to fit experimental conductivity data, thus allowing us to back out reasonable estimates for the unknown parameters. It is at this point that we should note one of the advantages of using a transport model developed in such a fashion. By fitting the BFCM to conductivity data we are able to extract critical information on all the unknown parameters. We could then use such parameters in the transport model to predict water transport. However, the use of the parameters found from fitting the BFCM to conductivity data to predict water transport is beyond the scope of this work and has been left as possible future work. We focus instead on the development of the conductivity model and on determining reasonable values for the parameters.

12 Conductivity

12.1 Conductivity Data

We start with the conductivity data of SES [29] reported for Nafion 117 in the E-form (no heat treatment), measured using a four-electrode AC impedance method. We assume that the ability to fit to this data is indicative of an ability to represent data for Nafion in any form (i.e. normal or shrunken form). However, in order to compare the ability to fit to the data we have chosen the E-form since this is what Thampan uses to compare his model to. Since the membranes used in fuel cells are typically heated in the manufacture of the membrane electrode assembly, it may be more appropriate to fit to the data for a membrane in the N or S form.

In the experimental work of SES, a sample pretreated in the conventional way [29] was fixed in an apparatus where two platinum electrodes feed current to the membrane while two platinum needles measured the corresponding potential drop. Data was collected for

samples at various temperatures. For each temperature the activity (p/p$_{sat}$(T)) of the water vapor the membrane was equilibrated with was varied and the corresponding conductivity was measured to allow for the plotting of conductivity as a function of water vapor activity over a range of temperatures (Fig. 13). SES calculated the conductivity in the plane of the membrane using the relation

$$(12.1) \quad \sigma_{SES} = \frac{l}{R_{mem}A},$$

where R_{mem} is the measured resistance of the membrane, l is the distance between the reference electrodes (the platinum needles) and A is the cross sectional area of the membrane calculated by assuming that the membrane is 200 μm thick [29].

Even though this conductivity data is taken for a Nafion 117 membrane and is measured in the plane of the membrane, we would expect that it would provide a reasonable measure of the conductivity in the direction normal to the surface of the membrane, since the properties of Nafion are expected to be reasonably isotropic, as there is no apparent ordering of the macromolecules in any preferential direction, other than that the sulfonate sites tend to cluster together. In addition we assume that the membrane is heterogeneous.

One must consider, however, that since the conductivity is not measured across the membrane in the direction normal to the surface, the membrane surfaces may have some effect on the conductivity. However, we have neglected surface effects and we assume that conductivity data measured by SES represents the conductivity of all 1100 *EW* Nafion membranes since they all have the same molecular structure, the only difference is the thickness.

The conductivity data (in S cm^{-1}) collected was fitted with a third degree polynomial of the form [29]

$$(12.2) \quad \sigma_{SES} = a + bx + cx^2 + dx^3,$$

where x is the relative humidity $\left(x = 100 \dfrac{p}{p_{sat}(T)} \right)$. The coefficients a, b, c and d can be found in the paper of SES for various temperatures. We will use the values for the E-form of Nafion for 30°C in the fitting process:

$$(12.3) \quad \begin{aligned} a &= -8.01 \times 10^{-3}\,\mathrm{S \cdot cm^{-1}} \\ b &= 6.72 \times 10^{-4}\,\mathrm{S \cdot cm^{-1}} \\ c &= -11.6 \times 10^{-6}\,\mathrm{S \cdot cm^{-1}} \\ d &= 11.8 \times 10^{-8}\,\mathrm{S \cdot cm^{-1}} \end{aligned}\,,$$

and 70°C

$$(12.4) \quad \begin{aligned} a &= -1.56 \times 10^{-3}\,\mathrm{S \cdot cm^{-1}} \\ b &= 1.21 \times 10^{-4}\,\mathrm{S \cdot cm^{-1}} \\ c &= 1.01 \times 10^{-6}\,\mathrm{S \cdot cm^{-1}} \\ d &= 3.95 \times 10^{-8}\,\mathrm{S \cdot cm^{-1}} \end{aligned}$$

The data for 30°C is used to fit the parameters since the sorption isotherm data is available from a number of different sources at or near 30°C.

The data at 70°C will be used to see how the parameters vary with temperature, since this temperature better falls within the range of reasonable fuel cell operating temperatures. We want to be certain that we can predict the conductivity at this temperature. We do not fit to the data at 70°C since sorption isotherm data at this temperature is not presently available and we only currently have one source of sorption isotherm data for 80°C. Note also that the conductivity data is only available for an E-form Nafion 117 membrane at 70°C but not at 80°C.

12.2 Sorption Isotherms

One of the difficulties is that the conductivity data of SES is given as a function of activity $(\sigma = \sigma(a))$ of the water vapor the membrane is equilibrated with, whereas our model and the models of SZG [39] and TMT [41] give conductivity as a function of λ, which we recall is the number of water molecules sorbed by the membrane per sulfonate head. Sorption isotherms provide water content (λ) as a function of the water vapor activity (see Figure 21 Below).

Casting conductivity as a function of λ, rather than activity, is more physical in that this relates to the number of waters per sulfonate head and allows a clearer view of how the number of waters sorbed by the membrane per sulfonate head affects the conductivity; for instance, this illustrates quite clearly what is the minimum numbers of waters that must be sorbed before the membrane becomes significantly conductive. Also, λ appears in our transport equations, while *a* does not.
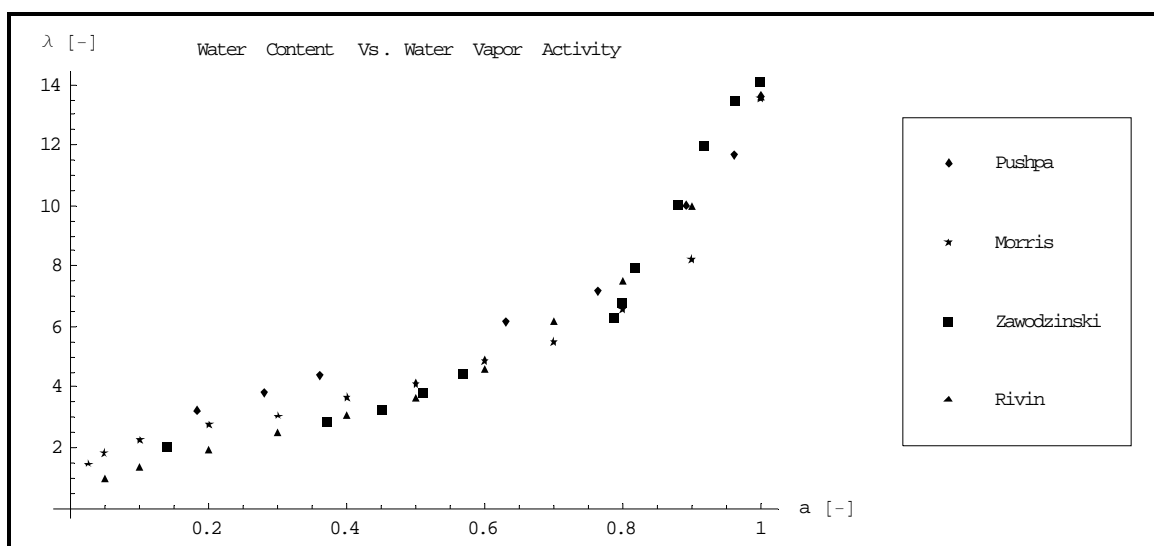
Figure 21: Water content in number of water molecules per sulfonate head (λ) plotted against activity (a) of water vapor the membrane is equilibrated with for 1100 *EW* Nafion membranes at 30°C (Zawodzinski), 25°C (Pushpa and Morris) and a range between 20 and 32°C (Rivin) [30].

It is at this point that we should make a careful note of the type of Nafion membranes used to collect the above information. Zawodzinski, Springer, Davey et al. [14] (hereafter reffered to as ZSD), Morris and Sun [62] and Pushpa, Nandan and Iyer [63] all

used Nafion 117, an 1100 *EW* membrane, in their experimental measurements. Rivin, Kendrick, Gibson et al. [64] report on 1100 *EW* membranes of varying thickness (Nafion 112, 115 and 117). We assume that since all of these membranes are of the same equivalent weight, with only varying thickness, the data should well represent the Nafion 1100 *EW* family of membranes, since thickness should only have a minor influence on sorption due to possible surface effects. However, of these authors only ZSD note that the temperature history (pretreatment) may have some effect on the sorption of water, and that the number of waters sorbed by a vapor-equilibrated membrane varies with temperature history (see Table 3 below).

Table 3: Effect of Temperature History on Water Uptake (λ) for Liquid Equilibrated Membranes [14]

Membrane	No thermal treatment Re-hydration temperature 27°C<T<94°C	Dried at 105°C Re-hydration temperature		
		27°C	65°C	80°C
Nafion 117	$\lambda = 21$	$\lambda = 12$	$\lambda = 14$	$\lambda = 16$

We know that there should be a noticeable jump in the number of waters sorbed when going from a membrane equilibrated with saturated water vapor to a liquid-equilibrated membrane (cf. Schroeder's Paradox). All data presented in Fig. 21 indicate that roughly 14 waters are sorbed per sulfonate head when equilibrated with saturated vapor. Close examination of Table 3 shows that for the liquid-equilibrated membrane, the one with no thermal pretreatment will sorb 21 waters per sulfonate head, as opposed to a maximum of 16 for the pretreated membranes. Given that we anticipate a large jump in water content, we conclude that the data presented is for membranes with no heat treatment (E-form) since the jump from 14 to 21 is more significant than that from 14 to 16 for the heat-treated case. We also note that the jump in water content from 14 to 21 can be seen in the data collected by Kreuer [18]. From this point on all sorption data is assumed to be for Nafion membranes in the E-form (no heat treatment).

12.2.1 1100 EW Nafion Sorption Isotherm Fit at 30°C

In order to change the experimentally measured data of SES from being a function of relative humidity *x* to a function of water content we need the activity (*a*) as a function of water content (λ). We can use the available sorption isotherm data with λ as the

independent variable and activity as the dependant variable and use a least squares fit of a third degree polynomial in order to get $a = a(\lambda)$. The resulting expression for activity as a function of water content is

(12.5) $a = b_0 + b_1\lambda + b_2\lambda^2 + b_3\lambda^3$.

The coefficients were found to be

(12.6)
$$\begin{aligned}
b_0 &= -0.246 \\
b_1 &= 0.232 \\
b_2 &= -0.0147 \\
b_3 &= 3.149 \times 10^{-4}
\end{aligned}$$

In addition a regression analysis of the sorption isotherm curve fit was performed to determine the standard deviation (standard error (SE)) of the fit to the data. The largest standard error was found to be

(12.7) $SE = 0.03843$.

The largest standard error was added or subtracted from the least squares fit to estimate the error in our curve fit,

(12.8) $a = b_0 + b_1\lambda + b_2\lambda^2 + b_3\lambda^3 \pm SE$.

This error estimate was then plotted, along with the curve fit (See Figure 22 below), to ensure that a reasonable number of data points lay within and outside the error bounds (roughly 50/50) and that the curve fit provided a reasonable representation of the data.

Figure 22: Plot of sorption isotherm data for 1100 EW Nafion membranes at 30°C with curve fit and dotted lines showing error estimate.

12.2.2 1100 EW Sorption Isotherm Fit at 80°C

We assume that the data available at 80°C is for a membrane with no heat-treatment (E-Form) and we apply the same procedure as described above on the available Nafion 117 data at 80°C. A polynomial of the form

$$(12.9) \quad a = b_0 + b_1\lambda + b_2\lambda^2 + b_3\lambda^3 + b_4\lambda^4$$

was fit, using a least squares fit, to the available data [65]. A higher degree fit (fourth degree) was used for the data at 80°C as it provided a better representation of the data than the lower degree fit used at 30°C. The coefficients were found to be

$$
\begin{aligned}
b_0 &= -0.00562 \\
b_1 &= 0.0146 \\
(12.10)\ b_2 &= 0.0685 \qquad . \\
b_3 &= -0.0115 \\
b_4 &= 5.60\times10^{-4}
\end{aligned}
$$

The largest standard error was found to be

$$(12.11)\ SE = 0.0312\ .$$

Once again the largest standard error was added or subtracted from the least squares fit to estimate the error in our curve fit,

$$(12.12)\ a = b_0 + b_1\lambda + b_2\lambda^2 + b_3\lambda^3 + b_4\lambda^4 \pm SE\ .$$

The error estimate was then plotted, along with the curve fit (See Figure 23 below), to ensure that a reasonable number of data points lay within and outside the error bounds (roughly 50/50) and that the curve fit provided a reasonable representation of the data.
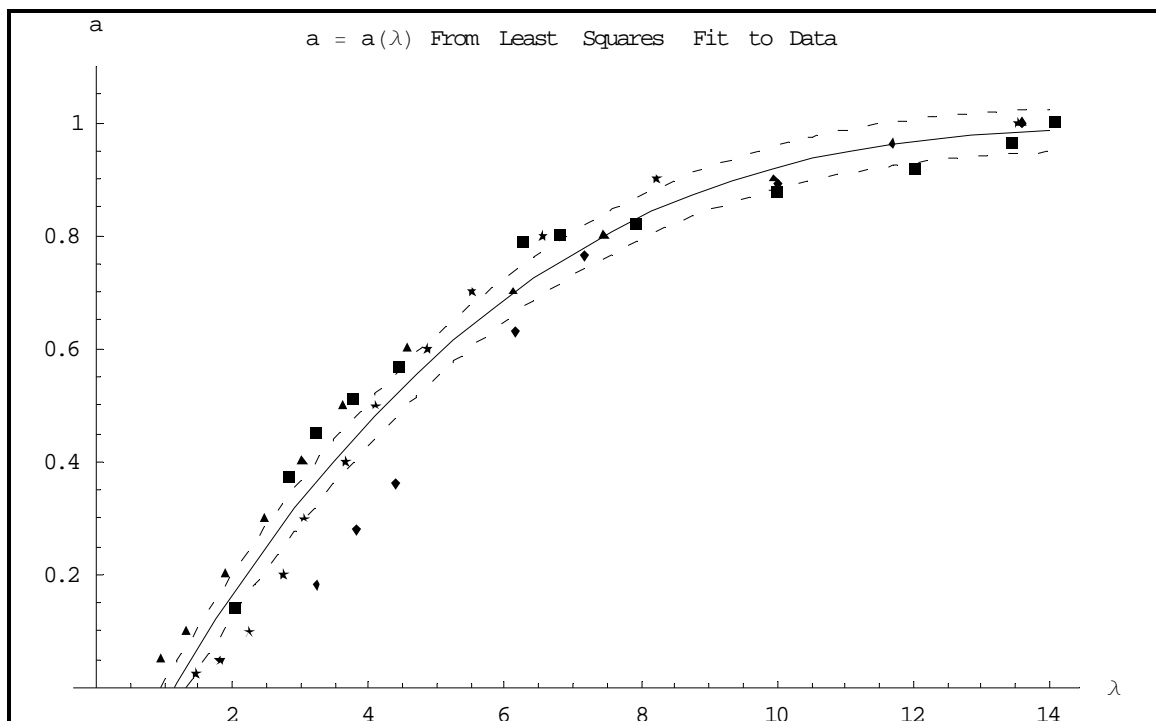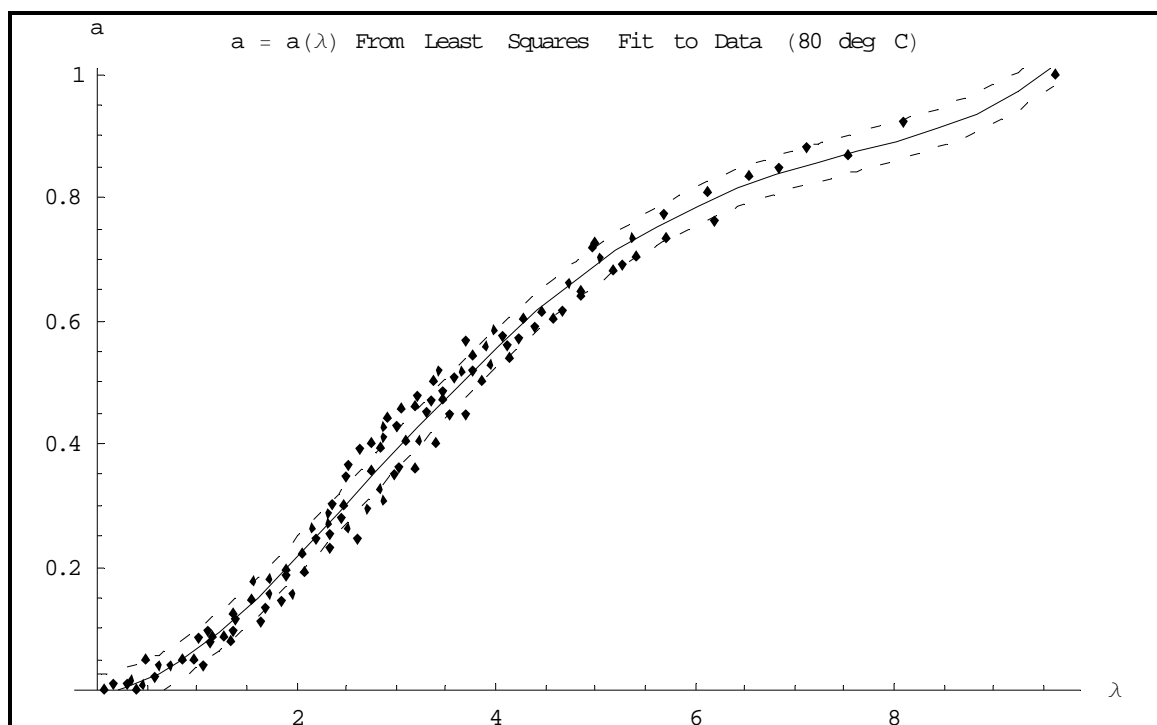

Figure 23: Plot of sorption isotherm data for 1100 EW Nafion at 80°C [65] with curve fit and dotted lines showing error estimate.

We now have the data available to plot the conductivity as a function of the water content. We should also note the behavior of the curve fit at low water contents. As

previously discussed there is some dispute over whether the plot should cross through the origin or not. Since the conductivity data of Sone drops to zero below relative humidity of approximately 12% (activity of 0.12) we are not concerned with what happens below this relative humidity, since no transport occurs. The water content that gives us an activity of 0.12 ($\lambda \sim 1.75$) lies within the portion of the sorption curve that is above the x-axis on both sorption curves, thus it does not matter if they do not terminate at the origin since we are not interested in the conductivity behavior in that region. However, the slope of the sorption isotherm curves near the origin may be slightly different if in fact they were to go through the origin, thus an element of error may be introduced due the relaxation of the condition that the curves must go through the origin.

12.3 Conductivity Model

The conductivity data measured by SES was measured using alternating current, on a membrane that was uniformly equilibrated with water vapor. We can assume that there is no initial gradient in water content $\left(\dfrac{\partial \lambda}{\partial x} = 0\right)$. Since the current alternates direction rapidly we can assume that no significant transport of water is occurring. This last assumption means that no gradient in water content is developed as the alternating current is passed through the membrane. Applying these assumptions to the transport equations derived above (Eqn. (11.11)) we have

$$(12.13) \quad \left\{ \begin{array}{c} \hat{N}_1' \\ \hat{N}_2' \end{array} \right\} = \frac{-\hat{c}}{(\lambda-\gamma)^2 \chi} \left\{ \begin{array}{c} \left(\dfrac{\alpha^2}{\hat{D}_{12}} + \dfrac{\alpha(\lambda-\gamma)}{\hat{D}_{2M}^e} \right)\Theta \\ \\ \dfrac{\alpha(\lambda-\gamma-\alpha)}{\hat{D}_{12}}\Theta \end{array} \right\} \hat{\nabla}\hat{\Phi} .$$

Since we have assumed that we can neglect water transport as we are using alternating current (AC), we neglect the transport of the water species and only consider transport of hydronium ions.

We reintroduce the determinant (χ) to get

$$(12.14) \; \hat{N}_1' = \frac{-\hat{c}}{\lambda - \gamma} \frac{\dfrac{\alpha^2}{\hat{D}_{12}} + \dfrac{\alpha(\lambda - \gamma)}{\hat{D}_{2M}^e}}{\dfrac{\alpha}{\hat{D}_{12}\hat{D}_{1M}^e} + \dfrac{\lambda - \gamma - \alpha}{\hat{D}_{12}\hat{D}_{2M}^e} + \dfrac{\lambda - \gamma}{\hat{D}_{1M}^e \hat{D}_{2M}^e}} \Theta \hat{\nabla}\hat{\Phi} .$$

Now, we reintroduce the dimensional quantities and simplify to get an expression for the pore averaged molar flux of hydronium ions

$$(12.15) \; N_1' = \frac{-c_t}{\lambda - \gamma} \frac{F}{RT} \frac{\dfrac{\alpha^2}{D_{12}} + \dfrac{\alpha(\lambda - \gamma)}{D_{2M}^e}}{\dfrac{\alpha}{D_{12}D_{1M}^e} + \dfrac{\lambda - \gamma - \alpha}{D_{12}D_{2M}^e} + \dfrac{\lambda - \gamma}{D_{1M}^e D_{2M}^e}} \nabla\Phi .$$

The current density is related to the ionic fluxes by

$$(12.16) \; i = F\sum_{i=1}^{n} z_i N_i .$$

We require molar fluxes based on the surface area of the *membrane*, rather than pore averaged fluxes based on the *pore* area. Recall that we use the Bruggeman correction to convert pore-averaged fluxes to molar fluxes based on the surface area of the *membrane*, thus we have

$$(12.17) \; i = F(\varepsilon - \varepsilon_0)^q N_1' = F(\varepsilon - \varepsilon_0)^q \frac{-c_t}{\lambda - \gamma} \frac{F}{RT} \frac{\dfrac{\alpha^2}{D_{12}} + \dfrac{\alpha(\lambda - \gamma)}{D_{2M}^e}}{\dfrac{\alpha}{D_{12}D_{1M}^e} + \dfrac{\lambda - \gamma - \alpha}{D_{12}D_{2M}^e} + \dfrac{\lambda - \gamma}{D_{1M}^e D_{2M}^e}} \nabla\Phi .$$

Conductivity is defined as

$$(12.18) \quad \sigma \equiv \frac{-i}{\nabla \Phi},$$

therefore,

$$(12.19) \quad \sigma = \left(\varepsilon - \varepsilon_0\right)^q \frac{c_t F^2}{RT(\lambda - \gamma)} \cdot \frac{\dfrac{\alpha^2}{D_{12}} + \dfrac{\alpha(\lambda - \gamma)}{D_{2M}^e}}{\dfrac{\alpha}{D_{12}D_{1M}^e} + \dfrac{\lambda - \gamma - \alpha}{D_{12}D_{2M}^e} + \dfrac{\lambda - \gamma}{D_{1M}^e D_{2M}^e}}.$$

Recall that we have an expression for the porosity ε as a function of water content, Eqn. (9.20).

12.3.1 Dissociation Model

The degree of dissociation α can be determined by using the thermodynamic equilibrium model of TMT [41]

$$(12.20) \quad \alpha = \frac{(\lambda + 1) - \sqrt{(\lambda + 1)^2 - 4\lambda\left(1 - \dfrac{1}{K_{A,C}}\right)}}{2\left(1 - \dfrac{1}{K_{A,C}}\right)},$$

where $K_{A,C}$ is the equilibrium constant for proton solvation in terms of mole densities [41]

$$(12.21) \quad K_{A,C} = K_{A,C,298} \exp\left[-\frac{\Delta H^0}{R}\left(\frac{1}{T} - \frac{1}{298}\right)\right] \quad \text{and}$$

$$(12.22) \quad \begin{aligned} \Delta H^0 &= -52.3\,kJ/mol \\ K_{A,C,298} &= 6.2 \end{aligned}.$$

We plot the degree of dissociation in Fig. 24 and we can see that the first two waters sorbed by the membrane ($\lambda = 2$) cause a significant portion of the protons to dissociate from the sulfonate heads to form hydronium ions.
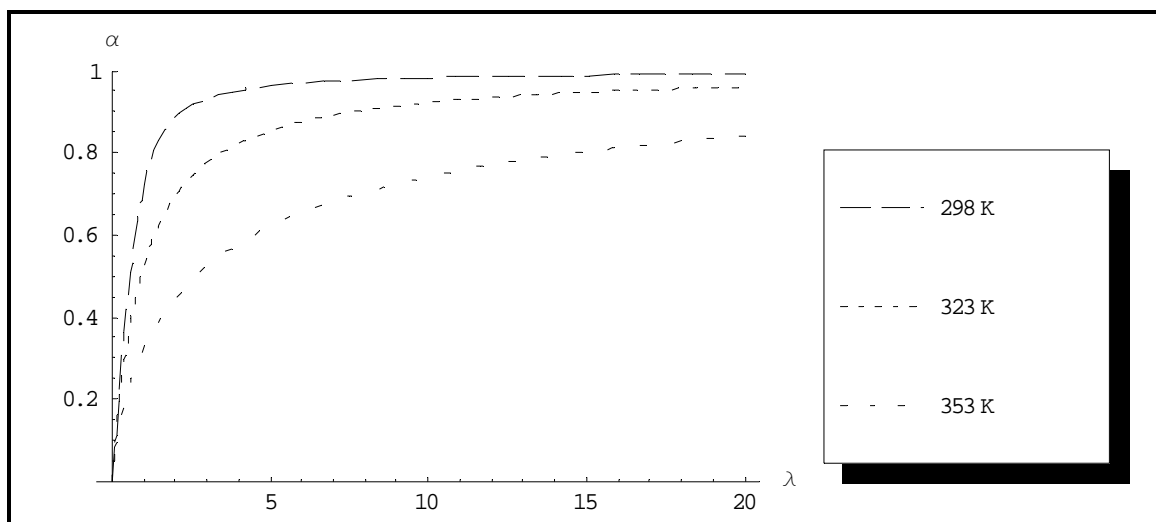

Figure 24: Degree of dissociation α for various temperatures, calculated using equilibrium model of TMT.

12.3.2 Functional Dependence of Diffusion Coefficients on Water Content (λ)

12.3.2.1 Hydronium-Water Interaction *(D_{12})*

We assume that the interaction between the water and the hydronium ions does not depend on water content. The Stefan-Maxwell coefficients for systems of nonideal fluids are concentration dependent, but this dependence is not as significant as the concentration dependence of the Fick diffisuvities [55]. In one extreme case the Stefan-Maxwell coefficients varied only by a factor of 1.5 while the Fick diffusivities varied by a factor of 20 [55]. It is therefore expected that the error introduced in neglecting the weak dependence of D_{12} on water content would be insignificant, even in the presence of large composition gradients within the membrane.

12.3.2.2 Hydronium-Membrane Interactions *(D^e_{IM})*

We do not have knowledge of the membrane interaction terms. It seems reasonable that the interactions between the membrane and various species should depend on the water content due to changes in the geometry of the membrane and the proximity of the species

to the membrane. However, we are unsure of this dependence. In order to try to fit our model to the conductivity data we attempt to estimate the nature of the dependence of the membrane interaction terms by considering the nature of the forces acting on the species. We start with the interaction between hydronium ions and the membrane.

We have assumed in the BFM that the membrane is a "dust" with which the particle interacts to generate friction. We would assume that the more volume V there is, the less likely are interactions between membrane and hydronium ions; in addition, the more surface area SA there is, the more likely are interactions, so the friction coefficient between the membrane and hydronium ions $\left(f_{1M}\right)$ should have the dependence

$$(12.23)\ f_{1M} \propto \frac{SA}{V},$$

i.e. the larger the surface area (SA) the larger the friction, the larger the volume (V) the smaller the friction. Since D_{1M}^{e} has the significance of an inverse friction coefficient we would anticipate that

$$(12.24)\ \begin{aligned} D_{1M}^{e} &\propto \frac{V}{SA} = \frac{\pi (r)^{2} L}{2\pi r L}, \\ D_{1M}^{e} &\propto r \end{aligned}$$

where we have assumed an approximately cylindrical pore with radius r and length L. The above result makes sense in that as the radius grows with swelling the hydronium ions are able to move more freely ($D^{e}{}_{1M}$ grows).

12.3.2.3 Water-Membrane Interactions ($D^{e}{}_{2M}$)

The interactions between the membrane and the water molecules are different than those between the membrane and the hydronium ions. However, the likelihood of interactions increases with surface area and decreases with volume, so we would anticipate a similar dependence of D_{2M}^{e} on volume and surface area as we found for D_{1M}^{e}. Thus,

$$(12.25) \quad D^e_{2M} \propto \frac{V}{SA}.$$
$$D^e_{2M} \propto r$$

12.3.2.4 Dependence of Pore Radius (*r*) on λ

Assuming that the pores within the membrane are approximately cylindrical we have that

$$(12.26) \quad V = \pi r^2 L.$$

We also know that the volume of the pore is proportional to the water content

$$(12.27) \quad V \propto \lambda,$$

therefore,

$$(12.28) \quad r^2 L \propto \lambda.$$

We are interested in the dependence of the radius on water content, which is anticipated to be of the form

$$(12.29) \quad r = \lambda^{1/s}$$

where *s* is some constant. Therefore, we would expect a power law relationship of the above form, relating radius to λ. Plugging this into the above expressions for membrane diffusion coefficients we would anticipate the following dependence of the membrane diffusion coefficients on water content

$$(12.30) \quad D^e_{1M} \propto \lambda^{1/s}$$

and

(12.31) $D^e_{2M} \propto \lambda^{1/s}$.

These relations will be used when we attempt to fit our theoretical curve to the data provided by Sone.

12.3.3 Summary of Conductivity Model Development

In the BFCM developed in the previous sections (Eqn.12.19), results from simplifying the binary friction transport model (Eqn. 11.11), according to the conditions of the AC impedance experiments used to measure conductivity. The use of AC impedance measurements allows us to neglect water transport and gradients in water content (λ). This model requires the determination of several parameters (Table 4) using constitutive relations, complementary models or empirical data.

Table 4: Parameters required for implementation of the BFCM

Parameter	Determination
α, fraction of dissociated acid heads	Eqn. 12.20
ε, porosity	Eqn 9.20
ε_0, threshold porosity	Empirical fit
q, Bruggeman exponent	1.5 [41]
D_{12}, diffusion coefficient (hydronium – water)	Empirical fit
D^e_{1M}, diffusion coefficient (hydronium – membrane)	Eqn. 12.30, Empirical fit
D^e_{2M}, diffusion coefficient (water – membrane)	Eqn. 12.31, Empirical fit
s, exponent for diffusion coefficients	Empirical fit
γ, number of water molecules "stuck" to sulfonate heads	Empirical fit

A model is available for the dissociation behavior, which provides the fraction of dissociated acid groups (Eqn. 12.20), and porosity can be determined from a constitutive relation (Eqn. 9.20), with the value of q commonly taken to be 1.5 [41].

D_{12} does not depend on water content, and we have proposed a functional dependence of the diffusion coefficients D^e_{1M} and D^e_{2M} on water content (Eqns. 12.30 and 12.31), however, the values of D_{12}, D^e_{1M} and D^e_{2M}, and of the exponent s are unknown. The threshold porosity ε_0 and the number of fixed waters per sulfonate head γ are also unknown. By fitting the BFCM to experimental conductivity data we will obtain estimates for D_{12}, D^e_{1M}, D^e_{2M}, ε_0, γ, and s. Once determined, these parameters could be

reintroduced into the binary friction transport model (Eqn. 11.11) to predict water transport, however, this is beyond the scope of this work.

13 Determining Conductivity Model Parameters

The parameters required in the model developed in the preceeding sections (D_{12}, D_{1M}^e and D_{2M}^e, ε_0, γ, and s) are determined based on the experimental data of SES at two temperatures, 30 and 70°C. Since in our model $\sigma = \sigma(\lambda)$, SES data $\sigma = \sigma(a)$ needs to be converted. The conversion involves a curve fit of the sorption isotherms. Prior to determining the model parameters and analyzing the validity of the values obtained, we first examine the error introduced by converting SES's conductivity data.

13.1 Fitting Conductivity at 30°C

13.1.1 Introduction of Error Due to Fit to Data

The conductivity plot of SES (Eqns. (12.2) and (12.3)) was modified to plot the conductivity as a function of water content by using Eqn. (12.8). We used this range of activity values to plot the range in which the conductivity data may lie by substituting Eqn. (12.8) into Eqn. (12.2) (See Figure 25).

We should stress that Figure 25 accounts only for the error in fitting the sorption isotherm data and doesn't include experimental errors associated with the measurements of conductivity versus water vapor activity. However, since any fit that lies within this error estimate would fall well within any estimate of the total error, a fit to this data is considered satisfactory.
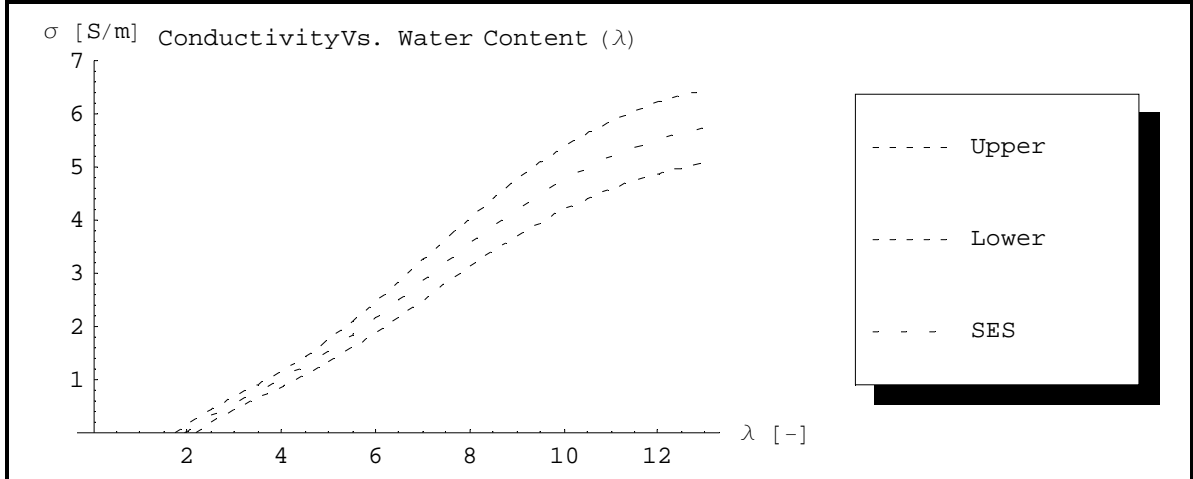
Figure 25: Conductivity for E-form of Nafion 117 versus water content (λ) at 30°C plotted using least squares fit to sorption isotherm data. Standard error in sorption isotherm curve fit is used to provide an estimate of expected error and thus a range within which any curve fit should lie.

13.1.2 Fitting The Curve

Our model has several parameters, which we can be adjusted to provide a fit to the above curve. The choices should however be constrained by physical considerations.

The threshold porosity is defined as

$$(13.1) \quad \varepsilon_0 = \frac{\lambda_{min} - \gamma}{\lambda_{min} + \dfrac{V_{M,M}}{V_{M,2}}},$$

where λ_{min} is the minimum amount of water that must be sorbed by the membrane for the pore liquid phase to be sufficiently well connected to allow for transport through the membrane. Examining Fig. 25, it is clear that λ_{min} should lie somewhere between 1.5 and 2, since this is the approximate range where the conductivity bounds intersect the x-axis.

The diffusion coefficient D_{12} does not vary with water content, so we assume it is a constant at this point and use it as a reference diffusion coefficient. Introducing proportionality constants in relations (12.34) and (12.35) we get

$$(13.2) \quad D_{1M}^e = D_{12} A_1 \lambda^{1/s},$$

and

(13.3) $D_{2M}^e = D_{12} A_2 \lambda^{1/s}$.

A_1, A_2, s and the magnitude of D_{12} can be varied to obtain a fit that lies within the upper and lower curves of Figure 25. As an additional guide in fitting the conductivity curve we calculated the relative error of our conductivity fit relative to the experimental curve of SES

(13.4) $\%error = 100\left(\dfrac{\sigma_{SES} - \sigma}{\sigma_{SES}}\right)$.

The relative error in the conductivity was plotted (see Fig. 26) as a function of water content to keep this error within a reasonable range while obtaining a fit that fell within the range of conductivity values defined by the standard error in the sorption isotherm curve fit.

Implementing the conductivity model the values for the parameters we obtained were

(13.5) $\lambda_{min} = 1.65$,

(13.6) $D_{12} = 6.5 \times 10^{-9} \, m^2 \, s^{-1}$,

(13.7) $s = 1.3$,

(13.8) $A_1 = 0.084$

and

(13.9) $A_2 = 0.5$.

The minimum water content λ_{min} was chosen such that the conductivity threshold of our model closely matched the data of SES. A reasonable order of magnitude for D_{12} was chosen from a literature survey, A_1, $A_{2,}$ s, and the value of D_{12} were then varied such that the BFCM results lay within the error bounds at all times.

Considering the A_1 and A_2 parameters, these terms reflect the relative size of D^e_{1M} and D^e_{2M} respectively. Since hydronium ions have a net charge while water has no net charge, we expect the interaction forces between the membrane (with charged sulfonate heads) and the hydronium ions to be different than the forces between the membrane and water. In addition, we would anticipate the interaction forces to be larger between the hydronium ions and the membrane than the membrane and water because of the additional interaction forces due to the charge on the sulfonate heads and the hydronium ions. The larger the interaction forces between the membrane and a species, the smaller D^e_{iM} is, thus we assume A_1 is smaller than A_2 due to the additional forces.

In our fitting procedure we also found $\gamma = 0$ which implies that there were no water molecules that were so strongly bonded to the sulfonate heads that they did not contribute to transport.

This is an interesting result in that it indicates that all the waters sorbed by the membrane are participating in the transport that is occurring. Even though this parameter was found to be zero for Nafion membranes, it is recommended to leave this parameter in the model for generality. Other families of membranes may not behave in the same fashion, and this parameter may prove useful.

Analyzing the plot of absolute error (see Figure 26 below) we notice that over a wide range of λ values (approximately 2 to 14) the error is approximately equal to or less than 12.5%. Examining the plot of our conductivity curve compared to the conductivity curves resulting from our error estimate (Figure 27) we see that we are able to achieve a

fit within the anticipated range of conductivity values over the entire range of water contents.

Note that our absolute percent error only exceeds 12% as we approach water contents near two. Considering low water contents (λ of about 2), where our model error grows significantly, we compare our error to the maximum possible error introduced by the curve fit to sorption isotherm data (Figure 28). We see that error in the fitting of sorption isotherms (the only error estimate we have considered) can, at all water contents, introduce more error than the difference between our model and the measurement of SES. In addition, at low water contents the absolute error is small, while, the relative error is large since conductivity values are small.

Finally it should be noted that though the simple fitting procedure adopted is adequate for this phase of the work, and appears to yield satisfactory parameter estimates, more systematic procedures should be investigated in the future.
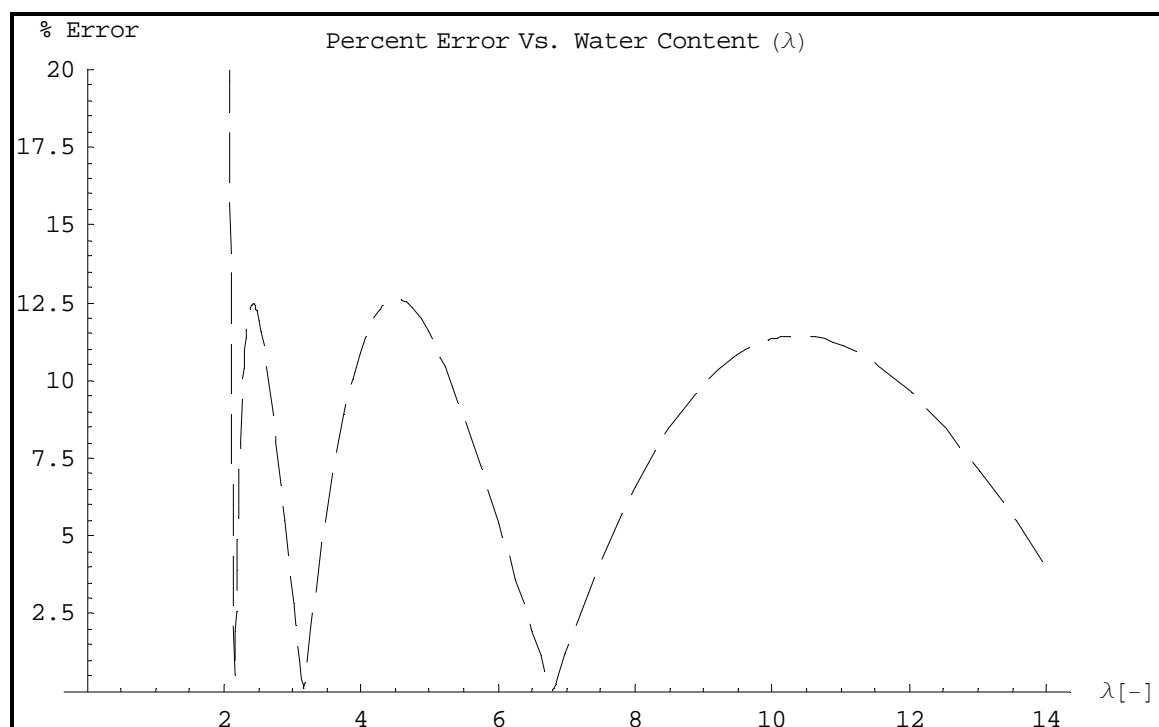
Figure 26: Plot of absolute percent error of BFCM relative to SES's experimental results at 30°C.
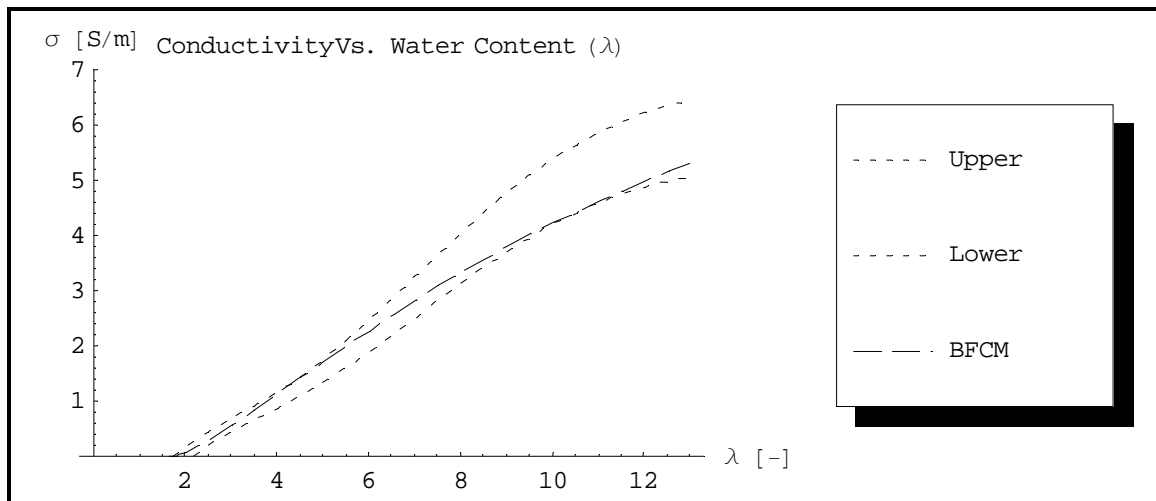
Figure 27: Plot of BFCM and anticipated upper and lower bounds on conductivity resulting from expected error in fit to sorption isotherm data at 30°C.
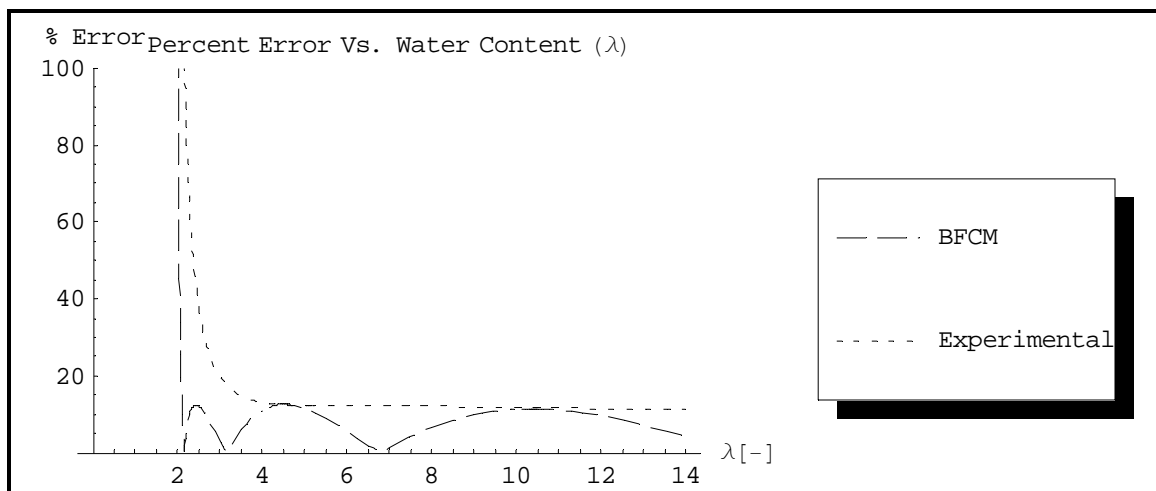

Figure 28: Plot of absolute percent error in BFCM compared to percent error due to error in fit to experimental data.

13.1.3 Analyzing Magnitude of Parameters

Although we have used several guides in fitting the parameters to the experimental data (i.e. percent error and ability to fall within the expected range of conductivity), it is beyond the scope of this work to perform an exhaustive analysis of the parameters involved. However, to verify that the obtained diffusion coefficients (D_{12}, D^e_{1M} and D^e_{2M}) are reasonable, we have varied the parameter D_{12} by an order of magnitude (larger and smaller) and then selected A_1 and A_2 values for the best possible fit to the conductivity data of Sone at 30°C.

First we decreased the value of D_{12} by one order of magnitude to 6.5×10^{-10} m^2 s^{-1} (Figure 29). The value of the fit parameters A_1 and A_2 were found to be 1.2 and 10 respectively. Then we increased the value of D_{12} to 6.5×10^{-8} m^2 s^{-1} (Figure 30). The values of A_1 and A_2 were found to be .007 and .05 respectively.

σ [S/m] ConductivityVs. Water Content (λ)

Upper

Lower

BFCM

λ [-]
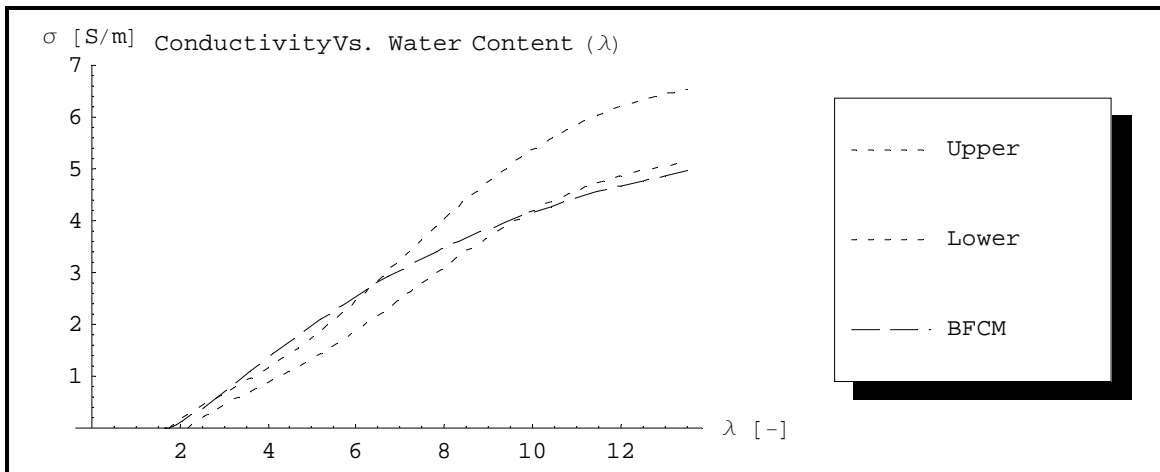
Figure 29: BFCM plotted against expected range of conductivity values for $D_{12} = 6.5\times10^{-10}$ m^2 s^{-1}.

σ [S/m] ConductivityVs. Water Content (λ)

Upper

Lower

BFCM

λ [-]
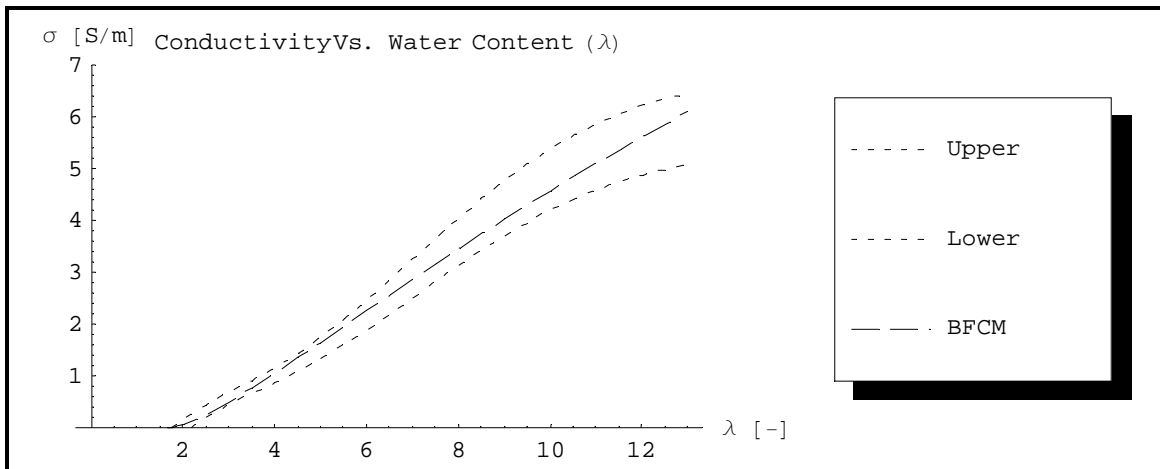
Figure 30: BFCM plotted against expected range of conductivity values for $D_{12} = 6.5\times10^{-8}$ m^2 s^{-1}.

From Figure 29 we note that this fit is very poor. Since larger D_{12} values provide a significantly better fit (Figures 27 and 30), this suggests that D_{12} should at least be on the order of 10^{-9} m^2 s^{-1}.

We note from Figure 30 that for D_{12} of 6.5×10^{-8} m^2 s^{-1} the curve lies closer to the centre of the error bounds than that for D_{12} of 6.5×10^{-9} m^2 s^{-1} (Figure 27). That said, there are a few points to support the choice of a D_{12} value of 6.5×10^{-9} m^2 s^{-1}. First, we note that any fit lying entirely within the error bounds given by the analysis the sorption isotherm data is considered entirely satisfactory.

The second point of note is regarding the order of the D_{12} values that provide a reasonable fit. In an attempt to determine what order of magnitude we would expect for D_{12} a survey of values reported in the literature was done. Verbrugge and Hill [49] do report a value of $\mathcal{D}_i$ of the Nernst-Planck equation for protons of 4.5×10^{-9} m^2 s^{-1}.

Considering that the Nernst-Planck equation is really a simplification of the Stefan-Maxwell equations where the solute species (in this case protons), is infinitely diluted by a solvent (in this case water), the $\mathcal{D}_i$ is really a Stefan-Maxwell diffusion coefficient. Therefore, we would anticipate our D_{12} value to be on the order of 4.5×10^{-9} m$^2 \cdot$s^{-1}, which suggests that $D_{12} = 6.5 \times 10^{-9}$ m^2 s^{-1} is a better choice since it is on the same order of magnitude.

A further point to note is that regardless of the order of magnitude of D_{12} we found that the $D^e{}_{1M}$ and $D^e{}_{2M}$ that provided for reasonable fits were of the same order of magnitude. For example for $D_{12} = 6.5 \times 10^{-10}$ m^2 s^{-1} we have (from 13.2 and 13.3)

$$(13.10) \quad D^e_{1M} = 7.8 \times 10^{-10} \lambda^{1/s} \ \text{m}^2 \ \text{s}^{-1}$$

and

$$(13.11) \quad D^e_{2M} = 6.5 \times 10^{-9} \lambda^{1/s} \ \text{m}^2 \ \text{s}^{-1},$$

while for $D_{12} = 6.5 \times 10^{-8}$ m^2 s^{-1} we found

(13.12) $D_{1M}^e = 4.55 \times 10^{-10} \lambda^{1/s}$ m^2 s^{-1}

and

(13.13) $D_{2M}^e = 3.25 \times 10^{-9} \lambda^{1/s}$ m^2 s^{-1}.

The fact that the membrane interaction terms remain relatively constant is encouraging in terms of the generality of the model and serves to reinforce the choice in magnitude for the parameters A_1 and A_2.

13.1.4 Comparison With Other Available Models

Both SZG [39] and TMT [41] have presented conductivity expressions for Nafion 117 membranes. SZG's model is the result of a curve fit to experimental data and is of the form

(13.14) $\sigma_{SZG}\left(T_{cell}\right) = \exp\left[1268\left(\dfrac{1}{303} - \dfrac{1}{273 + T_{cell}}\right)\right]\sigma_{30}$,

where T_{cell} is the cell temperature in degrees centigrade and σ_{30} is the conductivity (with units of S cm^{-1}) at 30°C [39] that is measured to be a linear function of λ,

(13.15) $\sigma_{30} = 0.005139\lambda - 0.00326 \quad (\lambda > 1)$.

At this point we should note that SZG also omit to report whether the membrane considered was in the E-form or some heat-treated form. We will assume that it is for the E-form and use it for comparison purposes.

TMT's conductivity expression is developed from a theoretical model and is of the form [41]

$$(13.16) \quad \sigma_{TMT} = \left(\varepsilon_{TMT} - \varepsilon_{TMT,0}\right)^q \left(\frac{\lambda_1^0}{1+\delta}\right) c_{HA,0}\alpha ,$$

with the acid group concentration within the pore fluid given by [41]

$$(13.17) \quad c_{HA,0} = \frac{1}{\lambda \overline{V}_2} ,$$

and the porosity and equivalent conductance given by [41]

$$(13.18) \quad \varepsilon_{TMT} = \frac{\lambda}{\dfrac{\overline{V}_M}{\overline{V}_2} + \lambda}$$

$$(13.19) \quad \lambda_1^0 = \lambda_{1,298}^0 \exp\left[-\frac{E_\eta}{R}\left(\frac{1}{T} - \frac{1}{298K}\right)\right].$$

We note that the above expression for porosity is similar to our expression (see Eqn. (12.33)), except for the term $(\lambda - \gamma)$ in the numerator of our expression, which allows for the possibility that there are γ waters per sulfonate head that are so strongly bonded to sulfonate heads that they do not contribute to transport. We assume they are part of the membrane and thus do not contribute to the water phase. In the case where γ is zero (e.g. for Nafion) our expression is identical to TMT's.

Note that α is the degree of dissociation as discussed previously; the other parameters used by TMT in their model are given in Table 5.

Table 5: Parameters for TMT's Model [41]

Parameter	Significance	Value
q	Bruggeman exponent	1.5
$\varepsilon_{Thampan,0}$	Percolation threshold volume fraction of water	Not given
$\lambda^0_{1,298}$	Equivalent conductance of hydronium ions at infinite dilution	349.8 S cm^2/mole
E_η	Activation energy for viscosity of water	14 kJ mol^{-1}
δ	$\delta = \dfrac{D^e_{12}}{D^e_{1M}}$	5.5 for vapor-equilibrated 0.6 for liquid-equilibrated
$V_{M,M}$	Molar volume of membrane	537 cm^3 mol^{-1}
$V_{M,2}$	Molar volume of water	18 cm^3 mol^{-1}

The conductivity models of TMT and SZG are compared to our model in Figure 31, which also shows the expected range of the data. SZG's model falls within the upper and lower bounds on conductivity given by the estimate of the error in sorption data for high water contents. TMT's model falls within the upper and lower bounds for low water contents, however, for higher water contents, the model deviates significantly from the experimental results.
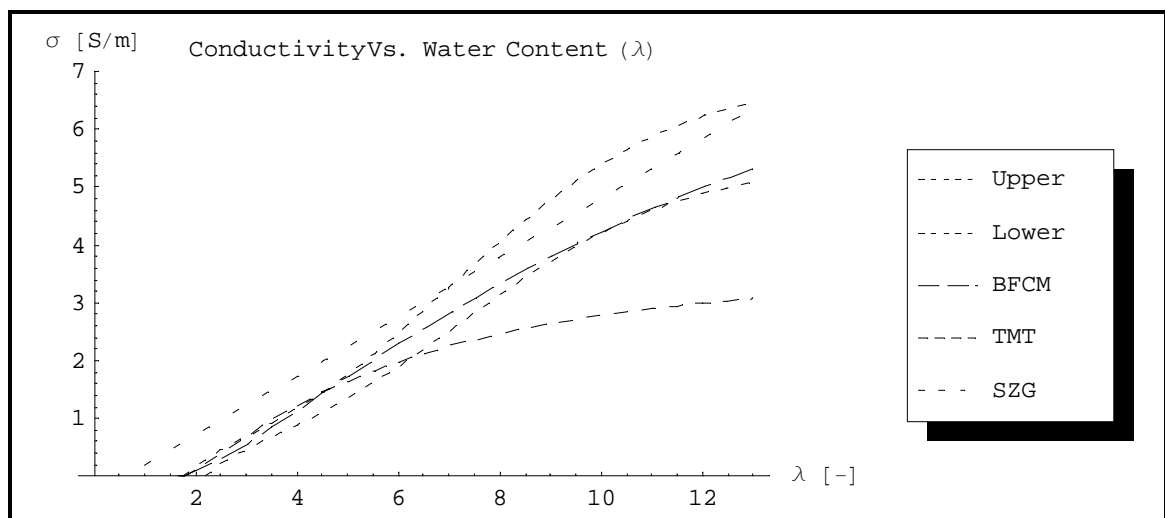
Figure 31: Comparison of various conductivity models against experimental data of Sone et al. for E-form Nafion 117 at 30°C.

The errors relative to the curve fit of SES is plotted in Figure 32 for our model and those of SZG and TMT. SZG's fit to the data is good at higher water contents only, while

TMT's model provides a good fit at lower water contents only. The proposed BFCM provides a good fit throughout the range, and lower errors at most values of λ.
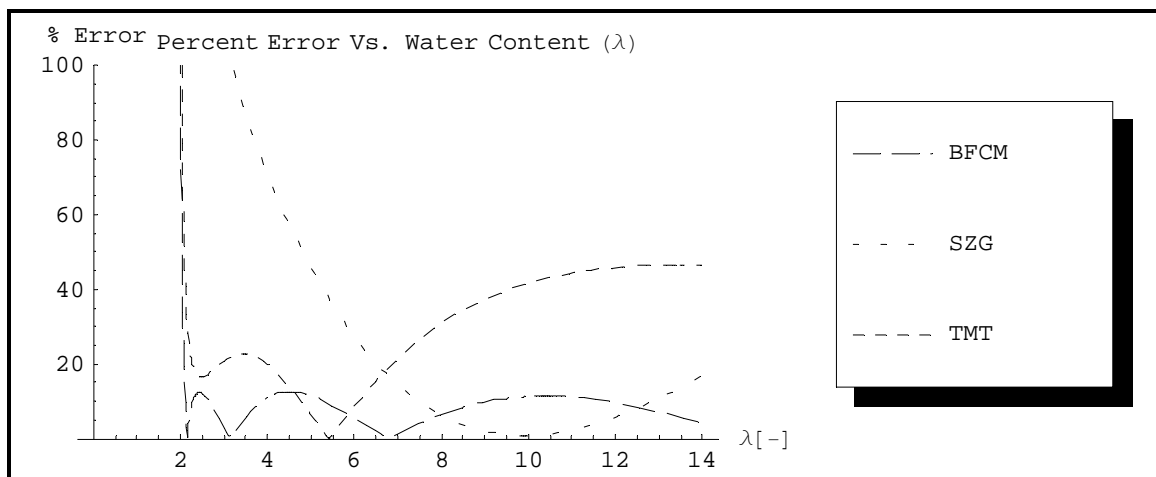

Figure 32: Plot of absolute percent error in various models relative to SES's experimental results at 30°C.

13.2 Fitting Conductivity at 70℃

13.2.1 Fitting Parameters

The only BCFM parameters assumed to depend on temperature are the diffusion coefficients, since the complementary model for calculating the fraction of dissociated sulfonate heads α already includes temperature dependence, γ was found to be zero at all temperatures and the minimum water content λ_{min} is not expected to be temperature dependent. For simplicity, the same functional dependence on temperature was assumed for all diffusion coefficients. We used the data of SES for 70°C with the sorption isotherm data for 80°C to obtain a plot of the conductivity as a function of water content at 70°C (Figure 33). Implementing a similar model as the one for 30°C, we altered the model slightly for 70°C by implementing the sorption isotherm fit at 80°C and the conductivity expression for 70°C. We then varied the value of D_{12}, and hence the reference diffusion coefficient, until the percent error fell within reasonable bounds over the entire range of water contents (Figure 34), and the conductivity curve fell within the error bounds defined by experimental error (Figure 35).
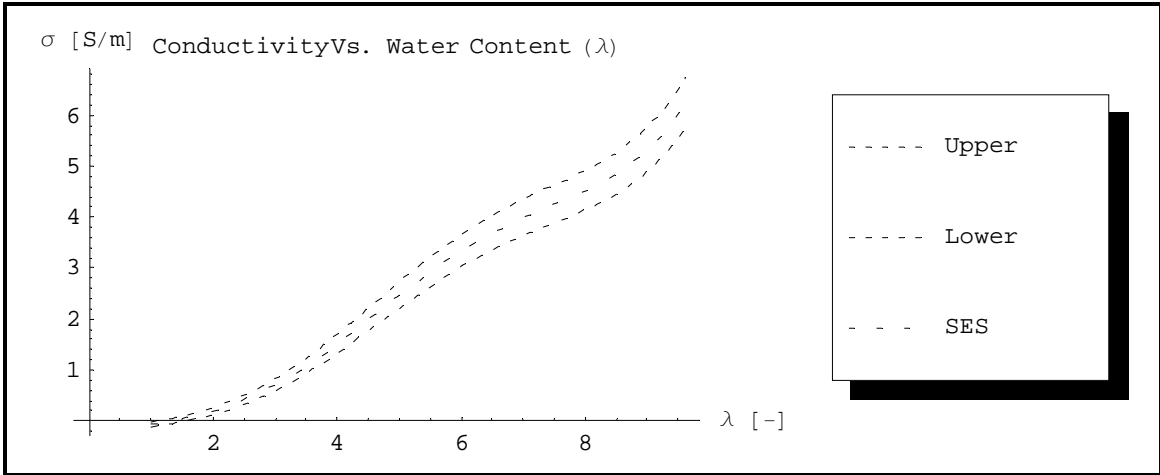
Figure 33: Measured conductivity for E-form of Nafion 117 versus water content (λ) at 70°C plotted using least squares fit to sorption isotherm data at 80°C. Standard error in sorption isotherm data is used to provide an estimate of expected error and thus a range within which any curve fit should lie.
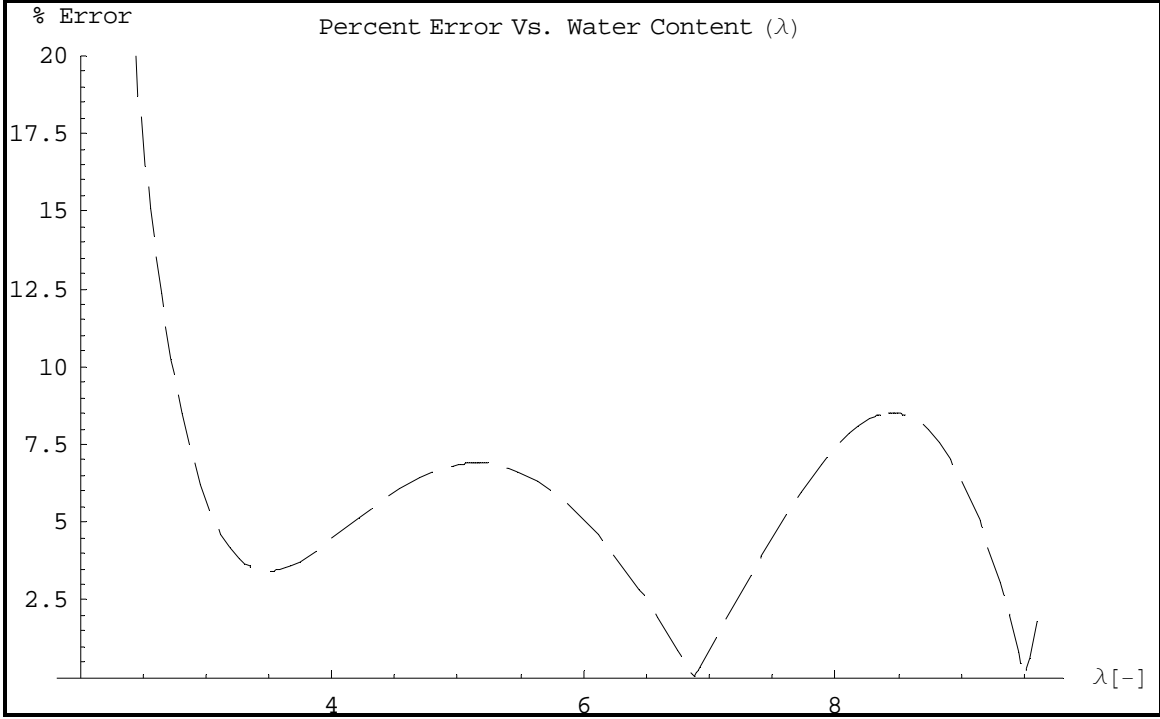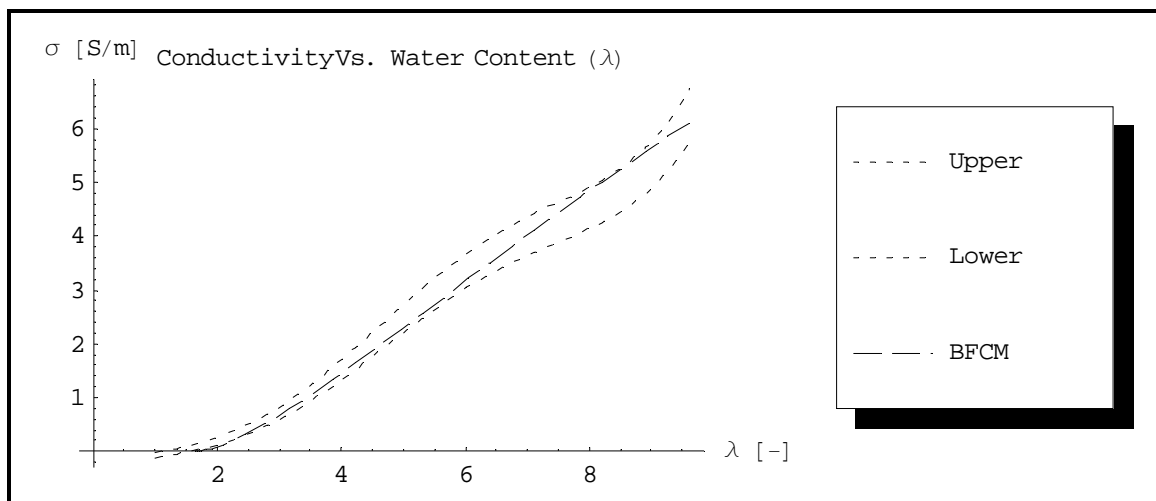

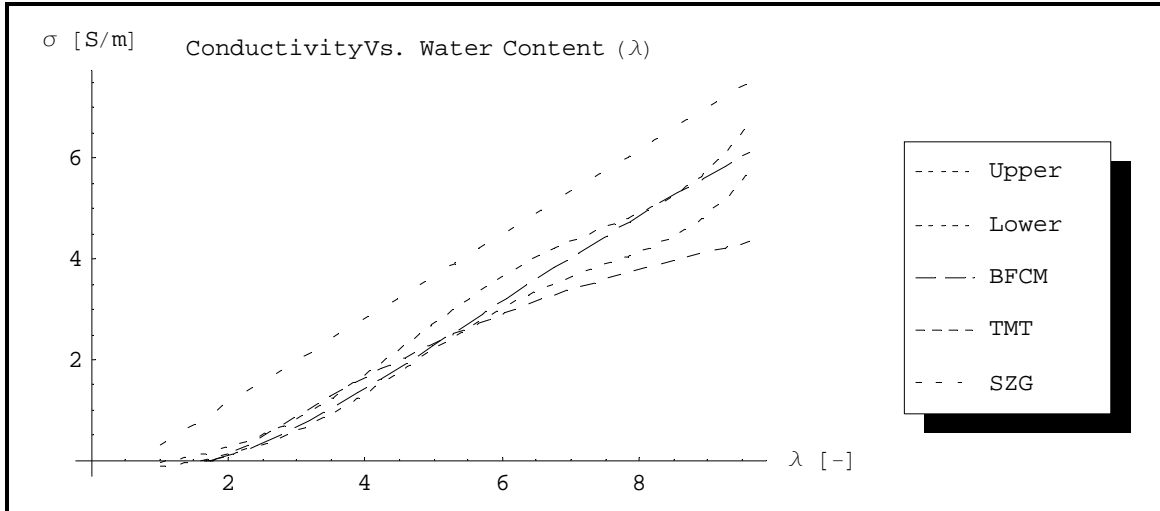**Figure 34: Plot of absolute percent error of BFCM relative to SES's experimental results at 70°C.**

Figure 35: Plot of BFCM and anticipated upper and lower bounds on conductivity resulting from error in fit to sorption Isotherm Data at 70°C.

13.2.2 Comparison With Other Models

As was done for our results at 30°C we can compare our results to the predictions of TMT and SZG at 70°C (Figs. 36 and 37). We note that SZG does not achieve a good fit to this data, having a minimum percent error of approximately 20% and lying outside the conductivity range at all water contents. There are a number of possible causes: we may not be comparing their expression to data for Nafion of the correct form (E, N or S); their temperature dependence is incorrect; or experimental errors in the conductivity measurements.

We note that TMT do not provide a good fit at higher water contents (approximately 20% error and outside the expected conductivity range), but at lower water contents (below λ of 3) TMT's model provides a comparable fit to ours. In general, our model has lower overall error and is able to to fall within the range of conductivity.

Figure 36: Comparison of conductivity models against experimental data of SES for E-form Nafion 117 at 70°C.
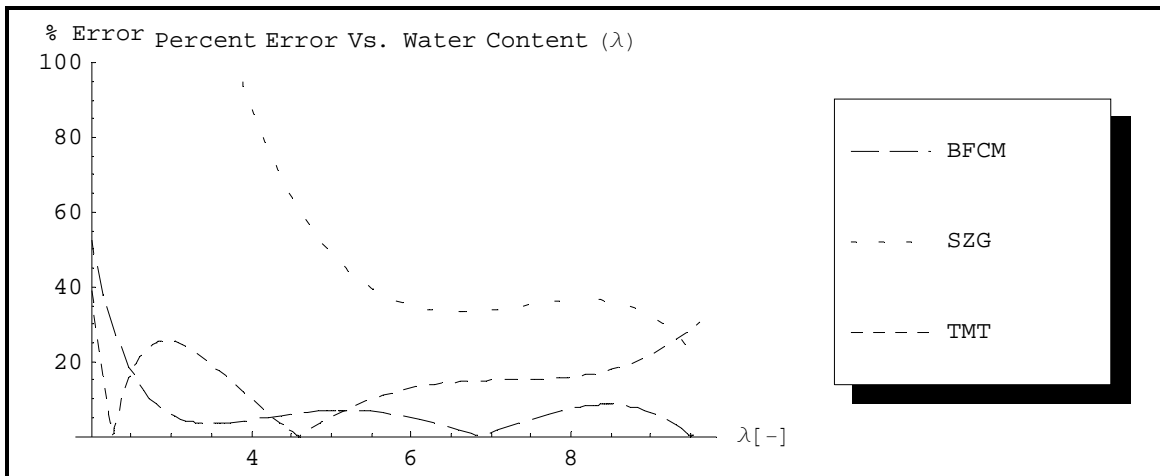
Figure 37: Plot of absolute percent error in various models relative to SES's experimental results at 70°C.

13.2.3 Temperature Dependence of Parameters

The reference diffusion coefficient (which we set to be D_{12}) varies with temperature:

$$(13.20)\ D_{12}\left(30°C\right) = 6.5 \times 10^{-9}\ \mathrm{m^2\ s^{-1}}$$

and

$$(13.21)\ D_{12}\left(70°C\right) = 1.35 \times 10^{-8}\ \mathrm{m^2\ s^{-1}}.$$

Assuming that all the diffusion coefficients vary in the same way, and that the variation is of Arrhenius-type, we used our data points to determine an activation energy (E_a), which is assumed to apply for all λ. Thus,

$$(13.22) \quad D_{12}(T) = 6.5 \times 10^{-9} \left\{ \exp\left[\frac{E_a}{R}\left(\frac{1}{303\ \mathrm{K}} - \frac{1}{T} \right) \right] \right\} \mathrm{m}^2\ \mathrm{s}^{-1}$$

with

$$(13.23) \quad \frac{E_a}{R} = 1899\ \mathrm{K}.$$

Also,

$$(13.24) \quad D_{1M}^{e} = D_{12} A_1 \lambda^{1/s}$$

and

$$(13.25) \quad D_{2M}^{e} = D_{12} A_2 \lambda^{1/s}.$$

We should note that the conductivity in SZG's model is also assumed to vary with an Arrhenius law with activation energy of

$$(13.26) \quad \frac{E_a}{R} = 1268\ \mathrm{K}.$$

The reason for assuming Arrhenius type temperature dependence is that molecules that are diffusing must overcome an activation energy barrier to move from one location to another. At higher temperature, more molecules will have sufficient energy to "clear" this energy barrier, with correspondly higher diffusion coefficients. This type of behavior

is modeled by an Arrhenius relation of the above form, similar to a chemical reaction with an activation barrier.
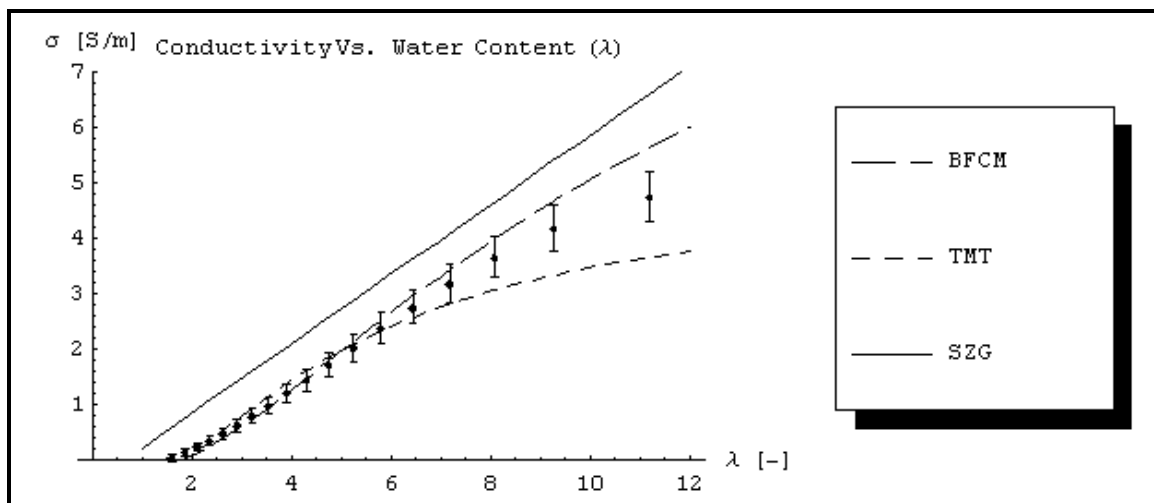
13.3 Predicting Conductivity at 45°C

13.3.1 Sorption Isotherm

In order to gauge the ability of our model to correctly predict the temperature variation of conductivity we decided to compare our theoretical curve to the data collected by SES at 45°C. One problem encountered when attempting this was a lack of reliable sorption isotherm data at temperatures near 45°C. Data was found for 50°C [62], however, this data was suspect since it showed more water was sorbed by a membrane which was at 50°C than one at 25°C. This is contrary to the expected decrease in amount of water sorbed as temperature increases [66].

Rather than use the suspect data, we decided to use the chemical model of Weber and Newman (WN) developed for determining λ for a vapor-equilibrated membrane [66]. This model was implemented and used to provide sorption isotherm data we could use in conjunction with SES's data at 45°C [29] to plot conductivity as a function of the number of sorbed waters. We used a standard error of ±0.038 on the activity (the same standard error as was used at 30°C) to provide error bars within which we would reasonably expect the conductivity to lie.

13.3.2 Comparison to Conductivity Data

Figure 38 shows the comparison of our model, and those of SZG and TMT, to the data at 45°C. SZG falls outside the error bars at all times and TMT provides the best fit at very low water contents. We note that although our model falls outside the error bars at high and low water contents, we are able to provide a better fit over a broader range of water contents.

Figure 38: Comparison of the ability of BFCM and those of SZG and TMT to predict the conductivity at 45°C.

Although we fall outside the error bars at very high and very low water contents we should consider that we are not using experimental data for sorption isotherm plots, but rather, in the absence of reliable data, a chemical model. Though this chemical model has been shown to generally agree with available data [66], it has not been rigorously validated at or near 45°C. This suggests, that even more error than anticipated might be introduced through the use of such a model as opposed to actual experimental data. Consider that a standard error of $\pm\,0.038$ at an activity near 1 ($\pm 3.8\%$ variation) can cause the conductivity to range between approximately 5.2 S m^{-1} and 4.4 S m^{-1} ($\pm\,8\%$ variation in conductivity approximately) at a water content of around 11. This indicates that the conductivity is highly sensitive to changes in the activity, and small errors in sorption isotherm models can have significant effect when determining conductivity as a function of λ.

Our ability to fit the data well over a broad range of water contents, coupled with some uncertainty in the sorption isotherm model, suggest that the BFCM is capable of reasonably predicting the temperature dependence of conductivity. In order to perform a more rigorous analysis of the temperature dependence more experimental data needs to be collected. Ideally sorption isotherm data and conductivity data, allowing for the

determination of conductivity as a function of water content, should be obtained for a wider range of temperatures to allow for a more systematic analysis.

13.3.3 Checking Sorption Isotherm Model of Weber and Newman

As a check on WN's chemical model for sorption we used his chemical model to translate the conductivity data of SES from being plotted as a function of activity to being plotted as a function of water content at 30°C (Fig. 39), and 70°C and 80°C (Fig. 40).
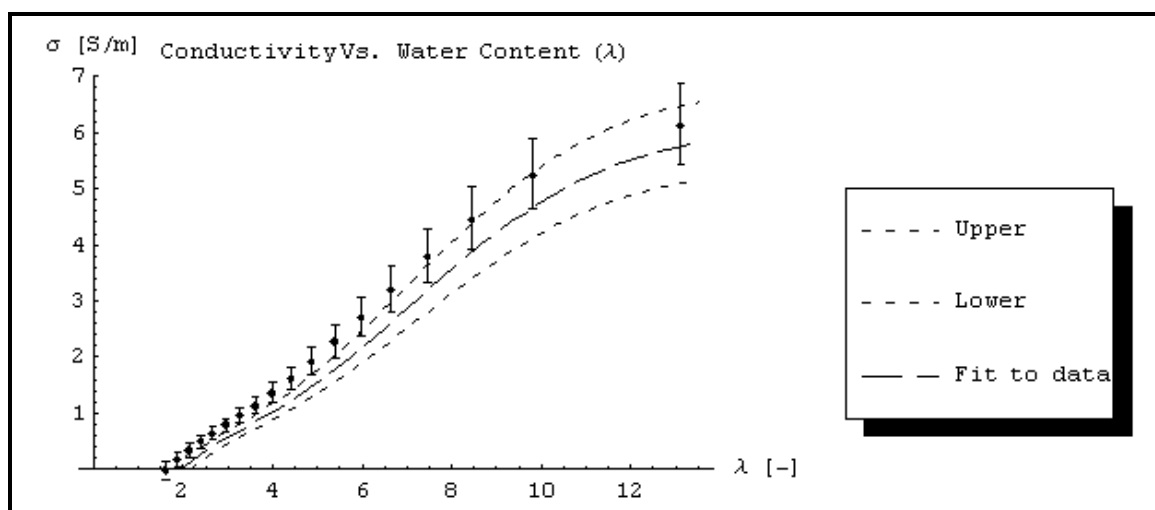

Figure 39: Plot showing translation of conductivity data of SES (30°C) using fit to sorption data at 30°C and chemical sorption model of WN (diamonds).
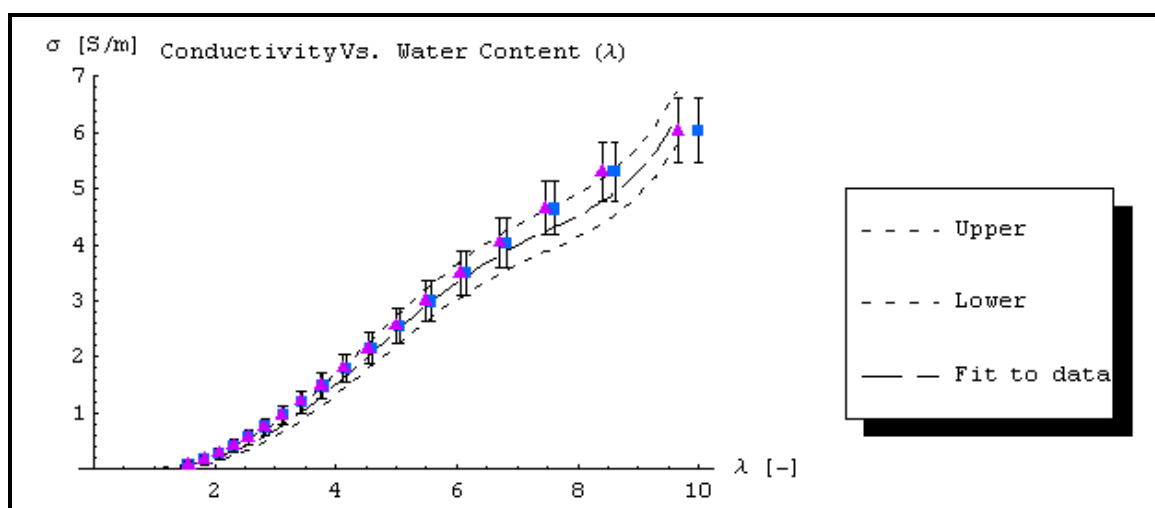

Figure 40: Plot showing translation of conductivity data of SES (70°C) using fit to sorption data at 80°C and chemical sorption model of WN at 70°C (triangles) and 80°C (squares).

For the case of 30°C, WN's conversion and the conversion using the fit to data overlap in the mid to high water content range. At lower water contents, the differences between the sorption isotherm model and the fit to the data for low water contents become more significant.

In the above conversions of the conductivity data at 70°C using the sorption isotherm model of WN at 70°C and 80°C (Fig. 40), we note that there is significant overlap of both over the entire range of water contents. Noting that we have used a fit to data at 80°C and Weber's chemical model at 70°C and 80°C, we conclude that the effect of a 10°C temperature variation on the sorption isotherms is small and that our use of the sorption data at 80°C to convert the conductivity data at 70°C is acceptable. WN's chemical model appears to provide a reasonable enough translation of the conductivity data, and should provide a useful basis to validate the temperature dependence behaviour of our model.

14 Further Discussion of Sorption Isotherm Models

In order to further examine the influence that different fits to the sorption isotherm data have on the translation of the conductivity data of SES we decided to convert the conductivity data using the sorption model of TMT [41] and our curve fit. We translated the data of SES at 30°C and at 70°C using our fits to the sorption isotherm data obtained above and a sorption isotherm provided by TMT (see Figs. 41 and 42).
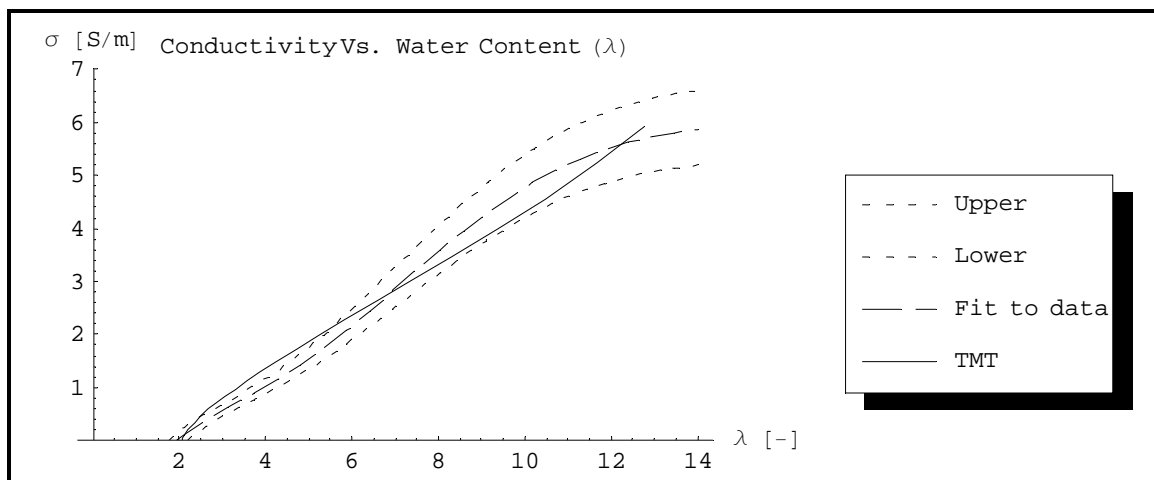
Figure 41: Conductivity data of SES (30°C) plotted against water content using our fit to sorption isotherm data and TMT's sorption model to translate activity to water content.

We note in Fig. 41 above the translation using the BET model yields a result that for the most part lies within the range given using our error prediction, deviating slightly at water contents in the range of λ between approximately 2.5 and 5.
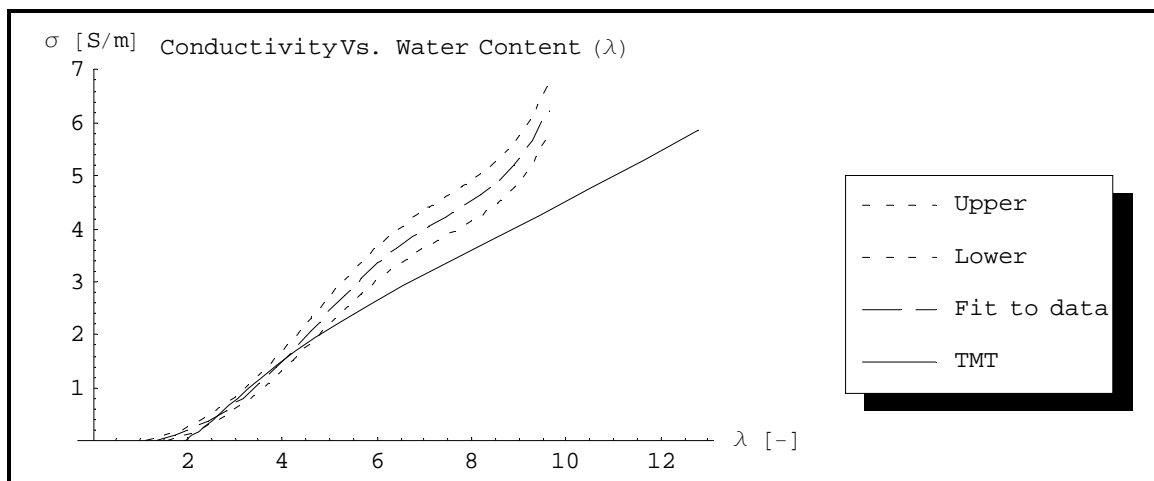
Figure 42: Conductivity data of SES (70°C) plotted against water content using our fit to sorption isotherm data and TMT's sorption model to translate activity to water content.

The first point to note in Figure 42 is that TMT has no temperature dependence in their sorption isotherm model. The sorption behavior is dependent on temperature [66]; not taking this dependence into account will surely affect the results. The curve using TMT's BET sorption isotherm model (at 70°C) deviates significantly at high water contents from the translation using our sorption isotherm fit, predicting a lower conductivity. If we plot TMT's theoretical conductivity model superimposed over the Figure 42 we can see that

15 Conductivity of Other PFSA Membranes

A preliminary investigation of the general applicability of the proposed BFCM was also perfomed by applying the model to membranes other than the family of Nafion 1100 *EW* membranes. To determine the model parameters, we used the experimental conductivity data of ZSD [14] for Membrane C (Chlorine Engineers, Japan) and Dow XUS 13204.10. Membrane C has the same side chain as 1100 *EW* Nafion but with a shorter backbone and an *EW* of 900, while Dow has a shorter side chain than 1100 *EW* Nafion but with the same backbone and an *EW* of 800 [14].

We decided to use these membranes for our evaluation of the ability of this model to reasonably predict the conductivity behavior of other membranes for several reasons. Since all these membranes are based on similar backbones, side chains and the same terminal sulfonate heads, we could assume that the dissociation behavior would be sufficiently similar to Nafion that we could use the same dissociation model. Other reasons for selecting these membranes for comparison is the availability of conductivity as a function of water content from ZSD's paper and we can determine all the parameters needed for the model. For example, we can calculate the molar volumes for the membranes, since we know the *EW*s and we can reasonably assume the densities of the dry membranes are the same as that for Nafion, thus [41]

$$(15.1) \quad V_{M,M} = \frac{EW}{\rho_{dry}} .$$

Furthermore, we can assume that, since these membranes have very similar macromolecular structures, the diffusion coefficients between the membrane and the diffusing species (D^e_{1M} and D^e_{2M}) will be the same.

We began by fitting our conductivity model parameters to the conductivity data for Nafion 117 provided by ZSD, noting that they use a different experimental apparatus to measure conductivity than SES, and in fact find slightly higher conductivity at 30°C than SES. The following model parameters were obtained:

(15.2) $\lambda_{min} = 1.65$,

(15.3) $D_{12} = 7.5 \times 10^{-9} \, m^2 \cdot s$,

(15.4) $s = 1.3$,

(15.5) $A_1 = 0.084$,

(15.6) $A_2 = 0.5$.

and

(15.7) $\gamma = 0$.

Note that these parameters are unchanged compared to the values in Eqns. (13.5), (13.6), (13.7), (13.8) and (13.9), except for D_{12}, which takes a slightly higher value. These parameters were found to provide a very reasonable fit to the experimental data for Nafion (see Fig. 44). In order to fit the conductivity data for the other two membranes we considered the differences between these membranes and Nafion and used this to make some reasonable assumptions about the parameters used.

Membrane C has the same side chain as Nafion but due to the smaller backbone it has a smaller *EW*, i.e. more sulfonate heads per unit mass of membrane and thus a higher concentration of heads. We anticipate that due to the similar side chain, clustering would be similar to that in Nafion, however, with clusters closer together. As a result we expect that λ_{min} will be smaller for Membrane C, but the other parameters should be relatively unaffected. Varying only λ_{min} we found that for a λ_{min} value of 0.3 we were able to provide a reasonable fit to the available data for Membrane C (Fig. 44).

The Dow membrane has the same backbone as Nafion but a shorter side chain and thus a smaller *EW*. Due to the fact that Nafion and Dow membranes have the same backbones we expect that λ_{min} should be similar for both membranes. It is presumed that smaller clusters will be formed in the Dow membrane and less water is sorbed from the vapor phase compared to Nafion [3]. As a result we expect that the porosity and tortuosity vary differently than in Nafion. Recalling the Bruggeman correction, we note that the Bruggeman exponent (*q*) has a suggested value of 1.5, however, it can be treated as a fitting parameter. Assuming within the Dow membrane the water forms smaller clusters separated by a similar distance to those in Nafion, we assume that for a given porosity the tortuosity will be larger, thus the parameter *q* should be smaller. With all other parameters kept the same as for Nafion, we found that a value of *q* = 1.25 provided a reasonable fit to the available data for the Dow membrane (Fig. 44).
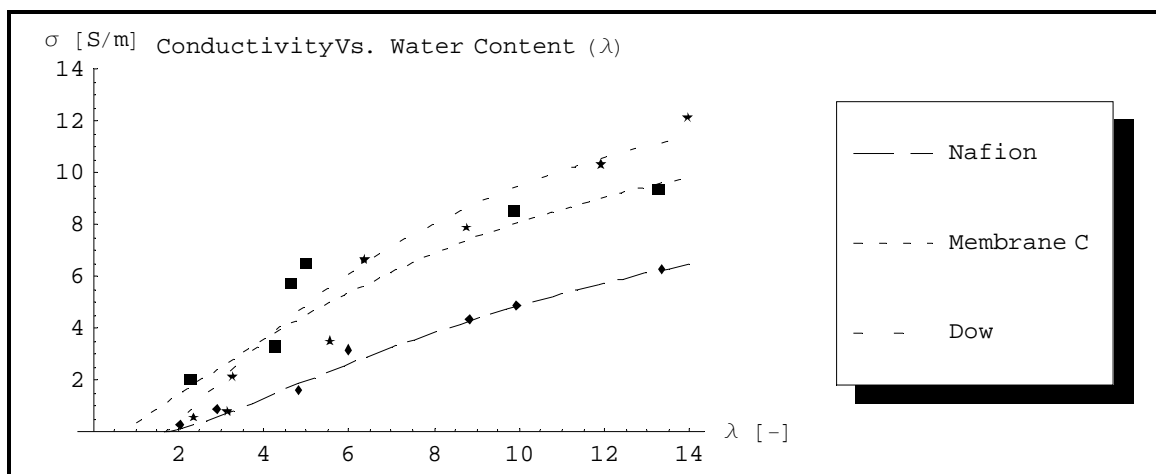
Figure 44: Predicting the conductivity of other membranes in the same family as Nafion at 30°C. Squares, Membrane C (Chlorine Engineers Japan) [14]; Stars, Dow 13204.10 [14]; Diamonds, Nafion 117 [14].

Clearly this is not a systematic analysis of the ability of our model to fit the conductivity of other membranes. Rather this preliminary analysis shows that the model can be applied to other membranes within the family of perfluorosulfonic acid membranes and provides a reasonable representation of the experimental data with only minor and *physically rational* changes in the fitting parameters. The sparsity of reliable and well-

documented data means that a more rigorous analysis will have to be deferred until comprehensive data sets for a variety of membranes become available.

16 A Guide For Future Work

16.1 Necessary Parameters For Conductivity Model Implementation

In closing our discussion of the conductivity model we turn our attention to summarizing what information is required in order to apply the BFCM to other membranes. This is done with the hope that this will be of some use in guiding those performing experimental investigations of membranes. We start with the fundamental properties of the membrane and transport phenomena.

In order to apply the model we need to know the *EW* and the dry density of the membrane, or the molar volume (required for the porosity portion of the model). The model requires knowledge of which species are involved in the transport within the membrane (e.g. water and hydronium). The model also requires specification of the fraction of dissociated acidic heads forming the charge carrying species (required for the counting portion of the model). Such information could be obtained experimentally or from a complementary dissociation model.

To find the values of the unknown parameters (i.e. λ_{min}, D_{12}, s, A_1, A_2 and γ), we require, at a minimum, conductivity data as a function of water content for a range of temperatures. If possible the best way to present data for use with this model is to have conductivity data measured as a function of water content for a range of temperatures. This allows for fitting directly to the data, without having to perform an exhaustive search for sorption isotherms. If conductivity data is given as a function of activity, then sorption isotherm data for the same type of membrane with the same pretreatment should also be documented, to allow for translation of the data.

In addition to treating the parameters as fitting parameters, it might be possible to develop experiments or molecular dynamics models, which can directly provide insight

into some of these parameters. Such simulations could, for example, provide valuable insight into the interaction forces between species, thus shedding more light on the D_{12}, D^e_{1M} and D^e_{2M} parameters (and thus A_1, A_2 and s). Researchers could report λ_{min} for each membrane, the water content below which conductivity falls below some critical level and thus becomes effectively zero. Investigating the possible lack of mobility of water molecules strongly attracted to the acidic heads would shed light on the value of the parameter γ, and whether it is useful to maintain this parmeter.

16.2 Further Verification of Parameters

As a final step, we could embed our transport model (Eqn. 11.11) into a computational fuel cell model. Using the parameters found by fitting to conductivity data, or from experimental investigation, we could then implement a fuel cell model for a known geometry and operating conditions. Building a working fuel cell of the same geometry we could run the fuel cell for the same operating conditions and collect the water output (condensing out all water present as steam also) from the fuel cells anode and cathode side. Comparing the predicted water crossover to the measured water crossover we could determine if our transport model is able to correctly predict the crossover of water.

In any case the further validation of this model requires the collection of more experimental data (both for Nafion and other membranes) and the implementation of more sophisticated fitting techniques. In this way we would be able to obtain even more accurate estimates of the unknown parameters and provide improved representation and predictions of the transport phenomena.

17 Conclusion

17.1 Conclusions

Nafion remains one of the most thoroughly studied PEMs, however, significant efforts are underway to research and develop other membranes that exhibit improved properties to fuel cell operation. These membranes include sulfonated polyetherketones and Flemion and Aciplex to name a few. Nonetheless, Nafion remains the most widely used and documented type of membrane.

We considered first the morphology and microstructure of the Nafion membrane, finding that the structure could be approximated as one of spherical clusters formed from groups of sulfonate heads and associated hydrating waters. Collapsed channels that swell when the membrane is equilibrated with liquid water connect the clusters. This description of the morphology was tied in with a description of the hydration behavior and how the number of water molecules sorbed per sulfonate head critically affects the conductivity exhibited by the membrane.

In addition we examined Schroeder's Paradox and found that one plausible explanation lies in considering the extra pressure of the liquid phase within the membrane when equilibrated with vapor due to the capillary pressure.

Having thoroughly investigated the sorption behavior of the membrane, and having discussed the concept of conductivity and how the sorption behavior affects conductivity, the transport properties of water were investigated. It was found that the introduction of the membrane reduced the conductivity compared to bulk solutions due to effects on the molecular scale as well as longer range effects such as geometrical restriction provided by the membrane. However, as water content within the membrane increases the conductivity approaches that in bulk water.

In the final sections of the literature review we considered the models of fuel cells and membranes and how they attempt to capture the transport phenomena that are occurring. The transport within the membrane is modeled both on a microscopic and macroscopic level. Microscopic models are key as they give us insight into physical processes occurring on the molecular level. Unfortunately the microscopic models are too complex to be integrated into a fuel cell model, and thus the focus shifts to macroscopic transport models for use in fuel cell models.

One common way to classify membrane models is as diffusion or hydraulic models. Diffusion models consider concentration gradients as the driving force for water fluxes

while hydraulic models consider pressure gradients as the driving force for water fluxes. Both models are valid in specific regimes; however, neither can completely represent and predict the observed behavior. A promising idea is to consider chemical potential gradients as the driving force for all fluxes.

Although there is some discrepancy between the various models used, and some controversy over the development of the equations, they can all provide insight into the operation of fuel cells and behavior of the PEM as long as one keeps in mind the limitations of the various models.

In the second part of this thesis we developed a transport model for polymer electrolyte membranes based on the Binary Friction Model. We investigated the driving forces in the binary friction model and found that the pressure gradient terms were negligible compared to the other driving force terms. The transport model was cast in a general form to allow for broad applicability and tailoring to suit other types of polymer membranes.

We then made several simplifications to the model to arrive at what we termed the Binary Friction Conductivity Model (BFCM). The BFCM model was developed to allow for predictions of conductivity, and was implemented to predict conductivity of 1100 *EW* Nafion membranes based on the four-electrode AC impedance method, in which water transport is negligible. The BFCM provides conductivity as a function of water content. In order to compare the model predictions with experimental results, we used curve fits to sorption isotherm data. These fits were used to translate the conductivity from being a function of activity of water vapor with which the membrane is equilibrated with, to conductivity as a function of the number of waters sorbed per sulfonate head.

We first used the conductivity data and sorption data at 30°C to determine the parameters of the conductivity model (λ_{min}, D_{12}, s, A_1, A_2 and γ). We then varied the reference diffusion coefficient (D_{12}) by an order of magnitude (larger and smaller) and found that the coefficients D^e_{1M} and D^e_{2M} were of the same magnitude no matter what the magnitude

of D_{12}, reinforcing our choice of magnitude for these parameters. The order of magnitude of D_{12} was reinforced by comparison to a literature value and by the ability to provide a reasonable fit to the data.

We also fit the conductivity data at 70°C and, assuming that all diffusion coefficients had the same Arrhenius-type temperature dependence, found the activation energy. We then used this to predict the conductivity at 45°C and established that this temperature dependence allowed us to provide a reasonable fit to the data.

At all temperatures we compared our model to those of TMT and SZG. Thampan et al. were able to provide a reasonable fit at low water contents for all the temperatures we investigated, while Springer et al. only provided a reasonable fit at high water contents for 30°C. The new BFCM model is able to provide a more consistent fit to the data *over the entire range* of water contents. To be fair, we should note that we are not certain that SZG's model is fit to data for E-form 1100 *EW* Nafion, TMT's model might yield improved predictions if temperature dependence of the sorption isotherms were accounted for.

The analysis shows that the BFCM model is more consistent in predicting conductivity as a function of temperature and water content for 1100 *EW* Nafion membranes in the E-form than other available models. A natural next step in the development of the transport model is to implement the parameter values obtained from fitting the BFCM to conductivity in a full membrane transport model. This is the inherent advantage of using such a model, the ability to gain insight into all the necessary transport parameters from fitting the conductivity data.

In order to show a broader generality to our model we then used the BFCM, with the diffusion coefficients we found from fitting to 1100 *EW* conductivity data of Zawodzinski et al. at 30°C, to predict the conductivity of a Dow and Membrane C membrane using only reasonable and physically consistent changes in parameters. The BFCMs ability to reasonably predict the trends in behavior of these membranes shows a

broader generality of the model. However, at present there is insufficient information for other membranes to rigorously assess the BFCMs ability to predict the behavior of a variety of different membranes.

17.2 Recommendations for Future Work

One of the biggest problems facing the developers of models for transport within the membranes is a lack of available experimental data. Thus, the majority of the following recommendations focus around acquiring more data for various membranes, and more rigorous presentation of data for comparison:

- Data collection and model development should be done for membranes in the same form as they are found within the fuel cell (i.e. the same pre-treatment).
- Measurment of more conductivity data for various membranes over a range of temperatures; conductivity should preferably be presented as a function of water content. If this is not possible then sorption isotherm data should be made available for membranes in the same form to allow for data translation.
- Implementaion of more rigorous fitting techniques for the determination of the model parameters.
- Experimental investigation of the unknown parameters. (λ_{min}, D_{12}, D^e_{1M}, D^e_{2M} and γ).
- Implementation of a fuel cell model using the transport model developed in this thesis coupled with the development of an experimental fuel cell, and their use to predict and experimentally verify the crossover of water using the transport model.

References

1. Beattie, P.D, Orfino, F. P., Basura, V. I., Zychowska, K., Ding, J. F., Chuy, C., Schmeisser, J. and S. Holdcroft. "Ionic conductivity of proton exchange membranes." Journal of Electroanalytical Chemistry **503**, 45-56 (2001)

2. Larminie, J. and Andrew Dicks. Fuel Cell Systems Explained. Ontario: John Wiley & Sons Ltd, 2000.

3. Weber, A. Z. and J. Newman. "Transport in polymer-electrolyte membranes." Journal of The Electrochemical Society **150,** A1008-A1015 (2003)

4. Chuy, C, Basura, V. I., Simon, E., Holdcroft, S., Horsfall, J. and K. V. Lovell. "Electrochemical Characterization of Ethylenetetrafluoroethylene-g-polystyrenesulfonic Acid Solid Polymer Electrolytes." Journal of The Electrochemical Society **147**, 4453-4458 (2000)

5. Ding, J., C. Chuy and S. Holdcroft. "Enhanced Conductivity in Morphologically Controlled Proton Exchange Membranes: Synthesis of Macromonomers by SFRP and Their Incorporation into Graft polymers." Macromolecules **35**, 1348-1355 (2002)

6. Ding, J., Q. Tang and S. Holdcroft. "Morphologically Controlled Proton-Conducting Membranes Using Graft Polymers Possessing Block Copolymer Graft Chains." Australian Journal of Chemistry **55**, 461-466 (2002)

7. Kerres, J, Ullrich, A., Haring, T., Baldauf, M., Gebhardt, U. and W. Preidel. "Preparation, Characterization and fuel cell application of new acid-based blend membranes." Journal of New Materials for Electrochemical Systems **3**, 229-239 (2000)

8. Kerres, J, Cui, W., Disson, R. and W. Neubrand. "Development and Characterization of Crosslinked Ionomer Membranes Based Upon Sulfonated and Sulfonated PSU, Crosslinked PSU Blend Membranes by Disproportionation of Sulfinic Acid Groups." Journal of Membrane Science **139**, 211-225, (1998)

9. Manea, C. and M. Mulder. "Characterization of polymer blends of polyethersulfone/sulfonated polysulfone and polyethersulfone/sulfonated polyetherketone for direct methanol fuel cell applications." Journal of Membrane Science **206**, 443-453 (2002)

10. Song, M. K, Kim, Y. T., Fenton, J. M., Kunz, H. R. and H. W. Rhee. "Chemically-modified Nafion/poly(vinylidene fluoride) blend ionomers for proton exchange membrane fuel cells." Journal of Power Sources **117**, 14-21 (2003)

11. Inzelt, G., Pineri, M., Schultze, J. W. and M. A. Vorotyntsev. "Electron and proton conducting polymers: recent developments and prospects." Electrochimica Acta **45**, 2403-2421 (2000)

12. Laporta, M., Pegoraro, M. and I. Zanderighi. "Perfluorosulfonated membrane (Nafion): FT-IR study of the state of water with increasing humidity." Physical Chemistry Chemical Physics **1,** 4619-4628 (1999)

13. Kreuer, K. D. "On the development of proton conducting polymer membranes for hydrogen and methanol fuel cells." Journal of Membrane Science **185**, 29-39 (2000)

14. Zawodzinski, T. A, Springer, T. E., Davey, J., Jestel, R., Lopez, C., Valerio, J. and S. Gottesfeld. "A Comparative Study of Water Uptake By and Transport Through Ionomeric Fuel Cell Membranes." Journal of The Electrochemical Society **140**, 1981-1985 (1993)

15. Tsou, Y.M., M. C. Kimble and R. E. White. "Hydrogen Diffusion, Solubility, and Water Uptake in Dow's Short-Side-Chain Perfluorocarbon Membranes." Journal of The Electrochemical Society **139**, 1913 (1992)

16. Yoshida, N. Ishisaki, T., Watakabe, A. and M. Yoshitake. "Characterization of Flemion membranes for PEFC." Electrochimica Acta **43**, 3749–3754 (1998)

17. Din, X. D. and E. E. Michaelides. "Transport of water and protons through micropores." AIChE Journal **44**, 35-47 (1998)

18. Kreuer, K. D. "On the development of proton conducting materials for technological applications." Solid State Ionics **97**, 1-15 (1997)

19. Basura, V. I., C. Chuy, P. D. Beattie and S. Holdcroft. "Effect of equivalent weight on electrochemical mass transport of oxygen in proton exchange membranes based on sulfonated α,β,β-trifluorostyrene (BAM) and sulfonated styrene-(ethylene-butylene)-styrene triblock (DAIS-analytical) copolymers." Journal of Electroanalytical Chemistry **501**, 77-88 (2001)

20. Savadogo, O. "Emerging membranes for electrochemical systems: (I) solid polymer electrolyte membranes for fuel cell systems." Journal of New Materials for Electrochemical Systems **1**, 47-66 (1998)

21. Sumner J. J., Creager, S. E., Ma, J. J. and D. D. DesMarteau. "Proton Conductivity in Nafion 117 and in a Novel Bis[(perfluoroalkyl)sulfonyl]imide Ionomer Membrane." Journal of The Electrochemical Society **145,** 107-110 (1998)

22. Wainright, J. S. Wang, J. T., Weng, D., Savinell, R. F. and M. Litt. "Acid-Doped Polybenzimidazoles: A New Polymer Electrolyte." Journal of The Electrochemical Society **142**, L121-L123 (1995)

23. Gierke, T. D., G. E. Munn and F. C. Wilson. "The morphology in Nafion Perfluorinated Membrane Products, as Determined by Wide- and Small-Angle X-Ray Studies." Journal of Polymer Science: Polymer Physics Edition **19**, 1687-1704 (1981)

24. Gierke, T. D. and W. Y. Hsu. "Ion-Transport and Clustering in Nafion Perfluorinated Membranes." Journal of Membrane Science **13**, 307-326 (1983)

25. Gierke, T. D. and W. Y. Hsu. "Elastic Theory for Ionic Clustering in Perfluorinated Ionomers." Macromolecules **15**, 101-105 (1982)

26. Gierke, T. D., G. E. Munn and F. C. Wilson. "Morphology of Perfluorosulfonated Membrane Products." ACS Symposium Series **180**, 195-216 (1982)

27. Yeager, H. L. and A. Steck. "Cation and Water Diffusion in Nafion Ion Exchange Membranes: Influence of Polymer Structure." Journal of The Electrochemical Society **128**, 1880-1884 (1981)

28. Kreuer, K. D., Ise, M., Fuchs, A. and J. Maier. "Proton and water transport in nano-separated polymer membranes." Journal de Physique IV **10**, 279-281 (2000)

29. Sone, Y., P. Ekdunge and D. Simonsson. "Proton Conductivity of Nafion 117 as Measured by a Four-Electrode AC Impedance Method." Journal of the Electrochemical Society **143**, 1254-1259 (1996)

30. Choi, P. and R. Datta. "Sorption in Proton-Exchange Membranes: An Explanation of Schroeder's Paradox." To be published in the Journal of The Electrochemical Society. (2003)

31. Elliot, J., Hanna, S., Elliot, A. M. S. and G. E. Cooley. "Atomistic simulation and molecular dynamics of model systems for Perfluorinated ionomer membranes." Physical Chemistry Chemical Physics **1**, 4855-4863 (1999)

32. Vishnyakov, A. and A. V. Neimark. "Molecular Simulation Study of Nafion Membrane Solvation in Water and Methanol." Journal of Physical Chemistry B **104**, 4471-4478 (2000)

33. Kreuer, K. D. "On the complexity of proton conduction phenomena." Solid State Ionics **136**, 149-160 (2000)

34. Zawodzinski, T. A, Derouin, C., Radzinski, S., Sherman, R. J., Smith, V. T., Springer, T. E. and S. Gottesfeld. "Water Uptake by and Transport Through Nafion 117 Membranes." Journal of The Electrochemical Society **140**, 1041-1047 (1993)

35. Kreuer, K. D. "Proton Conductivity: Materials and Applications." Chemistry of Materials **8**, 610-641 (1996)

36. Agmon, N. "The Grotthuss Mechanism." <u>Chemical Physics Letters</u> **244**, 456-462 (1995)

37. Eikerling, M. Kornyshev, A. A., Kuznetsov, A. M., Ulstrop, J. and S. Walbran. "Mechanisms of proton conductance in polymer electrolyte membranes." <u>Journal of Physical Chemistry B</u> **105**, 3646-3662 (2001)

38. Zawodzinski, T. A., Davey, J., Valerio, J. and S. Gottesfeld. "The Water Content Dependence of Electro-osmotic Drag in Proton-Conducting Polymer Electrolytes." <u>Electrochimica Acta</u> **40**, 297-302 (1995)

39. Springer, T. E., T. A. Zawodzinski and S. Gottesfeld. "Polymer electrolyte fuel cell model." <u>Journal of The Electrochemical Society</u> **138**, 2334-2342 (1991)

40. Berg, P., K. Promislow, J. St-Pierre, J. Stumper and B. Wetton. "Water management in PEM fuel cells." (2003)

41. Thampan, T., Malhotra, S., Tang, H. and R. Datta. "Modeling of conductive transport in proton-exchange membranes for fuel cells." <u>Journal of The Electrochemical Society</u> **147**, 3242-3250 (2000)

42. Paddison, S. J., R. Paul and T. A. Zawodzinski. "Proton friction and diffusion coefficients in hydrated polymer electrolyte membranes: Computations with a non-equilibrium statistical mechanical model." <u>Journal of Chemical Physics</u> **115**, 7753-7761 (2001)

43. Paul, R. and S. J. Paddison. "A statistical mechanical model for the calculation of the permittivity of water in hydrated polymer electrolyte membrane pores." <u>Journal of Chemical Physics</u> **115**, 7762-7771 (2001)

44. Paddison, S. J., R. Paul and T. A. Zawodzinski. "A Statistical Mechanical Model of Proton and Water Transport in a Proton Exchange Membrane." <u>Journal of the Electrochemistry Society</u> **147**, 617-626 (2000)

45. Eikerling, M., A. A. Kornyshev and U. Stimming. "Electrophysical Properties of Polymer Electrolyte Membranes: A Random Network Model." <u>Journal of Physical Chemistry B</u> **101**, 10807-10820 (1997)

46. Breslau, B. R. and I. F. Miller. "A hydrodynamic model for electroosmosis." <u>Industrial Engineering Chemistry Fundamentals</u> **10**, 554-565 (1971)

47. Verbrugge, M., and D. Bernardi. "Mathematical Model of a Gas Diffusion Electrode Bonded to a Polymer Electrolyte." <u>AIChE Journal</u> **37**: 1151-1163 (1991)

48. Verbrugge, M., and D. Bernardi. "A Mathematical Model of the Solid-Polymer-Electrolyte Fuel Cell." Electrochemical Society Journal **139**, 2477-2491 (1992)

49. Verbrugge, M., and R. F. Hill. "Transport Phenomena in Perfluorosulfonic Acid Membranes during the Passage of Current." Journal of the Electrochemical Society **137**, 1131-1139 (1990)

50. Verbrugge, M., and R. F. Hill. "Ion and Solvent Transport in Ion-Exchange Membranes." Journal of the Electrochemical Society **137**, 886-899 (1990)

51. Eikerling, M., Kharkats, Y. I., Kornyshev, A. A. and Y. M. Volfkovich. "Phenomenological Theory of Electro-osmotic Effect and Water Management in Polymer Electrolyte Proton-Conducting Membranes." Journal of the Electrochemical Society **145**, 2684-2699 (1998)

52. Fuller, T., and J. Newman. "Water and Thermal Management in Solid-Polymer-Electrolyte Fuel Cells." Journal of the Electrochemical Society **140**, 1218-1225 (1993)

53. Bernardi, D. M. "Water-Balance Calculations for Solid-Polymer-Electrolyte Fuel Cells." Journal of The Electrochemical Society **137**, 3344-3350 (1990)

54. Janssen, G. J. M. "A phenomenological model of water transport in a proton exchange membrane fuel cell." Journal of The Electrochemical Society **148**, A1313-A1323 (2001)

55. Taylor, R. and R. Krishna. Multicomponent Mass Transfer. John Wiley & Sons: Toronto, 1993.

56. Kerkhof, P. J. A. M. "A modified Maxwell-Stefan model for transport through inert membranes: the binary friction model." The Chemical Engineering Journal **64**, 319-343 (1996)

57. Mason, E. A. and A. P. Malinauskas. Gas Transport in Porous Media; The Dusty Gas Model. Elsevier: Amsterdam, 1983.

58. Krishna, R. and J. A. Wesselingh. "Review Article Number 50: The Maxwell-Stefan approach to mass transfer." Chemical Engineering Science **52**, 861-911 (1997)

59. Lightfoot, E. N. Transport Phenomena and Living Systems. John Wiley & Sons: Toronto, 1974.

60. Conway, B. E. Ionic Hydration In Chemistry and Biophysics. Elsevier Scientific Publishing Company: Netherlands, 1981.

61. Moran, M.J. and H. N. Shapiro. <u>Fundamentals of Engineering Thermodynamics</u>. John Wiley & Sons: New York, 1996.

62. Morris, D. R. and X. Sun. "Water-Sorption and Transport Properties of Nafion 117 H." <u>Journal of Applied Polymer Science</u> **50**, 1445-1452 (1993)

63. Pushpa, K. K., D Nandan and R. M. Iyer. "Thermodynamics of Water Sorption by Perfluorosulphonate (Nafion-117) and Polystyrene-Divinylbenzene Sulphonate (Dowex 50W) Ion-exchange Resins at 298±1 K." <u>Journal of The Chemical Society. Faraday Transaction I.</u> **84**, 2047-2056 (1988)

64. Rivin, D., Kendrick, C. E., Gibson, P. W. and N. S. Schneider. "Solubility and Transport Behavior of Water and Alcohols in Nafion (TM)." <u>Polymer</u> **42**, 623-635 (2001)

65. Hinatsu, J. T., M. Mizuhata and H. Takenaka. "Water Uptake of Perfluorosulfonic Acid Membranes From Liquid Water and Water Vapor." <u>Journal of The Electrochemical Society</u> **141**, 1493-1498 (1994)

66. Weber, A. Z. and J. Newman. "Transport in Polymer-Electrolyte Membranes II. Mathematical Model." <u>Journal of The Electrochemical Society</u> **151**, A311-A325 (2004)

Appendix A: Calculating Driving Force Coefficients

Summarizing the values for parameters presented in Section 10.2.2 we have

(A.1) $\Delta p_{ref} = 5 \times 10^5 \, Nm^{-2}$,

(A.2) $\Delta \Phi_{ref} = 0.3V$,

(A.3) $\overline{V}_2 18 \times 10^{-6} \, m^2 mol^{-1}$,

(A.4) $c_{ref} = c_t = \dfrac{1}{\overline{V}_2} = 55.6 \times 10^3 \, mol \cdot m^{-2}$,

(A.5) $F = 96485 \, Coulombs \cdot mol^{-1}$,

(A.6) $R = 8.3143 J \cdot mol^{-1} \cdot K^{-1}$,

(A.7) $T \approx 343K$,

(A.8) $\eta = 3.565 \times 10^{-4} \, kg \cdot m^{-1} \cdot s^{-1}$,

(A.9) $\left(z_1 = +1, z_2 = 0 \right)$,

(A.10) $\hat{c}_1 = \dfrac{c_1}{cref} = \dfrac{\alpha}{\lambda - \gamma} = X_1$,

(A.11) $\hat{v}_1 \approx \hat{v}_2 \approx \overline{V}_2 c_{ref} = 1$.

We can now plug in the above information into the coefficients and we have

(A.12) $\hat{v}_1 \beta = \hat{v}_2 \beta = \dfrac{\hat{v}_2 \Delta p_{ref}}{RTc_{ref}} = \dfrac{(1)(5 \times 10^5)}{8.314(343)(55.6 \times 10^3)} = 3.15 \times 10^{-3}$,

and

(A.13) $\Theta = \dfrac{F \Delta \Phi_{ref}}{RT} = \dfrac{96485(0.3)}{8.314(343)} = 10.1$.

UNIVERSITY OF VICTORIA
PARTIAL COPYRIGHT LICENSE

Title of Thesis:

Transport Phenomena in Polymer Electrolyte Membranes.

Author   _____
              Jeff Fimrite
              June 11, 2004

VITA

Surname: Fimrite   Given Names: Jeffrey Anders

Place of Birth: Edmonton, Alberta, Canada

Educational Institutions Attended

University of Victoria   1997-2004

Degrees Awarded

B.Eng (with distinction)   University of Victoria   2002

Honours and Awards

APEGBC Achievement Award	2003
University of Victoria Graduate Fellowship	2002
ASI (Advanced Systems Institute) Graduate Scholarship	2002
Cunliffe Engineering Scholarship	2001
Hugh and Lilian Salmond Engineering Scholarship	2001
Dean's List	2001
University of Victoria Faculty Scholarship	2000
University of Victoria President's Scholarship	2000
Faculty of Engineering Dean's Entrance Scholarship	1997
D. C. McKinnon Award	1997
Science Council of British Columbia	
Headed for Success Award	1997

Publications

None.